National Technical University of Ukraine
«Igor Sikorsky Kyiv Polytechnic Institute»
Ministry of Education and Science of Ukraine
National Technical University of Ukraine
«Igor Sikorsky Kyiv Polytechnic Institute»
Ministry of Education and Science of Ukraine

Qualifying scientific work
on the rights of the manuscript

Chen Linfei

UDC 621.331:629.3.065-622(043.3) +
544.642.076.2:[681.511:519.85](043.3)

DISSERTATION

IMPROVING THE OPERATING MODES OF THE ELECTROTECHNICAL COMPLEX OF HYDROGEN SUPPLY USING INTELLIGENT CONTROL IN THE ELECTRIC TRANSPORT SYSTEM

Specialty 141 – Electric power engineering,

Eectrical Engineering and Electromechanics

14 – Electrical engineering

Submitted for the degree of Doctor of Philosophy

The dissertation contains the results of the author’s own research.

All ideas, results, and texts of other authors have been properly cited

Chen Linfei

Scientific Supervisor:

Professor Sergii Boichenko

Kyiv – 2026

ABSTRACT

Chen Linfei. Improving the Operating Modes of the Electrotechnical Complex of Hydrogen Supply Using Intelligent Control in the Electric Transport System. Dissertation for the degree of Doctor of Philosophy (PhD) in Specialty 141 – Electrical Power Engineering, Electrical Engineering, and Electromechanics (Field of Knowledge 14 – Electrical Engineering). – National Technical University of Ukraine «Igor Sikorsky Kyiv Polytechnic Institute», Kyiv, 2026.

The dissertation «Improvement of Operating Modes of the Electrotechnical Hydrogen Supply Complex Using Intelligent Control in the Electric Transport System» is dedicated to the urgent scientific task of enhancing the energy efficiency, operational stability, and economic viability of «green» hydrogen infrastructure. Given the rapid electrification of the global transport sector, the local Hydrogen Refueling Station (HRS) has emerged as a critical electrotechnical complex bridging renewable energy source (RES) grids with Fuel Cell Electric Vehicles (FCEVs). However, its efficient operation is severely hindered by a complex «double-stochastic» environment, where the significant intermittency of renewable generation constantly conflicts with the high volatility of refueling demand.

Purpose. To enhance the energy efficiency and operational reliability of the electrotechnical hydrogen supply complex for electric transport by developing an intelligent automated control system for electrolyzer operating modes and energy conversion systems based on dynamic spatio-temporal «Source-Grid-Load-Storage» coordination.

Relevance. This research aims to eliminate the structural mismatch between intermittent renewable energy and the rigid processes of hydrogen production. By addressing the issues of significant thermal fatigue and degradation of the Membrane Electrode Assembly (MEA) caused by frequent start-stop cycles, this study extends the operational lifespan of megawatt-class electrolyzers and ensures the economic security of large-scale green transport networks.

Research Hypothesis. The application of a continuous electrothermal control topology in «hot standby» mode, based on a specialized type of Recurrent Neural Network (RNN) with deep long-term memory (LSTM – Long Short-Term Memory), will minimize the degradation of electrolysis cells and reduce the duration of transient processes during load changes. LSTM was specifically designed to overcome the «gradient vanishing» problem, allowing the system to effectively store and process long data sequences without losing the context of previous steps. This ensures the stability of the hydrogen supply system under the dynamic demand conditions of electric transport.

Object of Research – conversion and consumption of electrical energy in hydrogen production and supply systems operating in stochastic conditions for the needs of electric transport.

Subject of Research – the mode parameters of intelligent control of electrical equipment of hydrogen filling stations.

Research Tasks:

1. To comprehensively describe the electrotechnical system (from the power grid to the electrolyzer) and systematically analyze the dynamic characteristics, degradation

mechanisms, and operational constraints of megawatt-class PEM electrolyzers under intermittent power supply conditions, accounting for the non-linearity of characteristics during transient regimes.

2. To perform a critical analysis with comparative examples and characteristics of strengths and weaknesses based on a SWOT analysis.

3. To study the stochastic behavior patterns of FCEV fleet electrical networks and develop a multi-level load forecasting structure.

4. To formulate a macroscopic M/M/S/N queueing model integrated with microscopic vehicle thermodynamics for the quantitative estimation of instantaneous hydrogen mass flow.

5. To design an Automated Electrolyzer Control System (AECS) with a hierarchical architecture for real-time dynamic state management.

6. To justify the selection and adapt Long Short-Term Memory (LSTM) neural network algorithms for high-precision short-term (next-hour) demand forecasting.

7. To create a multiphysics (electrothermal) dynamic model of a multi-PEM electrolyzer cluster using equivalent circuit topologies.

8. To develop a Demand Response strategy allowing the complex to adapt to RES generation schedules (solar/wind) and electricity market prices.

9. To calculate the Levelized Cost of Hydrogen (LCOH) and perform a techno-economic comparative analysis of the AECS and traditional Rule-Based Control.

Chapter 1 analyzes the current state of hydrogen infrastructure development and the critical limitations of existing control methods. It is determined that modern HRS operate in an extremely complex «double-stochastic» environment. A comprehensive literature review indicates that traditional hysteresis (On/Off) control strategies suffer from «information blindness» – they react only to static pressure thresholds in storage tanks. This rigid approach causes significant thermal fatigue, mechanical stress in the MEA, and massive curtailment of renewable energy, failing to resolve the fundamental structural conflict between system efficiency and equipment lifespan.

Chapter 2 characterizes a pioneering multi-level load forecasting structure. Departing from the oversimplified static assumptions of previous studies, this section synthesizes macroscopic M/M/S/N queueing theory with microscopic non-linear vehicle thermodynamics (utilizing real gas equations of state) to generate high-precision dynamic load profiles. Mathematical modeling and statistical analysis revealed an acute «supply-demand deficit» driven by traffic surges, quantifying an extreme peak-to-trough ratio of 15:1 during morning and evening rush hours. The results mathematically prove that smoothing these surges solely through passive buffer storage is economically unfeasible due to the exponential increase in CAPEX, confirming the rigorous necessity for active, demand-oriented management.

Chapter 3 proposes the core architecture of the Automated Electrolyzer Control System (AECS). The system features a hierarchical structure that organically combines an AI-based load forecasting module (LSTM) with a Deterministic Finite Automata (DFA/FSM). By analyzing historical operational matrices, the LSTM network accurately predicts the aggregate demand for the subsequent hour. As an innovation, a «hot standby» operating mode is added to the FSM logic to dynamically decouple the thermal state of the electrolyzer stack from its electrical load. This enables proactive state transitions based on real-time predictive demand data and solar energy availability, transforming the electrolyzer from a passive load into a highly flexible energy router.

Chapter 4 describes the physical validation of the proposed AECS through rigorous multiphysics dynamic simulation in the MATLAB/Simulink environment. Using a 2RC equivalent circuit model combined with a feedback thermal integrator, the electrochemical transient processes of a megawatt-class PEM cluster were simulated. Experimental results demonstrated that providing a minimum holding current density (yielding a production rate of 3,0 kg/h, or approximately 3% of nominal load) balances internal heat generation with environmental dissipation. This precisely maintains the stack temperature above the critical 60°C threshold during idle periods. Consequently, this mechanism completely eliminates the thermal stress associated with cold starts and endows the PEM electrolyzer with the capability to ramp up power in milliseconds to meet sudden load surges.

Chapter 5 is dedicated to a comprehensive techno-economic evaluation of the commercial feasibility of the AECS. By comparing the intelligent AECS with standard Rule-Based Control (RBC) under a hybrid Time-of-Use (TOU) tariff, simulations showed exceptionally favorable economic indicators. The AECS successfully synchronized flexible hydrogen production with intermittent solar availability, increasing solar energy utilization from an initial 0% to 38,5%. Through intelligent tariff arbitrage and maximum asset protection, the system achieved a specific production cost to 2,92$/kg (approximately 19,96 CNY/kg based on current exchange rates), representing a significant reduction of 13,20%. Crucially, the implementation of the «hot standby» mode reduced harmful start-stop cycles by 98,3%, substantially decreasing associated depreciation costs. Furthermore, the validated fast transient characteristics confirm the system's ability to participate in the electricity market as a Virtual Power Plant (VPP), providing critical active power support to the grid.

Scientific Novelty: **1.** Further developed the methodology of intelligent control for electrolyzer operating modes. The use of an adaptive algorithm based on the LSTM neural network architecture is proposed, allowing for the forecasting of hydrogen demand from electric transport and real-time optimization of the fuel production schedule. **2.** Developed a comprehensive mathematical model of the electrotechnical hydrogen supply complex which, unlike existing models, accounts for the interconnection between power converter dynamic characteristics and non-linear electrochemical processes in the electrolyzer during operation from unstable renewable energy sources (RES). **3.** Proposed a dual-mode intelligent optimization strategy integrating the Arithmetic Optimization Algorithm (AOA) and the African Vulture Optimization Algorithm (AVOA), and constructed an AO–AVOA–BP neural network model for the high-precision state-of-health (SOH) forecasting of lithium-ion batteries.

Practical Significance: **1.** The developed AECS architecture, multi-level load forecasting algorithms, and electrothermal models provide a ready-to-use control paradigm for megawatt-scale commercial green hydrogen projects**. 2.** The proposed «hot standby» strategy reduces start-stop depreciation costs by over 98% and lowers the Levelized Cost of Hydrogen to 2,92$/kg (19,96 CNY/kg). Furthermore, the established dynamic thermal regulation principles will directly facilitate the transformation of hydrogen refueling stations from rigid industrial loads into flexible grid assets. A new approach to integrating a hydrogen refueling complex into the Smart

Grid system provides the possibility of the complex's participation in regulating the frequency and power of the power system, which increases the overall stability of the electric vehicle power supply network. **3.** The proposed integration of AO and AVOA optimization mechanisms significantly improves global search capabilities and local convergence performance of the BP neural network. A dynamic coordination strategy that solves the «impossible trinity» of hydrogen infrastructure (simultaneously achieving low cost, high RES penetration, and extended service life) has been mathematically interpreted and verified against traditional baseline models. On NASA and CALCE datasets, the AO–AVOA–BP model achieves reductions in MAE, RMSE, and MAPE of 72,9–85,7%, 69,6–85,2%, and 72,6–85,8%, respectively, compared to the baseline BP model. **4.** A matching method for hybrid vehicle power plants is proposed, combining orthogonal tests with Cruise software, supplemented by the development of control strategies for critical vehicle components on the MATLAB/Simulink platform. This can significantly reduce the number of experiments and the cost of developing electric vehicle powertrain prototypes.

The dissertation consists of 190 pages. The main body contains 24 figures and 20 tables, 51 formulas.

Keywords: green hydrogen, renewable energy sources, energy efficiency, electrotechnical hydrogen supply complex, intelligent control, Automated Electrolyzer Control System (AECS), hot standby, multi-level stochastic modeling.

АНОТАЦІЯ

Чен Лінфей. Удосконалення режимів роботи електротехнічного комплексу постачання водню з використанням інтелектуального керування в системі електротранспорту. Дисертація на здобуття наукового ступеня доктора філософії за спеціальністю 141 – Електроенергетика, електротехніка та електромеханіка (Галузь знань 14 – Електрична інженерія). – Національний технічний університет України «Київський політехнічний інститут імені Ігоря Сікорського», Київ, 2026.

Дисертація «Удосконалення режимів роботи електротехнічного комплексу забезпечення воднем з використанням інтелектуального керування в системі електричного транспорту» присвячена актуальному науковому завданню підвищення енергоефективності, експлуатаційної стабільності та економічної доцільності інфраструктури «зеленого» водню. З огляду на стрімку електрифікацію глобального транспортного сектору, локальна воднева заправна станція (ВЗС) стала критично важливим електротехнічним комплексом, що з'єднує мережі відновлюваних джерел енергії з електромобілями на паливних елементах (ЕМПЕ). Однак її ефективній роботі серйозно перешкоджає складне «подвійно-стохастичне» середовище, в якому значна переривчастість генерації відновлюваної енергії постійно конфліктує з високою волатильністю попиту на заправку.

Мета. Підвищення енергоефективності та експлуатаційної надійності електротехнічного комплексу постачання водню для електричного транспорту за рахунок розроблення інтелектуальної автоматизованої системи керування режимами роботи електролізерів та систем перетворення енергії на основі динамічної просторово-часової координації «Джерело – Мережа – Навантаження – Накопичувач».

Актуальність. Тема спрямована на усунення структурної невідповідності між переривчастою відновлюваною енергією та жорсткими процесами виробництва водню. Вирішуючи проблему значної термічної втоми та деградації мембранно-електродного блоку (МЕБ), спричинених частими циклами «пуску-зупинки», це дослідження спрямовано на збільшення експлуатаційного терміну служби електролізерів мегаватного класу та забезпечує економічну безпеку великомасштабних екологічних транспортних мереж.

Гіпотеза дослідження – застосування спеціалізованого типу рекурентної нейронної мережі (RNN) з глибокою довгостроковою пам'яттю в системі безперервної електротермічної топології керування в режимі «гарячого резерву» на базі (LSTM – Long Short-Term Memory) дозволить мінімізувати деградацію електролізних комірок і скоротити час перехідних процесів під час зміни навантаження.

Таким чином, удосконалення інтелектуальних систем керування електротехнічними комплексами постачання водню є **актуальним науково-прикладним завданням**, вирішення якого дозволить знизити вартість водневого палива, підвищити енергоефективність транспортної інфраструктури та забезпечити надійність енергосистеми в умовах енергетичного переходу.

Дисертаційна робота є складовою частиною науково-дослідної роботи кафедри автоматизації електротехнічних та мехатронних комплексів НН ІЕЕ КПІ ім. Ігоря Сікорського, зокрема, НДР «Розроблення та експериментальна валідація енергозабезпечення БПЛА з інтегрованою силовою установкою з водневими паливними комірками» (0126u000040).

Об'єкт дослідження – перетворення та споживання електричної енергії в системах виробництва та постачання водню, що функціонують у стохастичних умовах, для потреб електричного транспорту.

Предмет дослідження – режимні параметри інтелектуального керування електротехнічного обладнання водневих заправних станцій.

Завдання:

1. Комплексно описати електротехнічну систему (від мережі живлення до електролізера) та систематично проаналізувати динамічні характеристики, механізми деградації та експлуатаційні обмеження PEM-електролізерів мегаватного класу за умов переривчастого електропостачання з урахуванням нелінійності характеристик при перехідних режимах.

2. Виконати критичний аналіз з прикладами порівнянння та характеристиками слабких і сильних сторін (на базі SWOT-аналізу).

3. Вивчити стохастичні патерни поведінки електричних мереж парків електричних автомобілів (ЕМПЕ) та розробити багаторівневу структуру прогнозування навантаження.

4. Сформулювати макроскопічну модель масового обслуговування M/M/S/N, інтегровану з мікроскопічною термодинамікою транспортних засобів, для кількісної оцінки миттєвого потоку маси водню.

5. Спроєктувати автоматизовану систему керування електролізером (АСКЕ) з ієрархічною архітектурою для динамічного керування станами в режимі реального часу.

6. Обґрунтувати вибір та адаптувати алгоритми нейронної мережі з довгою короткочасною пам’яттю (LSTM) для високоточного короткострокового (на наступну годину) прогнозування попиту.

7. Створити мультифізичну (електротермічну) динамічну модель кластера з декількох PEM-електролізерів з використанням топологій еквівалентних схем.

8. Розробити стратегію керування попитом (Demand Response), що дозволяє комплексу адаптуватися до графіків генерації ВДЕ (сонячних/вітрових станцій) та цін на ринку електроенергії.

9. Розрахувати нормовану орієнтовну вартість водню (LCOH) та виконати техніко-економічний порівняльний аналіз між АСКЕ та традиційним керуванням на основі правил (RBC);

У *розділі* 1 здійснено аналіз поточного стану розвитку інфраструктури забезпечення воднем та критичні обмеження існуючих методів керування. Визначено, що сучасні ВЗС функціонують у надзвичайно складному «подвійно-стохастичному» середовищі. Комплексний огляд літератури свідчить, що традиційним стратегіям гістерезисного керування (Увімк./Вимк.) притаманна «інформаційна сліпота» – вони реагують лише на статичні порогові значення тиску в резервуарах. Такий жорсткий підхід спричиняє значну термічну втому, механічні напруження в МЕБ та масове обмеження використання відновлюваної енергії, що не дозволяє вирішити фундаментальний структурний конфлікт між ефективністю системи та терміном служби обладнання.

Розділ 2 характеризує новаторську багаторівневу структуру прогнозування навантаження. Відходячи від надто спрощених статичних припущень попередніх досліджень, цей розділ синтезує макроскопічну теорію масового обслуговування M/M/S/N з мікроскопічною нелінійною термодинамікою транспортних засобів (із застосуванням рівнянь стану реального газу) для генерації високоточних профілів динамічного навантаження. Математичне моделювання та статистичний аналіз виявили гострий «дефіцит пропозиції-попиту», зумовлений сплесками трафіку, кількісно оцінивши екстремальне співвідношення піку до спаду на рівні 15:1 під час ранкових та вечірніх годин пік. Результати математично доводять, що згладжування цих сплесків лише через пасивне буферне накопичення є економічно недоцільним через експоненціальне зростання капітальних витрат (CAPEX), що підтверджує сувору необхідність активного керування, орієнтованого на попит.

У *розділі* 3 запропоновано базову архітектуру автоматизованої системи керування електролізером (АСКЕ). Система має ієрархічну структуру, що органічно поєднує модуль прогнозування навантаження на базі штучного інтелекту (LSTM) із детермінованим скінченним автоматом (FSM). Аналізуючи історичні експлуатаційні матриці, мережа LSTM точно прогнозує сукупний попит на наступну годину. Як інновацію в логіку FSM додано робочий режим «гарячого резерву» для динамічного відокремлення теплового стану стека електролізера від його електричного навантаження. Це забезпечує проактивні переходи між станами на основі прогнозних даних навантаження та надходжень сонячної енергії в реальному часі, перетворюючи електролізер із пасивного навантаження на надзвичайно гнучкий енергетичний маршрутизатор.

У *розділі* 4 описано фізичну перевірку працездатності запропонованої АСКЕ за допомогою суворого мультифізичного динамічного моделювання в середовищі «MATLAB/Simulink». З використанням 2RC-моделі еквівалентної схеми у поєднанні з тепловим інтегратором зі зворотним зв’язком було змодельовано перехідні електрохімічні процеси PEM-кластера мегаватного класу. Результати експерименту продемонстрували, що подача мінімальної струмової щільності утримання (що забезпечує продуктивність 3,0 кг/год, або близько 3% від номінального навантаження) врівноважує внутрішнє виділення тепла з розсіюванням у навколишнє середовище. Це точно підтримує температуру стека вище критичного порогу в 60°C у періоди простою. Отже, цей механізм повністю усуває тепловий стрес, пов’язаний із холодними пусками, та наділяє PEM-електролізер здатністю нарощувати потужність за мілісекунди для задоволення раптових сплесків навантаження.

Розділ 5 присвячено комплексному техніко-економічному оцінюванню комерційної доцільності АСКЕ. Завдяки порівнянню інтелектуальної АСКЕ зі стандартним керуванням на основі правил (RBC) в умовах дії гібридного тарифу, диференційованого за часом (TOU), моделювання виявило надзвичайно сприятливі економічні показники. АСКЕ успішно синхронізувала гнучке виробництво водню з переривчастою доступністю сонячної енергії, збільшивши використання сонячної енергії з початкових 0% до 38,5%. Завдяки інтелектуальному тарифному арбітражу та максимальному захисту активів, система досягла питомої вартості виробництва на рівні 2,92 $/кг (19,96 юанів/кг), що становить суттєве зниження на 13,20%. Важливо, що впровадження режиму «гарячого резерву» зменшило шкідливі цикли пуску-зупинки на 98,3%, суттєво скоротивши відповідні амортизаційні витрати. Крім того, перевірені швидкі перехідні характеристики підтверджують здатність системи брати участь на ринку електроенергії як Віртуальна електростанція, надаючи критичну активну підтримку потужності мережі.

Наукова новизна *дослідження*:

1. Набула подальшого розвитку методологія інтелектуального керування режимами роботи електролізерних установок, за рахунок використання адаптивного алгоритму на основі нейромережі з архітектурою LSTM, що дозволяє прогнозувати попит на водень з боку електротранспорту та оптимізувати графік виробництва палива в реальному часі.

2. Розроблено комплексну математичну модель електротехнічного комплексу постачання водню, що, на відміну від існуючих, враховує взаємозв’язок між динамічними характеристиками силових перетворювачів і нелінійними електрохімічними процесами в електролізері під час роботи від енергоустановок на основі відновлюваних джерел енергії (ВДЕ).

3. Запропоновано дворежимну інтелектуальну модель оптимізації, що інтегрує алгоритм арифметичної оптимізації (AO) та алгоритм оптимізації африканського грифа (AVOA), а також будує нейронну мережеву модель AO–

AVOA–BP для високоточного прогнозування технічного стану літій-іонних акумуляторів.

Практичне значення.

1. Розроблена архітектура АСКЕ, алгоритми багаторівневого прогнозування навантаження та електротермічні моделі, що пропонують готову до використання парадигму керування для комерційних проєктів «зеленого» водню мегаватного класу.

2. Запропонована стратегія «гарячого резерву» зменшує амортизаційні витрати на пуск-зупинку на понад 98% і знижує нормовану вартість водню до 2,92 $/kg (19,96 юанів/кг). Встановлені принципи динамічного терморегулювання безпосередньо сприятимуть трансформації водневих заправних станцій із жорстких промислових навантажень у гнучкі. Новий підхід до інтеграції водневого заправного комплексу в систему «Smart Grid» забезпечує можливість участі комплексу в регулюванні частоти та потужності енергосистеми, що підвищує загальну стійкість мережі живлення електротранспорту.

3. Запропонована інтеграція механізмів оптимізації AO та AVOA значно покращує можливості глобального пошуку та продуктивність локальної конвергенції нейронної мережі BP. Математично інтепретовано та верифіковано відносно традиційних базових моделей стратегію динамічної координації, що вирішує «неможливу трійцю» водневої інфраструктури (одночасне досягнення низької вартості, високого проникнення ВДЕ та подовженого терміну служби). На наборах даних NASA та CALCE, порівняно з базовою моделлю BP, AO-

AVOA-BP досягає зниження MAE, RMSE та MAPE на 72,9–85,7%, 69,6–85,2% та 72,6–85,8% відповідно.

4. Запропоновано метод узгодження силової установки гібридного автомобіля, що поєднує ортогональні тести з програмним забезпеченням Cruise, доповнений розробкою стратегії керування критичними компонентами всього автомобіля на платформі MATLAB/Simulink. Це може значно зменшити кількість експериментів та вартість розроблення прототипу силової установки електричного автомобіля.

Дисертація складається з 190 сторінок. Основна частина дисертації містить 21 рисунок, 19 таблиць, 51 формулу.

Ключові слова: зелений водень, відновлювані джерела енергії, енергоефективність, електротехнічний комплекс забезпечення воднем, інтелектуальне керування, автоматизована система керування електролізером, гарячий резерв, багаторівневе стохастичне моделювання.

PUBLICATIONS PRESENTING THE MAIN FINDINGS OF THE DISSERTATION

***Journal Articles*:**

1. Wang, X., Liu, S., Ye, P., Zhu, Y., Yuan, Y., & **Chen, L.** (2023). Study of a Hybrid Vehicle Powertrain Parameter Matching Design Based on the Combination of Orthogonal Test and Cruise Software. *Sustainability*, 15(14), 10774. https://doi.org/10.3390/su151410774 (Web of Science & Scopus, Q2).

Conceptualization of the orthogonal testing method, validation of results according to the WLTC cycle,, Xingxing Wang and Linfei Chen; methodology and formal analysis, Xingxing Wang; software and validation, Shengren Liu and Peilin Ye; preparation of the manuscript and editing according to scientific publication standards, Peilin Ye and Linfei Chen; resources, Yu Zhu; data curation, Shengren Liu; writing – original draft preparation, Shengren Liu; writing – review and editing, Xingxing Wang and Linfei Chen; participation in the preparation of the interpretation of the obtained results, Shengren Liu; supervision, Yu Zhu; project administration, Xingxing Wang and Yinnan Yuan; funding acquisition, Yinnan Yuan and Linfei Chen.

2. Boichenko S., & **Chen, L.** (2024). Comparative analysis of hydrogen production, accumulation, distribution, and storage systems. *System Research in Energy*, 3 (79), 13–20. https://doi.org/10.15407/srenergy2024.03.013 (professional, category B).

Conceptualization, methodology, Sergii Boichenko; systematization and analysis of technical data on hydrogen production methods, types of storage devices and transport networks, formal analysis, Linfei Chen; writing – review and editing, – creation of a methodological basis for assessing the efficiency of hydrogen production, storage and distribution systems Linfei Chen and Sergii Boichenko.

3. Boichenko, S., **Chen, L.**, Korovushkin, V., & Biliakovych, O. (2025). PEST- and SNW-analysis of the use of liquid hydrogen as a motor fuel in aviation. *System Research in Energy*, 81(1), 61–73. https://doi.org/10.15407/srenergy2025.01.061 (professional,

category B).

Conceptualization, methodology, Sergii Boichenko; collection of analytical data, conducting a comparative analysis of technological, economic and environmental characteristics of hydrogen systems, Linfei Chen and Oleh Biliakovych; validation, verification of the obtained analytical results Linfei Chen and Vitalii Korovushkin; comparison of parameters of various hydrogen accumulation and storage technologies, Linfei Chen; writing – review and editing, Sergii Boichenko, Linfei Chen, Vitalii Korovushkin and Oleh Biliakovych; project administration, Sergii Boichenko.

4. Wang, X., Liang, S., Li, J., Ni, H., Zhu, Y., Lv, S., & **Chen, L.** (2025). Dual Modal Intelligent Optimization BP Neural Network Model Integrating Aquila Optimizer and African Vulture Optimization Algorithm and Its Application in Lithium-Ion Battery SOH Prediction. *Machines*, *13* (9), 799. https://doi.org/10.3390/machines13090799 (Web of Science & Scopus, Q2).

Conceptualization and methodology, Xingxing Wang; software and data curation, Junyi Li; compared results with other models, calculated errors (RMSE, MAE), constructed graphs of algorithm convergence, and proofread the text, Linfei Chen; validation and visualization, Shun Liang; formal analysis, Shuaishuai Lv; writing – original draft preparation, Shun Liang and Junyi Li; writing – review and editing, Xingxing Wang and Linfei Chen; resources and supervision, Hongjun Ni and Yu Zhu; project administration, Xingxing Wang and Yu Zhu; funding acquisition, Xingxing Wang and Hongjun Ni.

***Conference Presentations / Proceedings*:**

5. Chen, L., Boichenko, S. (2024, May). Pest-analysis of the use of liquid hydrogen as a motor fuel in aviation. [Oral presentation]. XXV International Scientific and Practical Online Conference "Renewable Energy and Energy Efficiency of the XXI Century", Kyiv, Ukraine. https://www.ive.org.ua/wp-content/uploads/Tezy_2024_Publication.pdf.

Conceptualization, methodology, Sergii Boichenko; collection of analytical data, conducting a comparative analysis of technological, economic and environmental characteristics of hydrogen systems, verification of the obtained analytical results, comparison of parameters of various hydrogen accumulation and storage technologies. Visualization of research results, preparation of presentations and report, Linfei Chen; writing – original draft preparation, Sergii Boichenko; writing – review and editing, Linfei Chen and Sergii Boichenko; project administration, Sergii Boichenko.

6. Chen, L., & Boichenko, S. (2024, November). Application of hydrogen fuel in automotive energy management: Material impact, environmental benefits, and safety considerations. [Oral presentation]. X International Scientific and Technical Conference "Energy Management: State and Prospects of Development – PEMS'2024", Kyiv, Ukraine. http://pems.kpi.ua/proc/issue/view/18723 .

Conceptualization, methodology, Sergii Boichenko; creation of a methodological basis for assessing the efficiency of hydrogen production, storage and distribution systems, as well as collection, systematization and analysis of technical data on hydrogen production methods, types of storage devices and transport networks, formal analysis, Linfei Chen; writing – original draft preparation, Linfei Chen; writing – review and editing, Linfei Chen and Sergii Boichenko; project administration, Sergii Boichenko.

7. Boichenko, S., & Chen, L. (2025, May). Hydrogen as a sustainable motor fuel fundamentals, focused content, definitions, challenges, implementation methods. [Oral presentation]. XXVI International Scientific and Practical Online Conference "Renewable Energy and Energy Efficiency of the XXI Century", Kyiv, Ukraine. https://www.ive.org.ua/?page_id=7225&lang=uk.

Conceptualization, methodology, Sergii Boichenko; formulation of hydrogen definitions, fundamental physical/chemical properties, and the core operational challenges of hydrogen engines. Visualization of research results, preparation of presentations and report, Linfei Chen; writing – original draft preparation, review and editing, Linfei Chen and Sergii Boichenko; project administration, Sergii Boichenko.

8. Chen, L. (2025, July). Intelligent automated electrolyzer control system for the production, accumulation and storage of hydrogen for refueling vehicles. [Oral presentation]. X International Scientific-Technical Conference «Theory and Practice of Rational Use of Traditional and Alternative Fuels & Lubricants» (Problems of Chemmotology), Kyiv, Ukraine. https://aemk.kpi.ua/wp-content/uploads/2025/07/Final-Program_01.07.2025.pdf .

Conceptualization, methodology, Sergii Boichenko; creating dynamic balancing algorithms, designing automation architecture, and modeling safe storage modes. The main volume of preparation of the publication text was completed. Visualization of research results, preparation of presentations and report, validation, Linfei Chen; writing – original draft preparation, review and editing, Linfei Chen and Sergii Boichenko; project administration, Sergii Boichenko.

9. Chen, L._(2025, April). Material compatibility, environmental impact, and safety considerations of hydrogen as a sustainable motor fuel [Oral presentation] / Linfei Chen, Sergii Boichenko // Modern technologies of fossil fuel processing: abstracts of the 8th International Scientific and Technical Conference., 16–17 April, 2025. https://repository.kpi.kharkov.ua/items/f1880959-b614-46be-83ed-79269c356e55.

Conceptualization, methodology, Sergii Boichenko; collected and analyzed data on hydrogen embrittlement, emissions, and safety hazard, prepared the initial draft, including background research and analysis, preparation of presentations and report, Linfei Chen; writing – original draft preparation, review and editing, Linfei Chen and Sergii Boichenko; visualization, Linfei Chen; project administration, Sergii Boichenko.

CONTENT

LIST OF SYMBOLS AND ABBREVIATIONS

Symbols:

A – Frontal area of the vehicle [m^2]

A_{cell} – Active area of a single electrolyzer cell [cm^2]

a_i – Polynomial coefficients for the compressibility factor model

b – Bias vector in LSTM neural network

C_D – Aerodynamic drag coefficient

C_{diff} – Diffusion capacitance [F]

C_{dl} – Charge double-layer capacitance [F]

C_{spec} – Specific electricity cost of hydrogen production [$/kg, CNY/kg]

C_{start} – Equivalent start-stop depreciation cost [$/kg, CNY/cycle]

C_{th} – Thermal capacitance [J/K] / Total thermal inertia

C_t – Cell state vector in LSTM at time step t

$\widetilde{C}_t$ – Candidate memory cell state in LSTM

D – Historical discrete load sequence

D(t) – Hydrogen demand rate drawn from the tank [kg/h]

$\widehat{D}_{LSTM}$ – Next-hour demand predicted by the LSTM model

d_t – Aggregated hydrogen demand at time step t [kg/h]

E_{bat} – Power battery capacity [kWh]

F – Faraday constant [96485 C/mol] / Mapping function for prediction

f – Rolling resistance coefficient / Grid frequency [Hz]

f_t – Forget gate vector in LSTM

ΔG – Gibbs free energy change

g – Gravitational acceleration [9.81 m/s^2]

h_t – Hidden state vector in LSTM at time step t

I – Current [A]

i – Current density [A/cm^2]

i_0 – Exchange current density [A/cm^2]

i_t – Input gate vector in LSTM

J – Global control objective function / Cost function

K_p – Proportional gain factor

k – Dummy variable for Poisson process

L – Queue length (average number of vehicles in the system) / Loss function

L_q – Queue length (average number of vehicles waiting)

M – Vehicle gross mass / curb mass [kg]

M_{design} – Station design capacity [kg/day]

M_{req} – Target daily demand [kg/day]

M_{total} – Cumulative daily hydrogen demand [kg/day]

$\dot{M}_{station}(t)$ – Station-level dynamic hydrogen mass flow rate [kg/h]

m – Mass of hydrogen gas [kg]

$\Delta\ m$ – Actual filling quantity / Net mass transferred [kg]

$\dot{m}_{H_2}$ – Hydrogen consumption rate [kg/h or kg/100km]

N – Maximum system capacity in queueing model [veh] / Total number of samples in MSE

N_{cells} – Number of cells in series per stack

N_{cycle} – Number of start-stop cycles

N_{daily} – Target service volume [veh/day]

N(t) – Stochastic number of vehicles arriving at time t

o_t – Output gate vector in LSTM

P – Absolute pressure [Pa or MPa] / Electrical power / Production rate [kg/h or kW]

P_{block} – Blocking probability in queueing system

p – Dropout rate in neural network regularization

$\dot{Q}$ – Heat transfer rate / Heat flux [W]

R – Ideal gas constant [8.314 J/(mol·K)] / Specific gas constant for hydrogen [4214 J/(kg·K)] / WLTC Range [km]

R^2 – Coefficient of Determination

R_{act} – Charge transfer (activation) resistance [Ω]

R_{conc} – Mass transport (concentration) resistance [Ω]

R_{mem} – Area-specific membrane resistance [$\Omega \cdot cm^2$]

R_{th} – Thermal resistance [K/W]

S – Hydrogen storage tank inventory level [kg] / Number of dispensers in queueing system

s – Sliding window step size / Laplace operator in complex frequency domain

T – Absolute temperature [K] / Total simulation duration [hours]

T_f – Forecast horizon in time-series prediction

T_p – Look-back window size in time-series prediction

t – Discrete time step

V – Voltage [V] / Internal water volume of the cylinder [m^3] / Vehicle velocity [m/s or km/h]

W – Learnable weight matrix in LSTM / Average wait time in system [hour]

W_q – Average wait time in queue [minute]

w – Weight factor in multi-objective optimization

X_t – Input feature matrix (observation vector)

x_t – Raw time-series data value

x'_t – Normalized input data value

Y_t – Target label / Future demand sequence

y_i – Actual ground truth value

$\hat{y}_i$ – Predicted value from the neural network

$\bar{y}$ – Mean of the observed data

Z – Compressibility factor

Z_{eq} – Equivalent impedance function

Greek Letters:

α – Road slope angle [rad] / Charge transfer coefficient

β_1, β_2 – Exponential decay rates for moment estimates in Adam optimizer

β_{road} – Road gradient coefficient

$\beta_{traffic}$ – Traffic congestion coefficient

Δ – Difference operator (e.g., Δt for time step size, Δm for mass difference)

δ – Rotating mass conversion coefficient

ϵ – Irreducible stochastic noise

η – Learning rate of the neural network optimizer

η_{act} – Activation overpotential [V]

η_{cap} – Daily capacity utilization factor

η_{diff} – Diffusion overpotential [V]

η_{ohm} – Ohmic overpotential [V]

η_t – Mechanical transmission efficiency

θ – Learnable parameters (weights and biases) of the neural network

λ – Arrival rate of vehicles [veh/h] / Electricity tariff or levelized cost [$/kWh, CNY/kWh]

μ – Mean value (e.g., μ_{P_0}, $\mu_{\Delta m}$)

ρ – Air density [1.225 kg/m^3]

σ – Standard deviation (power fluctuation) / Sigmoid activation function

τ – Integration dummy variable for time

Sub- and superscripts:

0 – Initial state (time zero)

act – Activation (kinetic) related

amb – Ambient environment

avg – Average

base – Baseline reference

bat – Battery

block – Blocking state

c – Cut-off state (final state)

cap – Capacity

cell – Single electrochemical cell (battery)

climb – Climbing condition

cmd – Command setpoint

conc – Concentration (mass transport) related

cool – Active cooling system

cruise – Steady-state cruising condition

D – Drag

daily – Daily summation

design – Design specification

diff – Diffusion related

dl – Double-layer related

emergency – Emergency threshold

eq – Equivalent

f, i, C, o – Forget, input, candidate, output (LSTM gating subscripts)

fc – Fuel cell

gen – Generation (heat)

grid – Utility power grid

i – Index variable

idle – Idle or Hot Standby state

init – Initialization state

life – Lifespan protection objective

lim – Limiting state (e.g., limiting current) loss – Dissipation or loss

max – Maximum physical or operational limit

mem – Membrane related

min – Minimum physical or operational limit

mot – Motor

night – Nighttime valley target

nom – Nominal state

off – Shutdown threshold

ohm – Ohmic related

on – Activation threshold

op – Operating state / Operational period

opt – Optimal setpoint

peak – Peak condition

q – Queue related

rated – Rated / Nominal capacity

real – Real / Actual condition

ref – Reference safety baseline

req – Required / Requested demand

rev – Reversible (thermodynamic) state

road – Road condition

solar – Solar / Photovoltaic related

spec – Specific normalized metric

stab – Stabilization objective

stack – Electrolyzer stack

start – Start-stop cycle related

station – Station level

sys – Lumped parallel system

target – Calculated target value

th – Thermal related

tn – Thermoneutral

total – Total cumulative

traffic – Traffic condition

Abbreviations:

AECS – Automated Electrolyzer Control System

AI – Artificial Intelligence

ALK – Alkaline Electrolysis

ARIMA – Autoregressive Integrated Moving Average

BESS – Battery Energy Storage System

BEV – Battery Electric Vehicle

BoP – Balance of Plant

BPTT – Backpropagation Through Time

BSFC – Brake Specific Fuel Consumption

BSG – Belt-integrated Starter Generator

CAPEX – Capital Expenditure

CD – Charge Depleting

CEC – Constant Error Carousel

CGH_2 – Gaseous Hydrogen

COTS – Commercial-Off-The-Shelf

CS – Charge Sustaining

CV – Coefficient of Variation

DSR – Demand Side Response

ECSA – Electrochemical Active Surface Area

EOS – Equation of State

EREV – Extended-Range Electric Vehicle

ESD – Emergency Shutdown

ETS – Electrotechnical System

EV – Electric Vehicle

FCEV – Fuel Cell Electric Vehicle

FSM – Finite State Machine

GLOSA – Green Light Optimal Speed Advisory

H35 / H70 – 35 MPa / 70 MPa Hydrogen Refueling Standard

HEV – Full Hybrid Electric Vehicle

HHV – Higher Heating Value

HIL – Hardware-in-the-Loop

HRS – Hydrogen Refueling Station

ICE – Internal Combustion Engine

IEC – International Electrotechnical Commission

IGBT – Insulated-Gate Bipolar Transistor

IIoT – Industrial Internet of Things

IPC – Industrial Edge AI Server / Industrial Personal Computer

ISG – Integrated Starter Generator

ISO – International Organization for Standardization

IT – Information Technology

ITS – Intelligent Transportation Systems

KOH – Potassium Hydroxide

KPI – Key Performance Indicator

LCOE – Levelized Cost of Energy

LCOH – Levelized Cost of Hydrogen

LH_2 – Liquid Hydrogen

LHV – Lower Heating Value

LSTM – Long Short-Term Memory

MAE – Mean Absolute Error

MEA – Membrane Electrode Assembly

MHEV – Mild Hybrid Electric Vehicle

MPC – Model Predictive Control

MSE – Mean Squared Error

MTBF – Mean Time Between Failures

NEV – New Energy Vehicle

NHPP – Non-homogeneous Poisson Process

NIST – National Institute of Standards and Technology

OBC – On-Board Charger

OCV – Open Circuit Voltage

OPC UA – Open Platform Communications Unified Architecture

OPEX – Operational Expenditure

OT – Operational Technology

P2G – Power-to-Gas

PEM – Proton Exchange Membrane / Polymer Electrolyte Membrane

PEMFC – Proton Exchange Membrane Fuel Cell

PEST – Political, Economic, Social, Technological (Analysis)

PFR – Primary Frequency Regulation

PFSA – Perfluorosulfonic Acid (Nafion)

PHEV – Plug-in Hybrid Electric Vehicle

PID – Proportional-Integral-Derivative

PLC – Programmable Logic Controller

PV – Photovoltaic

QoS – Quality of Service

RBC – Rule-Based Control

REFPROP – Reference Fluid Thermodynamic and Transport Properties Database

RES – Renewable Energy Sources

RMSE – Root Mean Square Error

RNN – Recurrent Neural Network

RTP – Real-Time Pricing

SAE – Society of Automotive Engineers

SCADA – Supervisory Control and Data Acquisition

SNW – Strengths, Neutrals, Weaknesses (Analysis)

SOC – State of Charge

SoH – State of Health

SPAT – Signal Phase and Timing

T40 – Temperature category for -40 °C pre-cooling

TCS – Thermal Control System

THS – Toyota Hybrid System

TOU – Time-of-Use

V2I – Vehicle-to-Infrastructure

V2X – Vehicle-to-Everything

VPP – Virtual Power Plant

VRE – Variable Renewable Energy

WLTC – Worldwide Harmonized Light Vehicles Test Cycle

ZEV – Zero-Emission Vehicle

INRTODUCTON

Research Background and Analysis of the Engineering Problem. As the global energy landscape transitions toward carbon neutrality, hydrogen has emerged as an irreplaceable zero-carbon secondary energy source, particularly for heavy-duty and long-haul transportation. Distributed on-site Hydrogen Refueling Stations (HRS), which integrate renewable energy with Proton Exchange Membrane (PEM) water electrolysis technology, have become critical infrastructure supporting the hydrogen transportation network. However, in actual operation, there exists a profound physical and operational logic conflict between the electric transport system and the hydrogen production system, which constitutes the starting point of this dissertation.

The core of this conflict lies in the «**Spatiotemporal Supply-Demand Mismatch**»: The arrival of vehicles at the HRS service end exhibits high stochasticity and discrete pulse-like characteristics (often following random processes such as the Poisson distribution), whereas the PEM electrolyzer at the production end requires a relatively steady-state continuous operation due to its electrochemical and thermodynamic constraints. Traditional control systems fail to fundamentally bridge this supply-demand gap caused by the randomness of traffic flow, leaving core hydrogen production equipment to operate in non-steady-state conditions for extended periods, severely restricting the overall reliability and economic viability of the hydrogen transport system.

Limitations of Existing Control Technologies and System Degradation Mechanisms. Currently, the most widely adopted control strategy for HRS in the industry is «Pressure-based Hysteresis Control». This control logic is entirely dependent on the current physical state of the hydrogen storage tank (i.e., the upper and lower limits of physical pressure thresholds). When the hydrogen inventory drops to the lower limit, the system starts at full load; when it reaches the upper limit, the system is passively forced to shut down.

This reactive control mode has three fatal limitations:

1. **Control Blindness:** The system has zero knowledge of future traffic flow demands. It can only passively respond to current pressure changes and is incapable of system-level prospective scheduling.

2. **Severe Equipment Degradation:** Faced with high-frequency fluctuating traffic flows, hysteresis control forces the PEM electrolyzer into frequent «start-stop» cycles (up to 37 start-stop events within 60 days, as demonstrated in the baseline test of this study). This binary (0 or 1) operational mode induces drastic mechanical stress (pressure alternation) and thermal stress (temperature gradient mutation), accelerating the mechanical fatigue and chemical degradation of the Membrane Electrode Assembly (MEA) and significantly shortening the service life of the electrolyzer.

3. **Grid Impact:** The frequent switching between full-load operation and shutdown leads to severe fluctuations in power output, causing significant load impacts on the front-end power supply network and weakening the system's compatibility with renewable energy sources or smart grids.

The Essence of Intelligent Control: A Paradigm Shift. To address the aforementioned limitations, this dissertation proposes the integration of «Intelligent Control» into the electric transport hydrogen supply system. The essence of this intelligent control is not merely system automation, but a paradigm shift from «reactive physical threshold control» to «proactive data-driven anticipation».

In the electric transport system, the core value of intelligent control is to act as a «Digital Shock Absorber» between stochastic external demand and steady-state internal production. Its essence is manifested in the reconstruction of two dimensions:

1. **Decoupling of Spatiotemporal Features:** Traditional hysteresis control transmits the stochastic shocks of traffic flow directly to physical equipment. In contrast, intelligent control establishes a «Predict-and-Control» framework. It filters and parses traffic flow at the information level, extracting deterministic patterns (such as the morning and evening «double-peak» characteristics) hidden within a stochastic background. Consequently, disordered external disturbances are transformed into an orderly internal production schedule.

2. **Continuous Reconstruction of Operational Topology:** Intelligent control abandons the traditional binary start-stop logic and introduces a continuous electrothermal control topology operating in a «Hot Reserve» mode. In this mode, the system no longer shuts down frequently. Instead, by sensing future demand changes, it translates control commands into a smooth «load-following» curve. The essential advantage of this continuous control is that by keeping the equipment running continuously in the partial-load region, it completely eliminates the start-stop transient processes that cause equipment degradation, thereby minimizing the drastic thermal and mechanical stress impacts.

Implementation Mechanisms of the Intellectual Guarantee. The continuous electrothermal control topology can be safely and reliably implemented in the «hot reserve» mode – without the risk of hydrogen depletion or overpressure hazards caused by sudden supply-demand mutations – at the expense of (and intellectually ensured by) the following three dimensions of algorithmic mechanisms:

First, a time-series pattern extraction and prediction mechanism based on Deep Learning.

The foundation of the system's intelligence stems from a Deep Long Short-Term Memory (LSTM) neural network. While traffic flow data is superficially filled with high-frequency random noise, the LSTM network, utilizing its unique gating mechanism, effectively filters this high-frequency noise. It accurately captures the low-frequency, decisive periodic patterns hidden behind long-term operational data (366 days), such as the deterministic «double-peak» demand characteristics that account for 62% of the variance. This robust generalization and prediction capability endows the control system with the «vision» to pre-adjust.

Second, a Dynamic Safety Buffer mechanism based on statistical error distribution.

In transportation systems, absolute prediction accuracy is unattainable. One of the intellectual cores of this dissertation is transforming prediction «uncertainty» into a quantifiable «deterministic physical boundary». By rigorously calculating the Root Mean Square Error (RMSE, tested at 8,37 kg in this study) of the LSTM model on the unseen test set, the system scientifically quantifies the potential supply-demand gap caused by random fluctuations. Based on this, a strict dynamic safety buffer inventory is established in the control strategy (the safety stock S_{ref} is set at 300 kg, providing a redundancy margin of $> 30 \times RMSE$). It is exactly this buffering mechanism, grounded in rigorous error statistics, that constitutes the mathematical foundation and intellectual guarantee allowing the system to confidently maintain continuous «hot reserve» operation and reject passive shutdowns.

Third, a smooth transformation mechanism for feedforward control commands.

Relying on high-accuracy LSTM demand prediction and an adequate RMSE safety margin, the control algorithm transforms the «step-like» full-load start-stop commands – originally triggered by pressure bottoming out – into «smooth feedforward» commands based on the integration of future hourly demands. This transformation significantly reduces the standard deviation (σ) of the electrolyzer's power output by 51,2%, truly realizing flexible, continuous production directed by an intelligent algorithmic brain.

Main Research Contents and Innovative Contributions. Based on the theoretical framework above, this dissertation is dedicated to solving the control optimization problem of hydrogen production systems under stochastic traffic loads. The main research contents and innovative contributions are reflected in the following three aspects:

1. **Establishment of a Robust Thermodynamic Benchmark Based on the Real Gas Equation of State:** Through Monte Carlo simulations of 100 random refueling scenarios, this study quantified the thermodynamic characteristics of the 70 MPa filling process, establishing a robust design benchmark of 4,5 kg/vehicle. It also proved that the physical fluctuation of a single filling (5,02%) is far less than the fluctuation of

traffic flow, fundamentally demonstrating the scientific feasibility of traffic-flow-driven demand modeling.

2. **Development of a High-Accuracy Short-Term Hydrogen Demand Prediction Model:** A deep learning model based on LSTM was developed, effectively overcoming the overfitting problems of traditional prediction methods when processing long-term, high-noise traffic data. The model achieved a high prediction accuracy with an RMSE of only 8,37 kg on the unseen test set, providing a reliable data prior for downstream control.

3. **Proposal of a «Predict-and-Control» Intelligent Collaborative Strategy Eliminating Start-Stop Stress:** This study innovatively integrated prediction results with an error-based safety buffer mechanism to design a continuous load-following control strategy. Simulation verification demonstrates that in a 60-day stochastic testing environment, this strategy successfully reduced the 37 start-stop cycles of the baseline system to exactly 0. This not only fundamentally eliminates the mechanical and thermal stresses that restrict electrolyzer lifespan but also significantly smooths the grid load, providing a complete theoretical guide and engineering paradigm for the control system design of next-generation highly reliable HRS.

CHAPTER 1.

LATEST ACHIEVEMENTS IN THE ELECTRIC TRANSPORT SYSTEM AND PROSPECTS FOR IMPROVING ELECTRICAL-TECHNICAL (ETS) HYDROGEN SUPPLY SYSTEMS

1.1. Modern classification of electric vehicles and the structure of the infrastructure of hydrogen refueling stations (HRS)

With the acceleration of the global energy transition and the advancement of decarbonization goals, the transportation sector is undergoing a fundamental paradigm shift from Internal Combustion Engine (ICE) vehicles to electrified drive systems [1]. The core carriers of this transformation are Electric Vehicles (EVs), while the key novel infrastructure supporting this system consists of charging networks and Hydrogen Refueling Stations (HRS). This Chapter provides a systematic classification of modern electric vehicles based on powertrain topology, referencing the latest International Electrotechnical Commission (IEC) standards and Society of Automotive Engineers (SAE) specifications [2]. Furthermore, it offers an in-depth analysis of the internal physical architecture of the HRS, viewing it as a complex Electrotechnical System (ETS).

1.1.1. The Six-Category Classification of Modern Electric Vehicles

In early academic definitions, electric vehicles were simply categorized into three types: Hybrid, Battery Electric, and Fuel Cell vehicles. However, with the iterative evolution of electrification technologies, modern EVs have differentiated into six distinct topological structures characterized by varying control logic and energy flow paths [3]. Based on the depth of motor intervention, energy replenishment method, and powertrain architecture, this study classifies them as follows:

1. Mild Hybrid Electric Vehicle (MHEV)

MHEV represents the entry-level stage of electrification, typically utilizing a 48V electrical system.

- Architectural Characteristics: Equipped with a small Belt-integrated Starter Generator (BSG) or Integrated Starter Generator (ISG) and a minimal battery capacity (< 1kWh).

- Operating Mode: The electric motor cannot independently drive the vehicle. Its primary functions are to facilitate rapid Start-Stop operations, provide Torque Assist during acceleration, and recuperate kinetic energy during braking.

- Significance: It serves as a low-cost transitional solution for traditional ICE vehicles, reducing fuel consumption by approximately 10–15%, but it cannot achieve zero-emission driving.

2. Full Hybrid Electric Vehicle (HEV)

HEV refers to non-plug-in hybrid vehicles capable of pure electric propulsion (e.g., the Toyota THS system).

- Architectural Characteristics: Features a high-voltage traction battery (typically >200V) and a powerful electric motor. Based on the mechanical coupling, architectures are divided into Series, Parallel, and Power-split configurations.

- Energy Source: Lacks external charging capability. All electrical energy is derived from the secondary conversion of fossil fuel (via the engine driving a generator) or regenerative braking.

- Limitation: Although thermal efficiency is high, its energy source remains entirely dependent on fossil fuels.

3. Plug-in Hybrid Electric Vehicle (PHEV)

PHEVs incorporate an On-Board Charger (OBC) and a larger capacity battery (typically 10 ~ 20kWh) into the HEV architecture.

- Architectural Characteristics: Retains a mechanical connection allowing the ICE to directly drive the wheels (usually Parallel or Power-split architecture).

- Operating Mode: Operates in «Charge Depleting (CD)» mode and «Charge Sustaining (CS)» mode. In CD mode, it functions as a BEV; once the battery is depleted and the vehicle enters CS mode, it reverts to HEV behavior.

4. Extended-Range Electric Vehicle (EREV)

EREV is a specific Series plug-in hybrid architecture, academically distinct from PHEVs.

- Architectural Characteristics: The ICE (referred to as the «Range Extender») is mechanically decoupled from the wheels, serving solely as a generator to charge the battery or supply power directly to the electric motor.

- Operating Mode: The vehicle is driven exclusively by the electric motor at all times. The engine operation is independent of vehicle speed, allowing it to run continuously on the optimal Brake Specific Fuel Consumption (BSFC) curve, thereby maximizing energy conversion efficiency.

5. Battery Electric Vehicle (BEV)

BEV represents the «Full Electrification» pathway.

Architectural Characteristics: The ICE, fuel system, and exhaust system are entirely eliminated. Energy is stored exclusively in a chemical battery pack and delivered to the motor via an inverter.

Technological Bottleneck: Despite having the highest «Grid-to-Wheel» efficiency, BEVs are limited by the gravimetric energy density of Lithium-ion batteries (currently approx. 250Wh/kg). This results in significant weight penalties and extended recharging times (30 minutes to several hours) for heavy-duty, long-haul transport, and low-temperature environments [4].

6. Fuel Cell Electric Vehicle (FCEV)

FCEV is the primary subject of this research and is regarded as the ultimate eco-friendly solution for heavy transport [5].

Architectural Characteristics: Essentially an «Electro-Electric Hybrid» system.

Primary Power Source: Proton Exchange Membrane Fuel Cell (PEMFC) stack, providing the Base Load.

Auxiliary Power Source: Traction battery, providing peak power for acceleration and absorbing regenerative braking energy.

Core Advantages: The high Lower Heating Value (LHV) of hydrogen (120MJ/kg) enables FCEVs to resolve the range and weight limitations of BEVs in heavy trucks, intercity buses, and aviation.

Infrastructure Dependency: The operation of FCEVs relies heavily on Hydrogen Refueling Stations (HRS). The refueling process (3–5 minutes) offers time utility comparable to conventional vehicles (tabl. 1.1).

Table 1.1 – Comparison of Core Characteristics and Key Considerations Across Electric Vehicle Technologies

Category	Core Characteristics	Key Notes
MHEV	Low-voltage (typically 48V) system assisting ICE; cannot drive purely on electric power	Entry-level electrification; improves fuel efficiency ~10–15%; examples: Audi A6 48V mild hybrid
HEV	ICE + electric motor; battery charged via regenerative braking/engine; no external charging port	Often classified as "energy-saving vehicle" (not NEV) in policies like China's; examples: Toyota Camry Hybrid
PHEV	Combines battery-electric drive (with external charging capability) + internal combustion engine (ICE); operates in pure EV mode for limited range	EV range typically 30–80 km; examples: BYD Qin PLUS DM-i, Toyota Prius Prime
EREV	Primarily BEV architecture with small onboard generator (ICE or turbine) that only charges the battery, never drives wheels directly	Distinct from PHEV: engine is purely a range extender; examples: Li Auto L-series
BEV	Solely powered by rechargeable battery pack driving electric motor(s); zero tailpipe emissions	Dominant EV type globally; requires external charging infrastructure; examples: Tesla Model Y, BYD Han EV, NIO ET7
FCEV	Generates electricity onboard via hydrogen-oxygen electrochemical reaction in fuel cell stack; powers electric motor; emits only water	Requires hydrogen refueling infrastructure; examples: Toyota Mirai, Hyundai Nexo

Important Clarifications:

- Hydrogen Internal Combustion Engine Vehicles (burning H_2 in modified ICE) are not classified as EVs – they lack electric propulsion and fall under alternative-fuel ICE vehicles.

- Solar-assisted EVs (e.g., Lightyear) remain BEVs with supplementary solar charging; solar input is insufficient for primary propulsion.
- Regional policy distinctions exist: In China, «New Energy Vehicles» (NEVs) officially include BEV, PHEV, EREV, and FCEV; conventional HEVs are categorized separately as energy-saving vehicles.

1.1.2. Structure and Classification Characteristics of Hydrogen Refueling Station (HRS) Infrastructure

The Hydrogen Refueling Station (HRS) serves as the critical physical node connecting the upstream hydrogen supply chain with end-user Fuel Cell Electric Vehicles (FCEVs). From the perspective of systems engineering and control theory, an HRS is not merely a fuel dispensing terminal but a complex Electrotechnical Complex integrating electrochemical reactions, non-linear thermodynamic processes, high-pressure fluid dynamics, and precision safety instrumentation systems [6]. Its engineering design must achieve an optimal balance among Process Safety, Refueling Efficiency, and Supply Chain Compatibility.As investigated by the author in previous studies [7], the internal infrastructure of an HRS heavily relies on its accumulation and storage systems. While liquid hydrogen offers high energy density, it requires energy-intensive cryogenic cooling. Therefore, high-pressure gaseous storage remains the most practical solution for modern HRS infrastructure, acting as the critical physical buffer between hydrogen production and vehicle distribution.

1. Classification Dimensions and Technical Selection

The architecture of modern HRSs exhibits high diversity, primarily determined by the hydrogen sourcing pathway, the target service vehicles (dictating pressure levels), and the station construction form. This classification (table 1.2) logic directly dictates the station's control strategy and equipment selection.

Table 1.2 – Main Classification Dimensions and Application Features of HRS

Dimension	Type	Technical Features & Application Context
Hydrogen Source	Off-site	Relies on tube trailers or liquid hydrogen tankers for transport. Suitable for early network deployment; occupies a smaller footprint due to the absence of production equipment, but OPEX is significantly impacted by logistics.
	On-site	Focus of this study. Utilizes water electrolysis or natural gas reforming. Eliminates transportation costs and fits distributed energy networks, but imposes higher demands on power grid capacity and land use.
Storage State	Gaseous Hydrogen (CGH_2)	Mainstream Technology (>90%). Characterized by technological maturity and lower costs, but suffers from low volumetric storage density and a larger physical footprint.
	Liquid Hydrogen (LH_2)	Future Trend. Utilizes cryogenic technology (-253°C). Offers high storage density, suitable for heavy-duty trucks and large-scale stations, but involves high equipment CAPEX and boil-off losses.
Refueling Pressure	35 MPa (H35)	Legacy Standard. Primarily serves commercial vehicles (buses, logistics trucks), as they accommodate larger tanks and are less sensitive to volumetric density.
	70 MPa (H70)	Modern Standard. Primarily serves passenger vehicles. High pressure enables driving ranges comparable to ICE vehicles but mandates efficient pre-cooling capabilities (-40°C) for the dispenser.
Refueling Capacity	Stationary	Permanent infrastructure with daily capacity typically >500 kg. Serves as core nodes for commercial operations, offering the highest safety and reliability.
	Skid-mounted	Modular design with daily capacity typically <500 kg. Features short deployment cycles (weeks), suitable for land-constrained areas or temporary pilot sites.
Site Integration	Dedicated Station	Dedicated solely to hydrogen refueling. Typically constructed near chemical industrial parks or within specific bus depots.
	Integrated Energy Station	Co-location of Oil-Hydrogen-Electricity. Leverages existing gas station land reserves, sharing personnel and non-process facilities, significantly reducing land acquisition hurdles and CAPEX.

2. Core Subsystem Architecture of On-site HRS

This research focuses on the On-site Water Electrolysis HRS. This system consists of five physically coupled subsystems, interacting closely through material flow (hydrogen), energy flow (electricity/heat), and information flow (control signals):

(1) Hydrogen Source Supply and Production Subsystem

- Technical Route: This research utilizes Proton Exchange Membrane (PEM) water electrolysis to produce "Green Hydrogen" from renewable energy sources.

- Key Indicators: To prevent poisoning of fuel cell catalysts (e.g., platinum), hydrogen purity must strictly adhere to the ISO 14687:2025 standard (≥ 99,97%) [8].

- Innovative Mode: Solar-powered electrolysis stations, similar to the Honda prototype, represent the emerging «Green Microgrid HRS» model, requiring control systems with extreme load-following capabilities.

(2) Deep Compression Subsystem

- Function: Serves as the energy consumption hub, boosting low-pressure hydrogen (~ 3,0 MPa) to operating pressure.

- Core Equipment: Multi-stage Diaphragm Compressor. This equipment accounts for approximately 32% of the total station investment. Although China achieved a 45% localization rate for 70 MPa units in 2024, high acquisition and maintenance costs remain industry pain points.

- Thermodynamics: Inter-stage Coolers are mandatory to remove heat from adiabatic compression and ensure efficiency.

(3) Cascade Storage Subsystem

- Tank Technology: Widely adopts Type III or Type IV high-pressure tanks. Gaseous storage accounts for over 90%, while liquid hydrogen deployment is limited due to boil-off losses.

- Safety Redundancy: Tanks must pass rigorous safety certifications, including 140 MPa overpressure tests and 800°C/30 min fire tests.

- Cascade Logic: Tanks are divided into Low (LP), Medium (MP), and High (HP) pressure banks. The control system minimizes compression work via «Cascade Filling» driven by pressure differentials.

(4) Dispensing and Thermal Management Subsystem

- Dispenser: Equipped with temperature/pressure-controlled nozzles and IR communication. Automatic shutdown is triggered upon detecting vehicle tank anomalies. Refueling takes 3-5 minutes.

- Pre-cooling: Per SAE J2601, hydrogen must be pre-cooled to -40°C (T40 category) for 70 MPa refueling to counteract the Joule-Thomson Effect[9].

(5) Control and Safety Instrumentation Subsystem

- Safety Monitoring: Integrates H_2 detectors, UV/IR flame detectors, and Emergency Shutdown (ESD) valves.

- Logic Control: Includes three-stage pressure relief and explosion-proof components. SCADA systems provide real-time monitoring.

- Research Focus: Current systems focus on safety interlocks but lack energy efficiency optimization and grid interaction, providing the entry point for the intelligent control algorithms proposed in this dissertation.

3. Global Status and Cost Structure Insights

Currently, global HRS development has entered a stage of large-scale expansion, characterized by a pattern of «Asia dominance, Europe following, and localized concentration in North America». According to the latest statistics from H2stations.org and relevant energy agencies, the cumulative number of HRSs globally exceeded 1,100 by the end of 2024[10].

- Asia-Pacific: The engine of global growth, accounting for over 60% of the total.

- China: Leads the world with 436 stations (as of Dec 2024), forming initial network effects in Guangdong and the Yangtze River Delta.

- South Korea: With strong government subsidies, operates over 170 stations, boasting one of the highest station densities globally.

- Japan: As a pioneer of the hydrogen society, maintains around 160 stations, focusing on passenger vehicle service networks.

- Europe: Approximately 270 stations. Germany is the absolute core with over 100 stations, primarily serving heavy-duty trucks and cross-border logistics.

- North America: Approximately 100 stations, with the vast majority (>80%) concentrated in California, USA, supporting local Zero-Emission Vehicle (ZEV) mandates.

However, despite the growth in numbers, widespread adoption is constrained by high costs and highly unbalanced regional distribution:

- CAPEX: Equipment costs account for over 70% of total investment [11]. A typical 500kg/35MPa stationary station costs approximately 10 million RMB (~1.4 million USD), and this cost can be even higher in Europe.

- OPEX: Electricity and labor costs constitute over 50% of operational expenses.

Conclusion: While FCEVs hold irreplaceable strategic advantages in heavy-duty and long-haul transport, the high cost of HRSs limits network density. Therefore, given that hardware costs are unlikely to drop significantly in the short term, developing efficient automated, unattended, and load-following control systems (as proposed in this research) represents a critical pathway to improving operational efficiency and reducing the Levelized Cost of Hydrogen (LCOH).

1.2. Interaction of hydrogen systems with traction networks of electric transport

The Hydrogen Refueling Station (HRS) is not merely a terminal facility supplying fuel to Fuel Cell Electric Vehicles (FCEVs); it acts as a critical hub connecting the Power Grid and the Traction Network within the macro-energy architecture. This cross-system interaction is primarily realized through the mechanism of «Sector Coupling», with the core technological pathway being «Power-to-Gas (P2G)» [12].

1.2.1. Characteristics of Electrolyzers as Flexible Grid Loads

With the increasing penetration of Variable Renewable Energy (VRE) sources such as wind and solar in the power grid, their inherent intermittency and volatility pose significant challenges to the supply-demand balance. Traditional power systems lack large-scale, long-duration energy storage means, often leading to substantial «curtailment» of renewable generation.

In this context, the water electrolyzer within an on-site HRS demonstrates superior «Demand Side Response (DSR)» capabilities[13]:

1. Controllable Load: PEM electrolyzers possess millisecond-level power regulation response speeds and can operate flexibly within a range of 0 ~ 100% of their rated power, enabling real-time tracking of fluctuating renewable energy generation curves.

2. Bidirectional Interaction:

- As a Consumer: When grid load is low or renewable energy is surplus (low electricity prices), the HRS operates at full load, converting excess electrical energy into stored hydrogen chemical energy.

- As a Service Provider: When grid load is high (high electricity prices), the HRS reduces power or even shuts down (relying on storage tank inventory to maintain refueling services), thereby alleviating grid stress and providing auxiliary services such as Peak Shaving and Frequency Regulation.

3. Time-Shifting: Through the «Power-Hydrogen-Refueling» conversion, electrical energy, which is difficult to store, is transformed into easily storable hydrogen. This realizes energy transfer across time scales (from hours to days), effectively resolving the mismatch between the demand of the electric transport traction network and the renewable energy generation curve.

1.2.2. SNW Analysis of Infrastructure Compatibility

To systematically evaluate the compatibility and operational bottlenecks of integrating hydrogen systems into the electric transport network (such as heavy-duty and aviation sectors), an SNW (Strengths, Neutrals, Weaknesses) analysis was performed by the author [14]. The analysis reveals that while the «Strengths» of hydrogen lie in its absolute zero-emission profile, critical «Weaknesses» emerge at the infrastructure level. Specifically, the high capital costs of high-pressure storage and the inefficient energy management between the power grid and the electrolyzers severely hinder system compatibility, dictating the need for operational optimization.

1. Strength

- Decarbonization Potential: Hydrogen systems provide the only viable zero-emission solution for hard-to-electrify heavy transport sectors (e.g., long-haul trucks, intercity trains), complementing the limitations of existing Battery Electric Vehicle (BEV) traction networks.

- Energy Security: Producing hydrogen from local renewable energy sources reduces the transport system's dependence on imported fossil fuels.

2. Neutral

- Utilization of Existing Assets: Existing natural gas grids can theoretically be retrofitted to transport hydrogen (blending or pure hydrogen repurposing), though this requires technical upgrades and material verification.

- Grid Capacity: Although HRSs are high-power loads, if coordinated with intelligent control strategies (such as off-peak operation proposed in this study), their occupancy of distribution grid capacity is manageable and does not impose excessive pressure for capacity expansion.

3. Weakness

- High Initial Investment (High CAPEX): Establishing an HRS network requires expensive specialized equipment (e.g., 90MPa compressors, cryogenic pre-cooling units), resulting in significantly higher initial capital expenditure compared to charging stations.

- Conversion Efficiency: The "Power-Hydrogen-Power" round-trip efficiency is approximately 30% ~ 40%, lower than the 70% ~ 80% of direct charging. This necessitates the utilization of low-cost curtailed renewable electricity to compensate for the efficiency disadvantage.

- Lack of Standardization: Current refueling protocols and interface standards are still evolving, posing challenges to infrastructure compatibility across different regions.

So, the interaction between hydrogen systems and electric transport traction networks exhibits significant complementarity. While disadvantages in efficiency and cost exist, leveraging the flexible regulation capability of electrolyzers through intelligent control strategies can significantly amplify their advantages in energy absorption and grid auxiliary services.

1.3. Overview of the problems of energy efficiency and stability of operating modes of electrolysis plants

When integrating electrolyzers into microgrids containing Renewable Energy Sources (RES) and fluctuating electric transport loads, electrolysis plants no longer operate under ideal steady-state conditions. Stochastic fluctuations in input power and frequent Start-Stop cycles lead to significant degradation in energy efficiency and equipment lifespan. This Chapter analyzes the core problems affecting the efficiency and stability of electrolysis plants from electrochemical and systems engineering perspectives.

1.3.1 Comparison of dynamic characteristics of alkaline (ALK) and proton exchange membrane (PEM) electrolysis

The two most commercially widely used hydrogen production technologies exhibit distinct dynamic response characteristics, which determine their compatibility with fluctuating power sources [15]:

1. Alkaline Electrolysis (ALK):

Thermal Inertia Limitation: ALK systems typically operate at 60 ~ 80 . Due to the use of liquid electrolyte (KOH solution), they possess high thermal capacity, resulting in cold start times of 30-60 minutes.

Narrow Dynamic Range: To prevent gas crossover (H_2 and O_2) through the porous diaphragm, which poses safety risks, the minimum operating load of ALK is typically restricted to 20% ~ 40% of the rated power.

Response Hysteresis: Its power regulation rate is relatively slow (approx. 0,2 ~ 20% P_{nom}/s), making it difficult to track millisecond-level fluctuations of wind and solar power.

2. Proton Exchange Membrane (PEM) Electrolysis ：

Fast Response: PEM utilizes a solid polymer electrolyte, offering high proton conductivity and a compact structure. Its power regulation rate can reach 100% P_{nom}/s, providing excellent grid frequency response capabilities.

Wide Operating Range: PEM can operate between 0 ~ 160% of rated load (strong short-term overload capability), with a cold start time of only 5–10 minutes.

To more intuitively demonstrate the differences between the two technologies in dynamic scenarios, table 1.3 provides a detailed comparison of key technical parameters.

Table 1.3 – Comparison of Technical Characteristics between ALK and PEM Electrolysis

Comparison Dimension	ALK	PEM
1. Technology Maturity	Mature Commercially established for >100 years; stable technology with a robust supply chain.	Early Commercial Rapid development over the last 20 years; currently transitioning from demonstration to large-scale deployment.
2. Electrolyte	Liquid High-concentration Potassium Hydroxide solution (KOH, 20-30 wt%). Corrosive, requiring periodic maintenance.	Solid Solid Polymer Electrolyte (PFSA/Nafion). Compact structure with no risk of corrosive liquid leakage.
3. Current Density	Low 0.2 ~ 0.8A/cm^2. Results in bulky stack size and a larger physical footprint.	High 1.0 ~ 3.0A/cm^2. Compact stack design; footprint reduced by ~50% compared to ALK.
4. Dynamic Response Rate	Slow < 20% P_{nom}/s. Limited by the thermal inertia of the liquid electrolyte and bubble management issues.	Very Fast ~ 100\% P_{nom}/s (millisecond level). Ideal for tracking rapid fluctuations in wind and solar power.
5. Operating Load Range	Narrow 20% ~ 100%. Gas crossover at low loads poses explosion risks, limiting deep peak-shaving capabilities.	Wide 0% ~ 160%.Supports short-term overload and can maintain standby at near-zero load without crossover risks.
6. Cold Start Time	Long 30 ~ 60 minutes. Requires preheating the large volume of electrolyte to operating temperature.	Short 5 ~ 10 minutes. Capable of rapid Black Start.

Continuation of the tabl. 1.3

7. Gas Purity (Raw)	Lower Requires deoxygenation and drying; product gas often contains alkali mist.	High Direct output is high purity; requires only simple drying to reach >99.99%.
8. Output Pressure	Low < 30 bar (often atmospheric). Requires energy-intensive mechanical compressors downstream.	High 30 ~ 80 bar. Electrochemical compression reduces the energy consumption of downstream mechanical compression.
9. Materials & Cost	Low Cost Utilizes non-precious metal catalysts (Ni, Co, Fe). Lower CAPEX.	High Cost Relies on precious metal catalysts (Pt, Ir) and Ti bipolar plates. Higher CAPEX, though decreasing with scale.
10. Application Scenario	Stable Load Suitable for grid-connected hydrogen production or steady industrial supply (e.g., ammonia synthesis).	Fluctuating Load Suitable for distributed energy microgrids, Hydrogen Refueling Stations (HRS), and RES integration.

Selecting the appropriate water electrolysis technology is fundamental to the energy efficiency of the HRS. Based on the comprehensive comparative analysis conducted by the author in [7], there is a stark contrast between traditional Alkaline (ALK) and Proton Exchange Membrane (PEM) electrolyzers, as clearly demonstrated in Table 1.3. While ALK is a mature technology that currently holds advantages in capital cost and stack lifespan, its slow dynamic response and narrow operating range make it fundamentally unsuitable for highly stochastic renewable energy inputs. In contrast, PEM electrolyzers possess overwhelming advantages, exhibiting a wide dynamic load range (0-160%), millisecond-level response times, and significantly faster cold starts. Therefore, for the specific scenario focused on in this research – Hydrogen Refueling Stations powered by fluctuating renewable energy – PEM technology is the indisputable optimal choice. Its superior capabilities allow the modern electrotechnical complex to effectively execute «load-following» strategies and provide rapid frequency response for grid auxiliary services.

1.3.2 Degradation mechanisms of Membrane Electrode Assemblies (MEA) under fluctuating loads

Although PEM is suitable for dynamic operation, prolonged exposure to fluctuating conditions accelerates the physical and chemical aging of its core component—the Membrane Electrode Assembly (MEA)[16]. The primary degradation mechanisms include:

1. Frequent Start-Stop Cycles：

This is the most damaging operating condition. When the electrolyzer switches from operation to Open Circuit Voltage (OCV), drastic potential changes at the anode cause dissolution and redeposition of the catalyst layer (typically IrO_2), leading to permanent loss of Electrochemical Active Surface Area (ECSA).

2. Low Load & Gas Crossover

At low current densities, the gas production rate decreases, while the gas permeation rate through the membrane remains relatively constant. This causes a sharp increase in impurity concentrations in the product gas (i.e., higher O_2 in H_2), forcing a safety shutdown if the explosion limit (4%) is exceeded, thereby triggering additional start-stop penalties.

3. Mechanical Stress

Rapid power fluctuations induce alternating cycles of temperature and pressure, causing expansion and contraction of the membrane. Long-term mechanical fatigue leads to membrane thinning or even pinholes, ultimately resulting in stack failure.

1.3.3 Energy efficiency characteristics and the "Efficiency-Stability" trade-off

Electrolyzer efficiency is not determined by a single parameter but exhibits highly non-linear characteristics.

1. Polarization Curve Analysis

The relationship between cell voltage V_{cell} and current density i follows the polarization curve[17]:

$$V_{cell} = V_{rev} + \eta_{act} + \eta_{ohm} + \eta_{diff} \quad (1.1)$$

Where η_{act} is activation overpotential, η_{ohm} is ohmic overpotential, and η_{diff} is diffusion overpotential.

Efficiency Paradox: In the low current density region, although ohmic losses are low, parasitic power consumption (BOP systems, e.g., pumps and fans) dominates, resulting in low system efficiency; in the high current density region, ohmic overpotential increases significantly, causing a sharp drop in stack efficiency. Therefore, an «Optimal Efficiency Range» exists.

2. The Control Dilemma

To extend lifespan, the system tends towards stable operation (reducing $\Delta P/\Delta t$); to absorb renewable energy and respond to refueling demand, the system requires flexible operation.

Traditional control strategies (such as simple hysteresis or PID) cannot resolve the coupled contradictions among «fluctuating input, non-linear efficiency, and lifespan constraints». This creates an urgent need to introduce advanced control strategies based on Model Predictive Control and Artificial Intelligence (AI) to optimize performance under multiple constraints.

1.4. Justification of the need for intelligent control methods

The Hydrogen Refueling Station (HRS), serving as a «dual-stochastic system» connecting the random renewable energy supply side and the random transport demand side, presents an operational optimization problem that is inherently a multi-objective, strongly constrained, and non-linear dynamic programming problem. Traditional deterministic control methods can no longer adapt to the complexity of modern energy systems. This Chapter first employs the PEST model to analyze external drivers, then deeply dissects the limitations of traditional control strategies, thereby establishing the necessity of transitioning to active predictive control.

1.4.1 External environment evaluation based on PEST analysis

The transition towards a hydrogen-based electric transport system is deeply influenced by macro-environmental factors. According to the PEST analysis published by the author [14], Political and Social dimensions strongly support hydrogen deployment through global decarbonization mandates. However, the Economic and Technological domains present formidable barriers. The high levelized cost of hydrogen production and the efficiency-lifespan conflict of electrolyzers under fluctuating grid tariffs require a paradigm shift. Overcoming these external and internal barriers cannot rely solely on physical infrastructure expansion; it fundamentally justifies the necessity of developing an intelligent control methodology.

1. Political

Global «Carbon Neutrality» policies mandate that HRS must maximize the absorption of local green electricity. This implies that the control system must possess «Source-Load Coordination» capabilities to respond to grid dispatch instructions.

2. Economic

Time-of-Use (TOU) and Real-Time Pricing (RTP) mechanisms in electricity markets are becoming prevalent. To reduce the Levelized Cost of Hydrogen (LCOH), the control system must possess «Price Sensitivity», capable of automatically storing energy during low-price periods and shedding load during high-price periods.

3. Social

End-users have extremely high expectations for Quality of Service (QoS). A «Fuel Starvation» event would severely damage public confidence in FCEVs. Therefore, the system must possess «Demand Prediction» capabilities to ensure a safety margin in storage tanks at all times.

4. Technological

The development of Industrial IoT (IIoT) and Deep Learning makes it possible to collect massive historical data and train high-precision prediction models (e.g., LSTM). The maturity of technology supply provides the physical basis for the implementation of intelligent control.

1.4.2 The necessity of transition from «Passive Hysteresis Control» to «Active Predictive Control»

Current hydrogen refueling stations universally adopt the classical Hysteresis Control (On-Off Control) strategy. Its logic is based on real-time feedback of tank pressure: start the electrolyzer when pressure drops below $P_{\min}$, and stop when it exceeds $P_{\max}$.

This «Rule-based» passive strategy suffers from three core deficiencies:

1. Lag and Blindness: Traditional controllers «only see the present, not the future». They do not know that a bus will arrive in 10 minutes, nor that electricity prices will double in an hour. This Information Blind Spot renders the system unable to pre-stock hydrogen or avoid high electricity prices.

2. Lifespan Reduction due to Frequent Start-Stops: As discussed in Section 1.3, facing stochastic vehicle loads, hysteresis control forces the electrolyzer to frequently cross the P_{min} threshold, causing drastic power fluctuations and start-stop cycles. This not only accelerates MEA degradation but also wastes significant hydrogen and electricity due to repeated system purging.

3. Lack of Global Optimization Capability: PID or logic control can only ensure the stability of local physical quantities (e.g., pressure, temperature); they cannot integrate conflicting objectives such as «equipment lifespan», «operating cost», and «grid stability» into a single optimization function for trade-off analysis.

To resolve the aforementioned issues, intelligent control methods must be introduced. By incorporating Long Short-Term Memory (LSTM) networks for precise time-series prediction of hydrogen demand and renewable energy, combined with optimization algorithms, the system can transform from «post-event response» to «Look-ahead Planning» [18]. This is not only a requirement for technological upgrading but also the only path to achieving the economic viability and environmental friendliness of HRS.

Summary by Chapter

This chapter provides a systematic literature review and engineering characteristic analysis of Hydrogen Refueling Station (HRS) infrastructure within the modern electric transport system, covering levels from macro-energy network interaction to micro-electrolysis equipment operation mechanisms. Through in-depth analysis of existing technological bottlenecks and operational challenges, the following key conclusions are drawn, laying the theoretical foundation for the research objectives and technical roadmap of this dissertation:

1. Strategic Status of HRS as a Key Energy Hub

With the deepening of transport electrification, Fuel Cell Electric Vehicles (FCEVs) have been established as the only viable path for decarbonizing heavy-duty long-haul transport. On-site hydrogen production HRS not only resolves high hydrogen transportation costs but also realizes deep sector coupling between transport and power grids through «Power-to-Gas (P2G)» technology.

2. Superiority of PEM Electrolyzers as Core Control Objects

Comparative analysis demonstrates that Proton Exchange Membrane (PEM) electrolyzers significantly outperform traditional Alkaline Electrolysis (ALK) in dynamic response rate (~100% P_{nom}/s), wide operating load range (0~160%), and cold start time (5~10min). This makes them the optimal physical carrier for absorbing fluctuating renewable energy and adapting to stochastic refueling demands.

3. Limitations of Traditional Control Strategies and the Efficiency-Lifespan Conflict

Existing Hysteresis Control strategies exhibit significant lag and blindness when facing highly stochastic inputs (renewable energy) and outputs (vehicle loads). Frequent start-stop cycles not only lead to severe Membrane Electrode Assembly (MEA) degradation but also cause energy waste due to repeated purging, failing to achieve an optimal balance between «system efficiency» and «equipment lifespan».

4. Necessity of Introducing Intelligent Predictive Control

PEST analysis reveals that to respond to grid Time-of-Use pricing mechanisms and guarantee Quality of Service (QoS), the control system must possess «Look-ahead Planning» capabilities. Utilizing deep learning (e.g., LSTM) for precise prediction of hydrogen demand and energy supply, combined with multi-objective optimization based on predictive information, is the inevitable path to resolving the aforementioned conflicts.

CHAPTER 2.

MULTI-SCALE MODELING OF FCEV HYDROGEN CONSUMPTION AND STOCHASTIC REFUELING DEMAND PREDICTION

With the deepening process of transport electrification, Fuel Cell Electric Vehicles (FCEVs) have established themselves as a key pathway for the decarbonization of transport, owing to their advantages of long driving range, fast refueling, and zero emissions [19]. As the energy hub connecting the upstream hydrogen supply side and the downstream vehicle demand side, the operational efficiency of the Hydrogen Refueling Station (HRS) directly impacts the economic viability and reliability of the hydrogen transport network. In research concerning the optimal control of HRS, the Refueling Load serves not only as the service object of the system but also as the external disturbance input characterized by the highest degree of stochasticity and fluctuation. Therefore, establishing a high-fidelity and physically interpretable refueling load prediction model is a prerequisite for achieving «source-load» collaborative control of the HRS.

However, existing research on HRS load prediction often suffers from oversimplification of physical models. Traditional methods mostly focus on statistical laws at the macro level, such as using Non-homogeneous Poisson Processes to simulate the random arrival times of vehicles, while the actual refueling demand per vehicle is often assumed to be a fixed constant or a simple normal distribution [20]. This approach neglects the profound physical coupling mechanisms within the «Vehicle-Road-Station» system:

1. Vehicle Side (Micro-scale): The hydrogen consumption rate of an FCEV is not a fixed value but depends on the parameter matching of the powertrain (such as the power distribution between the fuel cell and the battery) and the energy management strategy[21].

2. Road Side (Meso-scale): Actual road traffic conditions (e.g., congestion, traffic light stops) and terrain features significantly alter the driving energy consumption of the vehicle, thereby determining the residual pressure (Initial Pressure, P_0) when the vehicle enters the station [22].

3. Interface Side (Micro-physics): Under high-pressure refueling conditions (70 MPa), hydrogen exhibits significant Real Gas Effects, and the assumption of ideal gas behavior leads to considerable errors in the calculation of refueling mass [23].

The absence of these physical details prevents traditional load prediction models from reflecting demand fluctuations in real-world scenarios, thereby limiting the robustness of subsequent control strategies.

To overcome the limitations of existing studies, this chapter aims to establish a «Multi-scale» framework for FCEV hydrogen consumption modeling and stochastic refueling demand prediction. This framework breaks the single-dimension prediction mode and systematically deconstructs the formation mechanism of the refueling load from the following three physical scales:

- Micro-scale: Powertrain Parameter Matching and Baseline Energy Consumption. Based on vehicle longitudinal dynamics, multi-objective optimization algorithms are utilized to match the key powertrain components of the FCEV, establishing the «Theoretical Baseline Hydrogen Consumption» under standard driving cycles. This part of the work is based on the author's previous research results on complex powertrain parameter matching and longitudinal dynamics simulation [24], providing rigorously validated physical underlying data for the subsequent load prediction.

- Meso-scale: Dynamic Condition Correction Considering V2X. Introducing Vehicle-to-Everything (V2X) and intelligent traffic information, the impact of real traffic flow on baseline hydrogen consumption is analyzed to accurately deduce the distribution of residual hydrogen storage states when vehicles enter the station [25].

- Interface-scale: Refueling Thermodynamics Based on Real Gas Equation of State. A compressibility factor correction model based on NIST data is introduced to establish the refueling mass conservation equation considering thermodynamic constraints, precisely calculating the actual refueling mass (Δm) and quantifying its sensitivity characteristics to initial state fluctuations [26].

Through the organic integration of the aforementioned multi-scale models, this chapter will ultimately generate an HRS stochastic refueling load profile containing both temporal distribution and quantitative distribution characteristics. This not only quantifies the contribution of vehicle optimization and intelligent traffic technologies to reducing HRS operational pressure but also provides a high-precision System Disturbance Model for the intelligent control strategies in the subsequent chapters of this dissertation.

2.1 Micro-scale: FCEV Powertrain Topology and Parameter Matching Optimization

In the multi-scale framework of HRS load prediction, the Micro-scale modeling focuses on the physical attributes of individual vehicles. The powertrain configuration and parameter matching of Fuel Cell Electric Vehicles (FCEVs) directly determine their energy conversion efficiency and hydrogen consumption rate. To ensure the physical fidelity of the load prediction model, this Chapter establishes the power demand model based on vehicle longitudinal dynamics and configures the powertrain parameters based on a commercial benchmark vehicle (Toyota Mirai II). This establishes the Baseline Hydrogen Consumption Characteristics under standard driving cycles, serving as the physical foundation for the subsequent meso-scale and interface-scale modeling. As successfully demonstrated in the author's previous study [24], establishing a robust longitudinal dynamics model is crucial for quantifying a vehicle's instantaneous energy consumption. In that prior work, a comprehensive powertrain parameter matching framework was developed, proving the effectiveness of combining Orthogonal Experimental Designs with advanced vehicle simulation platforms to optimize multi-source energy distribution. By adapting the established longitudinal dynamics equations and drawing upon the proven simulation methodology from this prior research, this Chapter extends the vehicle-side energy consumption modeling from Hybrid Electric Vehicles (HEVs) to Fuel Cell Electric Vehicles (FCEVs).

2.2.1 Powertrain Topology and Longitudinal Dynamics Modeling

This study investigates a «Fuel Cell Dominant» hybrid configuration, which is the mainstream topology for commercial FCEVs[2]. The system adopts an electric-electric hybrid mode, where the Proton Exchange Membrane Fuel Cell (PEMFC) serves as the Primary Power Source, responsible for providing the continuous drive power; while the high-rate Lithium-ion Battery (Cell) acts as the Auxiliary Energy Source (specifically, a «Power Buffer»), responsible for recovering braking energy and mitigating high-frequency power fluctuations.

The topology of the vehicle powertrain system is illustrated in fig. 2.1. Hydrogen is supplied from high-pressure tanks to the fuel cell stack. The generated electricity is regulated by a DC/DC boost converter to match the high-voltage bus, coupling with the battery pack to drive the traction motor, which ultimately propels the wheels.

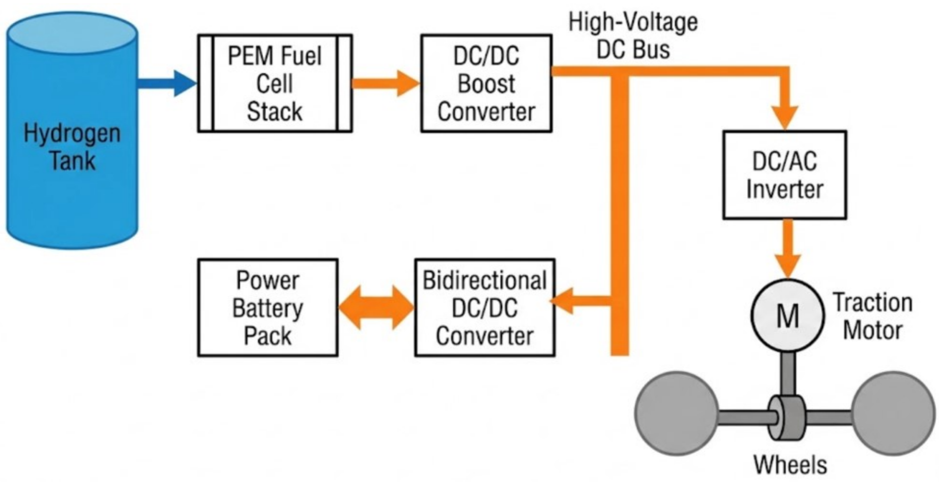

Figure. 2.1 – Topology of FCEV Powertrain System

To accurately quantify the real-time power demand (P_{req}) during vehicle operation, the vehicle longitudinal dynamics equation is established based on the balance of forces, consistent with the proven methodology applied in the author's previous simulation studies [24] and fundamental vehicle propulsion theories [27]:

$$P_{\mathrm{req}}=\frac{v}{1000\eta_{\mathrm{t}}}\left(\mathrm{Mg}f\cos\alpha+\mathrm{Mg}\sin\alpha+\frac{1}{2}C_{\mathrm{D}}A\rho\mathrm{v}^{2}+\delta M\frac{dv}{dt}\right) \quad (2.1)$$

Where:

P_{req}: Traction power demand at the motor shaft (kW).

v: Vehicle velocity (m/s).

M: Vehicle gross mass (kg).

g: Gravitational acceleration ($9.81 m/s^2$).

f: Rolling resistance coefficient.

α: Road slope angle (rad).

C_{D}: Aerodynamic drag coefficient.

A: Frontal area (m^2).

ρ: Air density ($1.225 kg/m^3$).

δ: Rotating mass conversion coefficient (set to 1.04).

η_{t}: Mechanical transmission efficiency (set to 0,93).

This physical model establishes a deterministic mapping between the driving cycle (velocity profile) and the energy demand.

2.2.2 Energy Management Strategy and Operational Modes

Based on the proposed topology, a Power Following Strategy is adopted. The core control logic is to utilize the fuel cell stack to meet the average power demand, ensuring it operates in high-efficiency regions, while using the battery to handle transient power shocks. The system primarily operates in three typical modes (as shown in fig. 2.2):

1. Steady-state Cruising Mode: When the vehicle travels at a constant speed, the power demand is stable. The fuel cell stack drives the motor directly. The battery remains in a Standby state to avoid unnecessary charge/discharge cycles and extend its lifespan.

2. Transient Acceleration Mode: During rapid acceleration or climbing, power demand surges instantaneously. Due to the dynamic response hysteresis of the fuel cell's air supply system, the battery instantly discharges to perform "Peak Shaving", compensating for the transient power gap.

3. Regenerative Braking Mode: During deceleration, the traction motor operates as a generator, converting vehicle kinetic energy into electricity to recharge the battery. This recovered energy is stored for the next acceleration event.

4.

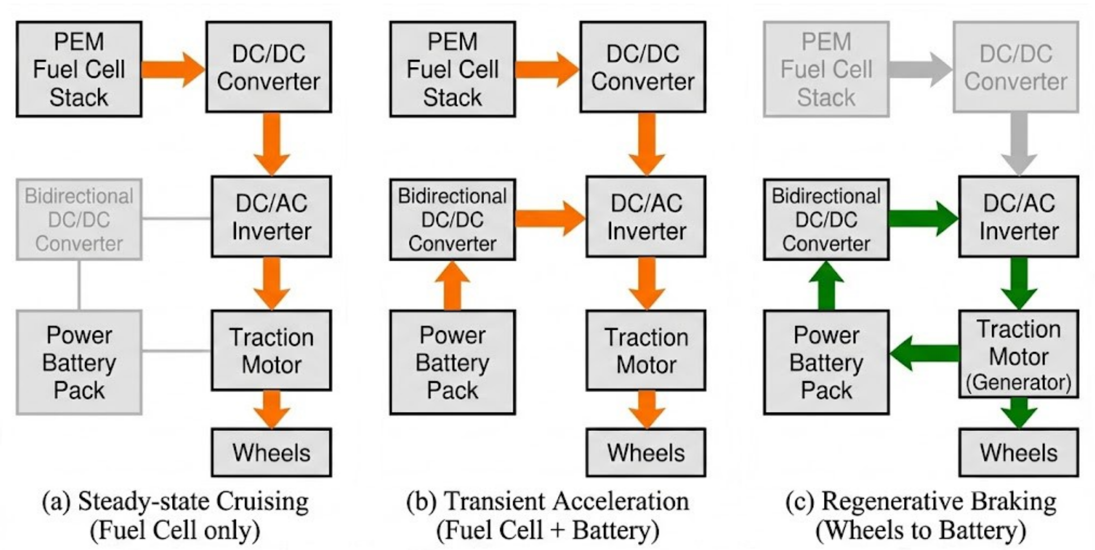

Figure 2.2 – Energy Flow Diagrams (Cruising, Acceleration, Regenerative Braking)

2.2.3 Powertrain Parameter Configuration based on Benchmark Vehicle

To ensure the engineering validity of the simulation model, the key powertrain parameters are configured based on the technical specifications of the Toyota Mirai II[28]. A distinctive feature of this configuration is the precise power matching between the fuel cell stack and the traction motor. The specific parameters are listed in table 2.1.

Table 2.1 – Key Parameters of the Target FCEV Model

Parameter	Symbol	Value	Unit	Description
Vehicle Curb Mass	M	1900	kg	Includes 3-tank H_2 system
Fuel Cell Rated Power	P_{fc}	128	kW	Primary Power Source
Traction Motor Peak Power	P_{mot}	134	kW	Max Output (182 Ps)
Power Battery Capacity	E_{bat}	1,24	kWh	High-rate Li-ion Power Buffer
Hydrogen Tank Capacity	M_{H2}	5,6	kg	Nominal @ 70 MPa
Aerodynamic Drag Coefficient	C_D	0,29	-	Streamlined body design
Frontal Area	A	2,8	m^2	Mid-size sedan standard
Rolling Resistance Coefficient	f	0,0085	-	Low rolling resistance tires
WLTC Range	R	650	km	Consumption ~0,86 kg/100km

2.2.4 Validation of Power Demand under Typical Scenarios

To validate the rationality of the parameter matching and the feasibility of the proposed topology, this study quantitatively calculates the power demand under three critical operating scenarios based on Eq. (2.1). The revised calculation results confirm the system's robustness.

1. Steady-state Cruising Verification (High Efficiency)

- Condition: Velocity v=100 km/h, Acceleration a = 0, Slope α = 0.

- Calculation: Substituting the parameters (M=1900, f = 0,0085, C_D = 0,29) into Eq. (2.1):

$$P_{cruise}=\frac{1}{0.93}\left(\frac{1900\cdot 9.81\cdot 0.0085\cdot 100}{3600}+\frac{0.29\cdot 2.8\cdot 100^3}{76140}\right)\approx 48{,}2\mathrm{kw} \tag{2.1}$$

- Analysis: The cruising power (48.2 kW) occupies approximately 37.6% of the fuel cell's rated power (128 kW). This ensures that the fuel cell operates in its high-efficiency region during highway driving, minimizing hydrogen consumption.

2. Peak Acceleration Verification (Critical Boundary Check)

- Condition: 0-100 km/h acceleration in 9,2s. Average acceleration $a \approx 2.99 \mathrm{m/s^2}$ (calculated at mean speed $v = 50$ km/h).

- Calculation: Considering the rotating mass factor $\delta = 1.04$:

$$P_{peak}=\frac{1}{0{,}93}\left(P_{road\_load}+\frac{1.04\cdot 1900\cdot 50\cdot 2.99}{3600}\right)\approx 126{,}5\ \mathrm{kW}$$

- Core Conclusion: The calculation shows that P_{peak}（126,5 kW）< P_{fc_rated} (128 kW). The result is significant: the peak demand is just within the capability of the fuel cell stack, with a tight margin of only 1,5 kW. This validates the «Fuel Cell Dominant» topology but simultaneously highlights the critical necessity of the battery buffer. Any additional load (e.g., air conditioning or steeper gradient during acceleration) would immediately require battery assistance, fully justifying the hybrid configuration logic.

3. Maximum Climbing Verification (Safety)

- Condition: Velocity v = 30 km/h, Slope 35% (≈19,3°).

- Calculation:

$$P_{\text{climb}} \approx 69{,}3\text{kW}$$

- Analysis: The power demand for extreme climbing corresponds to a 54,1% load of the fuel cell stack. This provides a sufficient safety margin to prevent power interruption under complex terrain conditions.

Through theoretical calculation and verification against real vehicle parameters, this Chapter establishes the physical baseline model of the FCEV. The results demonstrate that the powertrain system based on Mirai II parameters is physically robust and energy-efficient, providing a reliable baseline for the dynamic correction in the subsequent Meso-scale analysis.

2.3 Meso-scale: Dynamic Energy Consumption Analysis considering V2X Information

While Section 2.2 establishes the baseline physical model of the FCEV under ideal conditions, the actual hydrogen consumption in real-world driving is highly stochastic, influenced by traffic flow, road geometry, and driver behavior. To improve the prediction accuracy of the vehicle's state upon arrival at the station, this section introduces the Meso-scale analysis. Specifically, it quantifies the impact of Vehicle-to-Infrastructure (V2I) communication on energy conservation, which directly alters the distribution of the initial tank pressure (P_0).

2.3.1 Traffic and Terrain Correction Factors

In real-world urban driving, frequent acceleration and deceleration significantly increase energy demand compared to standard cycles (e.g., WLTC). The actual hydrogen consumption rate $\dot{m}_{H2}$ is corrected by introducing dynamic coefficients [29]:

$$\dot{m}_{\text{real}} = \dot{m}_{\text{base}} \cdot (1+\beta_{\text{traffic}}+\beta_{\text{road}}) \tag{2.2}$$

Where:

$\dot{m}_{\text{base}}$: Baseline consumption rate derived from the Section 2.2 model.

β_{traffic}: Traffic congestion coefficient, representing the additional energy cost of «Stop-and-Go» waves.

β_{road}: Road gradient coefficient, accounting for the gravitational work on non-flat terrains.

2.3.2 Energy Saving Potential of V2I Speed Guidance Strategy

With the advancement of Intelligent Transportation Systems (ITS), V2I communication allows vehicles to obtain signal phase and timing (SPAT) information in advance. This enables the Green Light Optimal Speed Advisory (GLOSA) strategy, which smooths the velocity trajectory to minimize unnecessary braking [30].

To quantify this benefit, a comparative numerical simulation was conducted based on the vehicle parameters defined in table 2.1.

1. Simulation Scenario Definition

The simulation is defined as a fixed-distance scenario of 1000 m crossing a signalized intersection.

- Baseline Scenario (Human Driver): Represents a typical aggressive driving style. The vehicle cruises at the speed limit (60 km/h), brakes late upon encountering a red light, waits for a complete signal cycle (20 s), and accelerates aggressively to merge into traffic.

- V2I Scenario (GLOSA Strategy): The vehicle utilizes V2I data to plan an optimal velocity profile. It decelerates early to coast through the intersection exactly when the light turns green, avoiding a complete stop.

2. Analysis of Simulation Results

The comparative results of vehicle kinematics and power demand are presented in fig. 2.3.

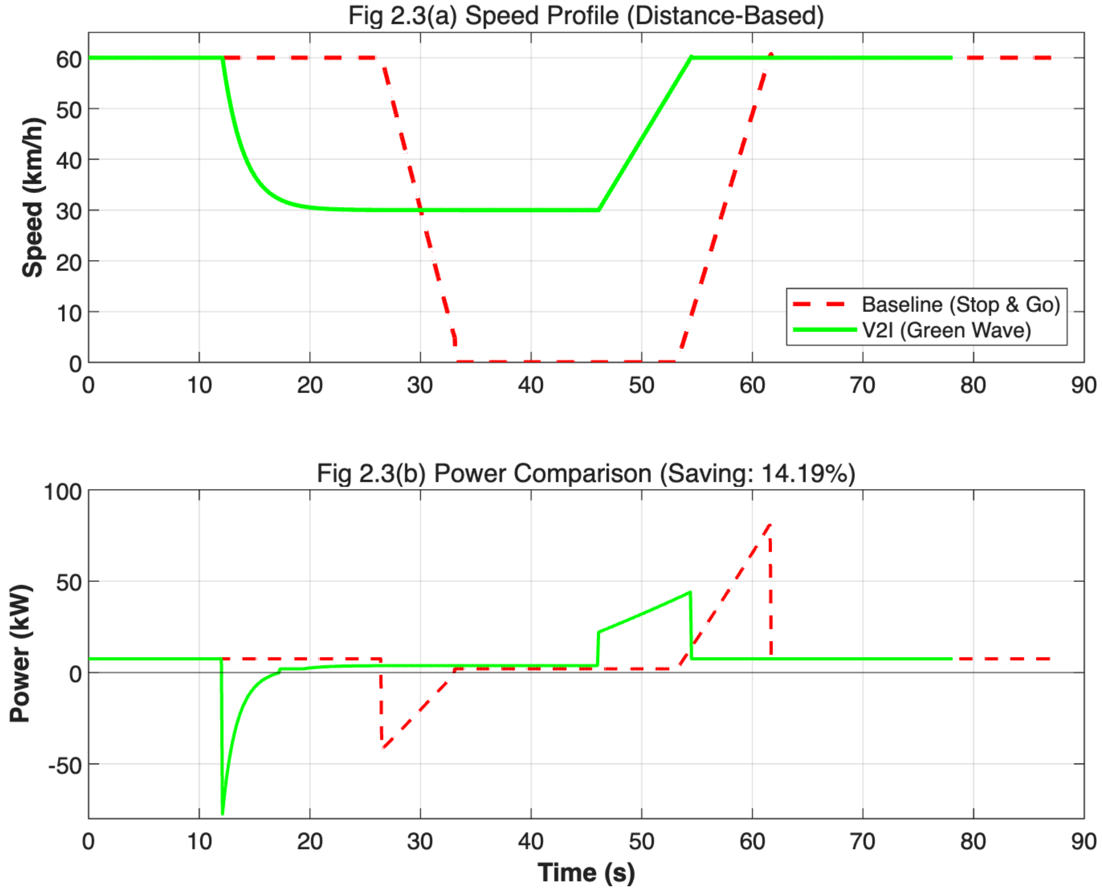

Fig. 2.3 – Comparative Simulation Results (Speed Profile & Power Demand)

- Kinematic Analysis (fig. 2.3, *a*): The Baseline vehicle (Red dashed line) experiences a complete cessation of motion ($v = 0$) for 20 seconds. In contrast, the V2I vehicle (Green solid line) maintains a non-zero velocity (min 30 km/h) throughout the process. By avoiding the «start-from-stop» maneuver, the V2I strategy significantly preserves the vehicle's kinetic energy.
- Power Demand Analysis (fig. 2.3, *b*):

- Peak Power Reduction: The Baseline vehicle requires a peak power output of over 80 kW to re-accelerate the 1900 kg mass from a standstill. The V2I vehicle, utilizing its momentum, reduces this peak demand drastically.

- Regenerative Braking Verification: It is observed that the power demand exhibits significant negative values (e.g., -80 kW at $t \approx$ 12s) during deceleration. This confirms the activation of the Regenerative Braking System modeled in Section 2.2, where the traction motor acts as a generator to recover kinetic energy into the battery buffer.

3. Quantitative Energy Saving

The simulation integrates the instantaneous power over the fixed 1000 *m* distance. The results are as follows:

- Baseline Energy Consumption: 635,58 kJ
- V2I Energy Consumption: 545,40 kJ
- Energy Saving Rate: 14,19%

This finding indicates that under connected traffic environments, FCEVs will consume significantly less hydrogen for the same trip, leading to a higher remaining State of Charge (SOC) upon arrival at the refueling station.

2.3.3 Modeling the Distribution of Initial Pressure (P_0)

The initial pressure (P_0) of the vehicle's hydrogen tank at the start of refueling is a critical boundary condition for the thermodynamic process in Section 2.4. Based on the energy consumption analysis, P_0 is modeled as a stochastic variable rather than a fixed value [31].

The distribution parameters are derived from two physical constraints:

1. Mean Value (μ_{P0}= 6,6 MPa): This value is calibrated based on the typical refueling behavior of FCEV users, corresponding to the «Low Fuel Level» warning threshold (approx. 9,4% SOC) of the 70 MPa storage system.

2.Coefficient of Variation ($CV = 31,19\%$): This high dispersion reflects the «Magnification Effect» of consumption variance on residual mass. While the V2I strategy reduces energy consumption by 14.19%, this saving disproportionately increases the remaining margin in the tank (e.g., doubling the residual pressure from 3 MPa to 6 MPa), leading to a wide statistical distribution in the boundary condition.

Therefore, P_0 is defined as a truncated normal distribution $N(6.6, 2.05^2)$ MPa, serving as the mass flow inlet boundary for the station-level simulation.

This section bridged the gap between the ideal vehicle physics (Micro-scale) and the real-world operational environment. The derived distribution of P_0 serves as the mass flow inlet boundary condition for the Interface-scale thermodynamic model in Section 2.4.

2.4 Interface-scale: Thermodynamic Modeling of the Hydrogen Refueling Process

Following the Meso-scale analysis, which quantified the stochastic impact of traffic conditions on the vehicle's arrival state (P_0), the Interface-scale modeling focuses on the thermodynamic behavior during the hydrogen transfer process from the dispenser nozzle to the on-board storage cylinder. The coupling of mass flow and heat transfer within the high-pressure system determines the actual refueling quantity and the instantaneous demand load. This section establishes the mass balance and real gas state equations to precisely calculate the single-vehicle refueling demand (Δm).

2.4.1 Real Gas Equation of State (EOS)

The on-board storage system of the target FCEV (Toyota Mirai II) operates at a nominal pressure of 70 MPa. Under such high-pressure conditions, hydrogen gas exhibits significant deviation from ideal gas behavior due to intermolecular repulsive forces and the non-negligible volume of gas molecules[23]. Using the ideal gas law would lead to substantial errors in mass estimation. Therefore, a Real Gas Equation of State is adopted to ensure physical fidelity:

$$PV = ZmRT \tag{2.3}$$

Where:

P: Absolute pressure inside the cylinder (Pa)

V: Internal water volume of the cylinder (m^3)

m: Mass of hydrogen gas (kg)

R: Specific gas constant for hydrogen (4214 J/(kg·K))

T: Gas temperature (K)

Z: Compressibility factor (dimensionless)

Compressibility Factor (Z) Model: Based on the NIST Reference Fluid Thermodynamic and Transport Properties Database (REFPROP), a polynomial fitting model is established for hydrogen gas within the operating range of interest (Pressure: 1–100 MPa, Temperature: 173–373 K)[26]. The mathematical expression for Z is derived as:

$$Z(P,T)=1+\sum_{i=1}^{n} a_i \left(\frac{P}{T}\right)^i \approx 1+1.8922\times10^{-6}\cdot\frac{P}{T} \tag{2.4}$$

This model corrects the density deviation. For instance, at 70 MPa and 340 K, calculation yields $Z \approx 1{,}3896$, indicating that the gas is significantly less compressible than an ideal gas (Z=1).

2.4.2 Mass Balance and Actual Filling Quantity Calculation

The refueling process is modeled as a thermodynamic transition from the Initial State (0) upon arrival to the Cut-off State (c) at the end of dispensing. The mass stored in the cylinder is a function of the thermodynamic state variables (P, T).As established in the classical thermodynamic modeling of hydrogen refueling [32], the lumped-parameter mass balance equations are formulated as follows:

1. Initial State Calculation

The initial hydrogen mass (m_0) remaining in the tank is determined by the arrival pressure (P_0) and the ambient temperature (T_0):

$$m_0 = \frac{P_0 V}{Z(\mathrm{P}_0,\mathrm{T}_0)\mathrm{RT}_0} \tag{2.5}$$

2. Final State Calculation

The final hydrogen mass (m_c) is determined by the target cut-off pressure (P_c) and the final gas temperature (T_c). It is critical to note that Tc is typically higher than the ambient temperature due to the heat of compression and the Joule-Thomson effect [33]:

$$m_c = \frac{P_c V}{Z(P_c,T_c)RT_c} \tag{2.6}$$

3. Actual Filling Quantity (Δm)

The net mass transferred from the station to the vehicle, defined as the Actual Filling Quantity, is the difference between the final and initial mass. This value represents the actual load demand imposed on the station's storage system [32]:

$$\Delta m = m_c - m_0 \quad (2.7)$$

2.4.3 Simulation Parameters and Boundary Conditions

To ensure consistency across the multi-scale framework, the geometric parameters are strictly aligned with the Toyota Mirai II specifications defined in Section 2.2. The thermodynamic boundary conditions, specifically the initial pressure (P_0), are adopted from the statistical distribution derived in the Meso-scale analysis (Section 2.3). The key parameters used for the calculation are listed in table 2.2.

Table 2.2 – Thermodynamic Calculation Parameters and Boundary Conditions

Parameter Name	Parameter Value	Unit	Selection Basis
Volume of On-board Hydrogen Storage Tank (V)	0,1422	m^3	Commercial 142.2L Type III hydrogen storage bottle
Initial temperature (T_0)	298	K	Ambient temperature reference value
Final temperature (T_c)	340	K	Temperature rise due to the Joule-Thomson effect
Initial pressure range (P_0)	3×10^6~10×10^6	Pa	Actual hydrogen refueling station survey data
Final pressure (P_c)	70×10^6	Pa	70MPa high-pressure hydrogen storage system standard
Hydrogen gas constant (R)	4214	J/(kg·K)	Hydrogen thermodynamic characteristic parameter

2.4.4 Stochastic Analysis of Refueling Demand

To quantify the impact of the stochastic arrival pressure on the station load, a Monte Carlo simulation was conducted, a robust methodology widely adopted in recent literature for forecasting spatial-temporal hydrogen refueling demand [34].

1. Sample Generation

Based on the truncated normal distribution model $P_0 \sim N(66, 2.05^2)$ derived in Section 2.3, 100 sample points of initial pressure were generated to ensure the physical fidelity of the input conditions. The distribution of these samples is shown in fig. 2.4.

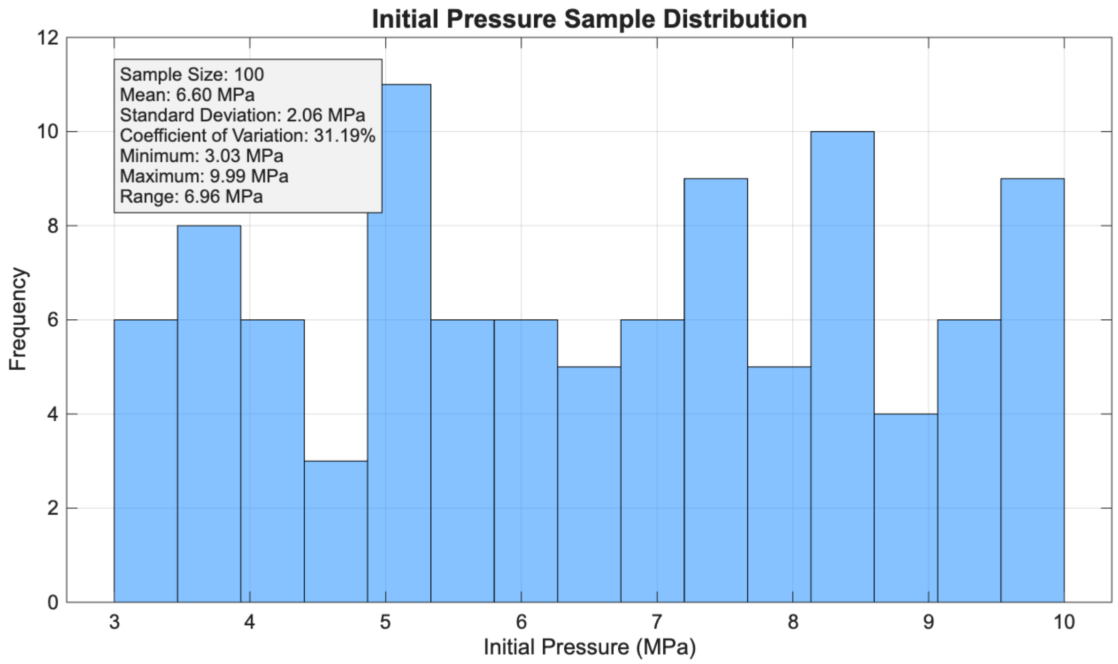

Fig. 2.4 – Probability Distribution of Initial Tank Pressure (P_0) of 100 Sampled FCEVs

2. Thermodynamic Response Analysis

The simulation results reveal the non-linear thermodynamic characteristics of high-pressure hydrogen refueling. As the initial pressure P_0 increases across the sample set, the initial compressibility factor Z0 exhibits a non-linear increasing trend (Fig. 2.5), confirming the necessity of using the Real Gas EOS for high-pressure corrections.

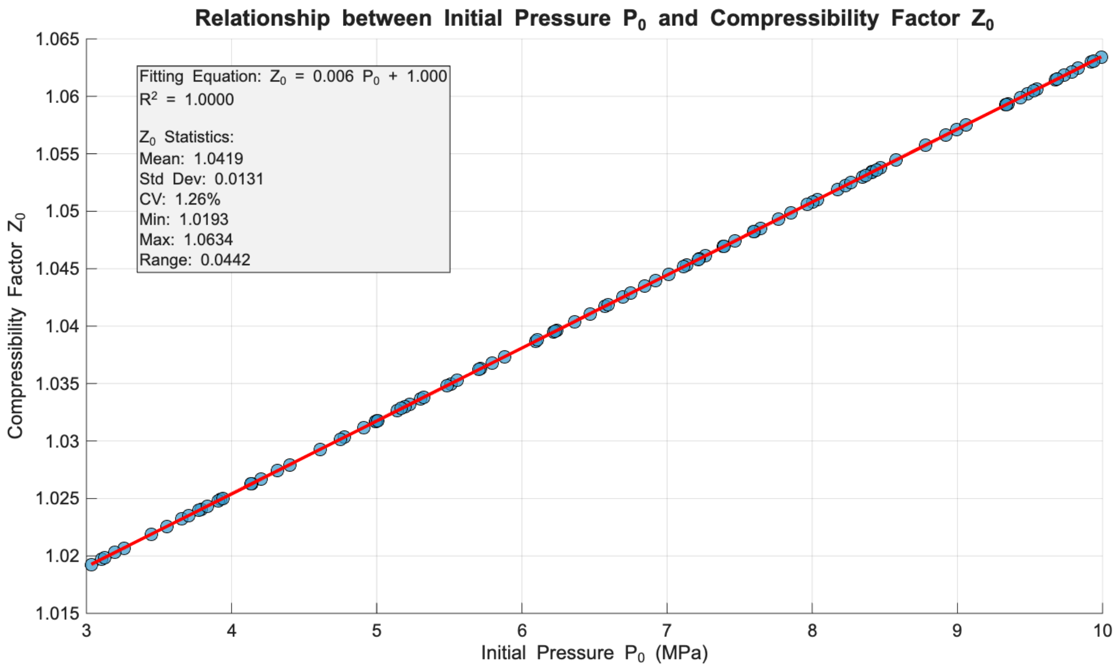

Fig. 2.5 – Influence of Initial Pressure on Compressibility Factor (*Z*)

Correspondingly, the initial hydrogen mass m0 shows a significant positive correlation with the initial pressure P_0 (fig. 2.6).

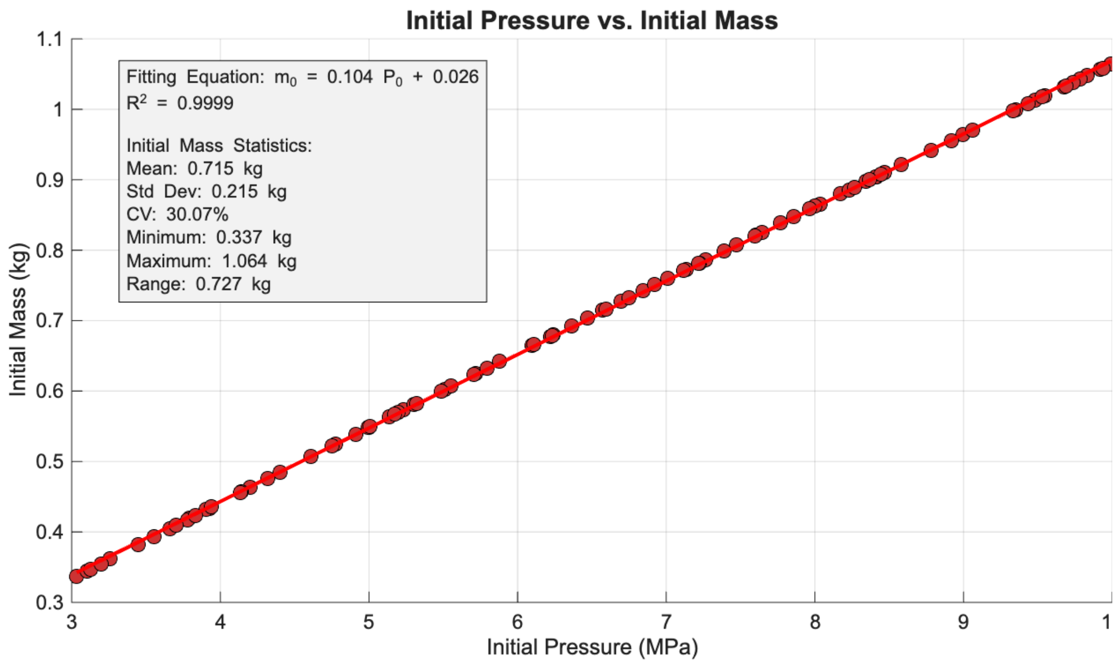

Fig. 2.6 – Relationship Between Initial Pressure (P_0)

and Initial Hydrogen Storage Mass (m_0)

To illustrate the calculation process more intuitively, the thermodynamic calculation results for selected typical initial pressure scenarios are listed in table 2.3.

Table 2.3 – Calculation Results of Hydrogen Storage Mass Under Different Typical Initial Pressures

Initial pressure P_0 (MPa)	Initial compressibility factor Z_0	Initial mass m_0 (Kg)	Final compressibility factor Z_c	Final mass M_c (Kg)	Actual filling quantity Δm (Kg)
3,0	1,0191	0,334	1,3896	5,000	4,666
4,0	1,0253	0,441	1,3896	5,000	4,559
5,0	1,0318	0,549	1,3896	5,000	4,451
6,0	1,0381	0,655	1,3896	5,000	4,345
7,0	1,0445	0,759	1,3896	5,000	4,241
8,0	1,0508	0,862	1,3896	5,000	4,138
9,0	1,0571	0,964	1,3896	5,000	4,036
10,0	1,0634	1,064	1,3896	5,000	3,936

3. Constraint on Final Mass and State of Charge (SOC)

A critical finding from the simulation is the thermodynamic constraint on the final mass mc. At the cut-off pressure of 70 MPa, the calculated hydrogen mass mc is approximately 5,0 kg.This value is lower than the nominal capacity of 5,6 kg (which is defined at standard temperature 288 K/15°C). This deviation is attributed to the Thermal Expansion Effect [33]. During the refueling process, the gas temperature rises from the initial ambient temperature (298 K/25°C) to a final temperature of 340 K (67°C), significantly reducing the gas density. Consequently, the actual State of Charge (SOC) reaches only about 89,3%. This result accurately reflects the physical limitation of «Hot Filling» processes where the pressure limit is reached before the full mass capacity is utilized. Influenced by this constraint, the relationship between the actual filling quantity Δm and the initial pressure is shown in fig. 2.7.

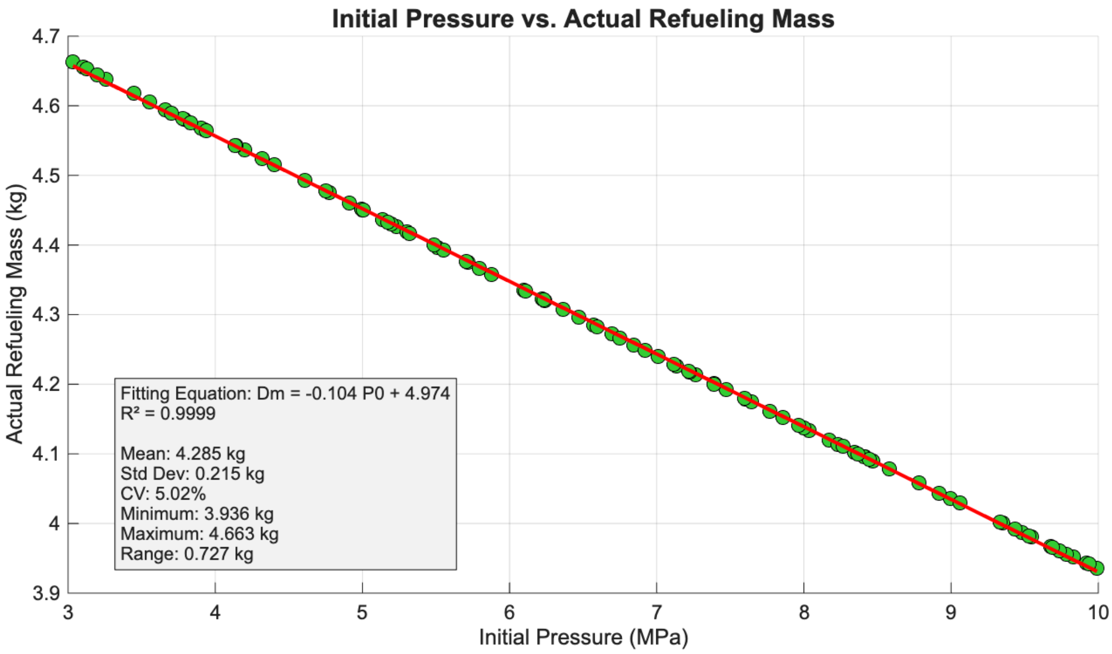

Fig. 2.7 – Law of the Effect of Initial Pressure on Actual Filling Quantity (Δm)

4. Statistical Conclusion

The statistical analysis of the actual filling quantity (Δm) for the 100 samples is summarized in table 2.4.

Table 2.4 – Statistical Analysis Results of FCEV's Initial Pressure Randomness and Filling Demand

Statistical indicators	Initial pressure P_0, (MPa)	Initial mass $m0$ (kg)	Actual filling quantity Δm (kg)
Mean	6,60	0,715	4,285
Standard Deviation	2,06	0,215	0,215
Coefficient of Variation	31,19%	30,07%	5,02%
Minimum Value	3,03	0,337	3,936
Maximum Value	9,99	1,064	4,663
Range	6,96	0,727	0,727

Although the vehicle's arrival state fluctuates significantly due to traffic conditions ($CV_{\mathrm{P0}} = 31{,}19\%$), the thermodynamic constraints of the high-pressure filling process dampen this variation, resulting in a relatively stable single-vehicle refueling demand with a coefficient of variation of only approx. 5%. The derived mean load of 4,285 kg/vehicle and its statistical characteristics will serve as the critical Mass Flow Input for the Macro-scale station load prediction in Section 2.5.

2.5 Macro-scale: Station-level Dynamic Load Prediction Based on Stochastic Queueing Model

Based on the single-vehicle refueling demand derived in Section 2.4 ($\mu_{\Delta m} \approx 4{,}285$ kg), the Macro-scale modeling aims to aggregate these discrete events into a continuous station-level hydrogen load profile. This section utilizes the M/M/S/N Queueing Theory to mathematically describe the stochastic arrival process of vehicles and quantify the dynamic operating load of the hydrogen refueling station (HRS).

2.5.1 Station Configuration and Operation Parameters

To ensure the engineering practicability of the model, a typical medium-scale commercial HRS is defined as the research object. The station is designed with a standard capacity of 500 kg/day to service a target fleet of 100 FCEVs per day, covering an operating window of 16 hours (06:00 – 22:00). The key configuration parameters are listed in table 2.5.

Operational Scenario Definition: Although the Toyota Mirai II (a passenger vehicle) is selected as the modeling object due to its precise technical parameters

(Section 2.2), this study defines the target user group as an Urban Ride-hailing/Taxi Fleet rather than private commuter vehicles. This definition justifies the specific peak refueling periods (07:00–10:00 and 15:00–18:00), which align with the typical shift-change patterns of commercial fleets.

Table 2.5 – Design Parameters of the Hydrogen Refueling Station

Parameter	Symbol	Value	Unit	Source / Remark
Station Design Capacity	M_{design}	500	kg/day	Standard Commercial Scale (Redundancy ≈16,7%)
Target Daily Demand	M_{req}	428,5	kg/day	Nominal Load (100 veh*4,285kg)
Target Service Volume	N_{daily}	100	veh/day	Design Target
Operating Hours	T_{op}	16	h	06:00–22:00
Average Arrival Rate	λ_{avg}	6,25	veh/h	100/16 = 6,25
Peak Arrival Rate	λ_{peak}	10,0	veh/h	Peak Factor ≈1,6
Number of Dispensers	S	3	-	Based on Queueing Optimization
Max System Capacity	N	13	veh	Queue Space Limitation

2.5.2 Stochastic Traffic Flow Modeling and Configuration Optimization

The arrival of FCEVs at the station is modeled as a stochastic process. Due to the limited space of the station, an M/M/S/N Queueing Model (Markovian arrival, Markovian service, S servers, Finite capacity N) is adopted.The theoretical foundation of this model is grounded in classical operations research, which strictly defines the state transition probabilities and blocking boundaries for finite-capacity multi-server systems [35].

Model Justification:

It should be noted that while the actual refueling time of FCEVs may exhibit characteristics of a normal distribution, the Exponential Distribution (Markovian) is adopted in this study for the service process. This assumption is based on two considerations:

1. Worst-Case Robustness: The exponential distribution possesses high variance. Using it generates a load profile with more severe fluctuations compared to deterministic models, providing a rigorous stress test for the downstream Automated Electrolyzer Control System (AECS) designed in Chapter 3.

2. Physical Constraints: The M/M/S/N model explicitly captures the blocking probability due to finite capacity (N), which is critical for urban HRS planning. As demonstrated in recent transportation engineering studies, incorporating queueing theory into station layout planning is critical for avoiding excessive capital investment while maintaining acceptable user wait times [36].

To determine the optimal station configuration, three typical plans are proposed for simulation analysis, as shown in table 2.6.

Table 2.6 – Configuration Plans for Hydrogen Refueling Dispensers

	Plan A	Plan B	Plan C
No. of hydrogen refueling machines (S)	2	3	4
System capacity (N)	7, 12, 17	8, 10, 13, 15	9, 14, 19

1. Performance Analysis under Off-Peak Conditions

First, the queuing performance of the three plans was simulated under the average arrival rate ($\lambda = 6,25$ veh/h) and peak arrival rate ($\lambda = 10,0$ veh/h). The results are summarized in table 2.7 and visualized in fig. 2.8.

Table 2.7 – Comparison of Performance Indicators for Different Plans

S	*N*	ρ	*L*	*Lq*	*W*, hour	*W*q, minute	Pblock
2	7	0,521	1,37	0,34	0,22	3,28	0,007
2	12	0,521	1,43	0,38	0,23	3,69	0,000
2	17	0,521	1,43	0,39	0,23	3,72	0,000
3	8	0,347	1,09	0,05	0,18	0,50	0,000
3	10	0,347	1,09	0,05	0,18	0,51	0,000
3	13	0,347	1,10	0,05	0,18	0,51	0,000
3	15	0,347	1,10	0,05	0,18	0,51	0,000
4	9	0,260	1,05	0,01	0,17	0,08	0,000
4	14	0,260	1,05	0,01	0,17	0,08	0,000
4	19	0,260	1,05	0,01	0,17	0,08	0,000

Analysis:

- Plan A (*S* = 2): While economical, it exhibits a significant risk of queuing during peak hours, with limited redundancy for equipment maintenance.
- Plan C (*S* = 4): Although it minimizes waiting time (< 0,1min), the equipment utilization rate is too low, leading to excessive capital investment and resource waste.
- Plan B (*S* = 3): Provides the optimal balance. It ensures a near-zero blocking probability while maintaining a reasonable equipment utilization rate.

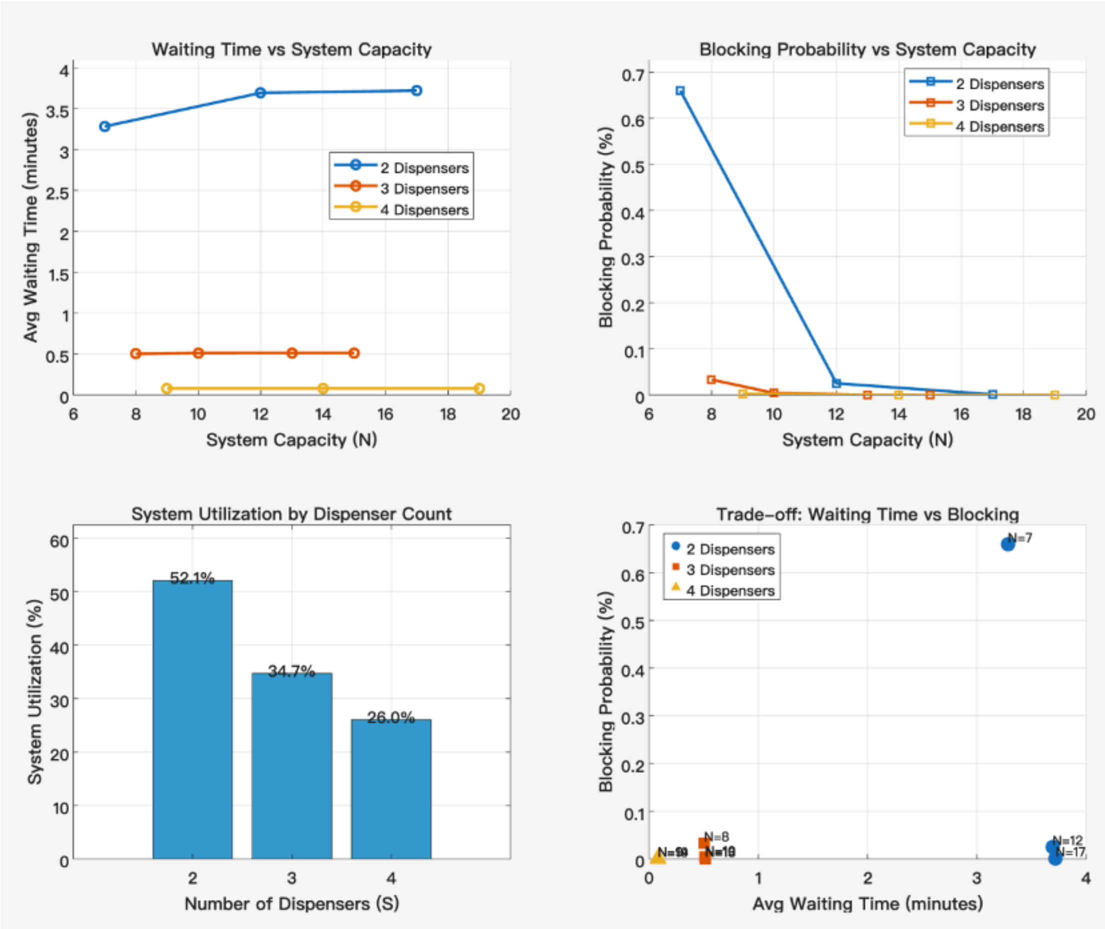

Figure 2.8 – Comparison Chart of Queuing Performance for Different Plans

2. Stress Test under Peak Conditions (Optimization)

To ensure reliability during rush hours, further analysis was conducted on the optimal Plan B (S = 3) under the peak arrival rate (λ= 10 veh/h) with varying system capacities (N). The results are shown in table 2.8.

Table 2.8 – Comparison of Performance Indicators for Plan B (S = 3) in Peak Period

N	ρ	L	Lq	W, hour	Wq, minute	Pblock
8	0,556	1,97	0,31	0,20	1,89	0,007
10	0,556	2,01	0,35	0,20	2,11	0,002
13	0,556	2,04	0,37	0,20	2,22	0,000
15	0,556	2,04	0,37	0,20	2,24	0,000

Selection Conclusion: As indicated in Table 2.8, when the system capacity is set to N=13, the blocking probability drops to 0.000, and the average waiting time is only 2.22 minutes. Therefore, the configuration of Plan B (3 dispensers, S = 3) with 13 vehicle spaces (N=13) is selected as the optimal design parameter.

2.5.3 Dynamic Hydrogen Load Profile Calculation and Characteristic Analysis

The station-level dynamic hydrogen mass flow rate, denoted as $\dot{M}_{\text{station}}(t)$, is the stochastic coupling of the macroscopic traffic arrival intensity and the microscopic refueling demand.

1. Mathematical Formulation

To rigorously describe the randomness of the load, the instantaneous hydrogen demand is modeled as a Compound Poisson Process. According to foundational stochastic process theory [37], this approach effectively decouples the random arrival rate from the stochastic individual service demand:

$$\begin{cases} \dot{M}_{\text{station}}(t) = \sum_{i=1}^{N(\text{t})} \Delta\, m_{\text{i}} \approx N(t) \cdot \mu_{\Delta\text{m}} \\ P(N(t) = k) = \dfrac{(\lambda(t))^{\text{k}} \text{e}^{-\lambda(\text{t})}}{k!} \end{cases} \tag{2.8}$$

Where:

- $N(t)$ is the stochastic number of vehicles arriving in hour t.
- $\mu_{\Delta\text{m}}$ is the mean refueling mass per vehicle (4,285 kg, derived in Section 2.4).
- $\lambda(t)$is the time-variant arrival rate parameter defined by the operational scenario in Section 2.5.1 (λ = 10during peaks, $\lambda = 4$ during off-peaks).

2. Simulation Results and Data Statistics

A 16-hour Monte Carlo simulation was conducted based on Equation (2.8). The application of Monte Carlo methods to capture spatial-temporal demand peaks has become a benchmark approach in forecasting alternative fuel infrastructure loads [38]. The resulting load profile (fig. 2.9) exhibits significant stochastic deviations from the theoretical baseline.

- Theoretical Mean: The design baseline fluctuates between 17,14 kg/h (Off-Peak) and 42,85 kg/h (Peak).

- Stochastic Extremes: The simulation records a Peak-to-Valley ratio of 15:1, with the instantaneous load ranging from a minimum of 4,29 kg/h (11:00) to a maximum of 64,28 kg/h (08:00).

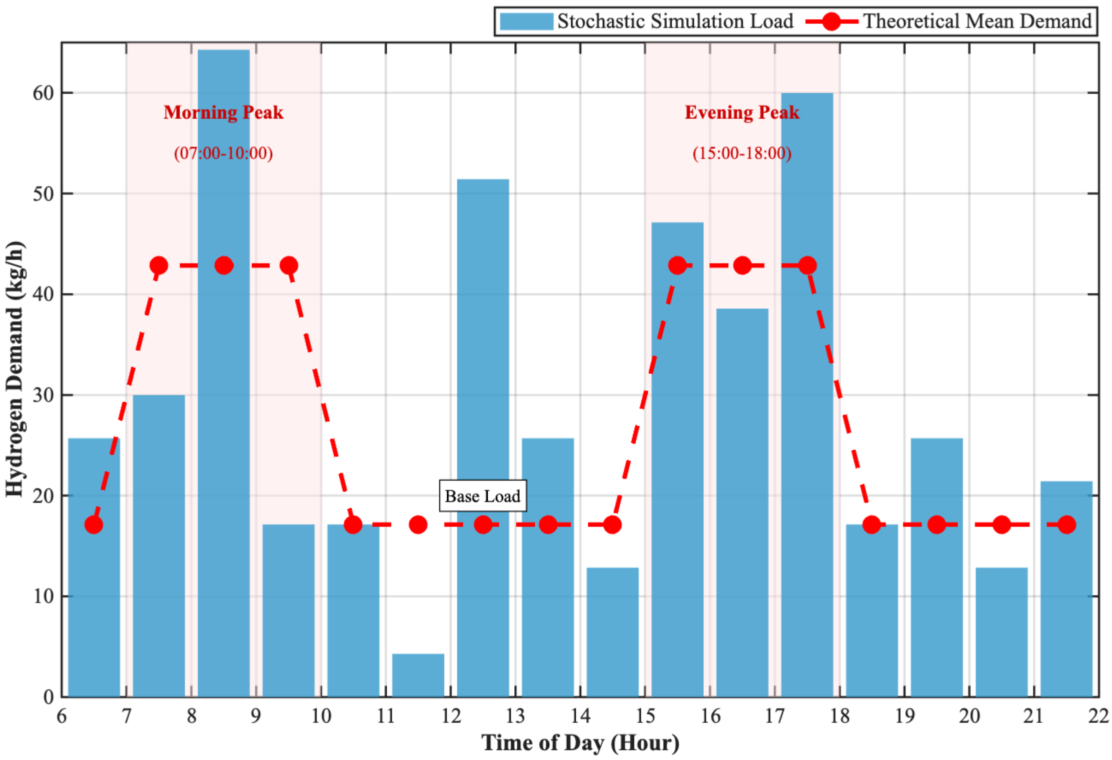

Figure 2.9 – Simulated Daily Hydrogen Demand Profile

Data Highlight: The profile reveals three distinct operational surges at 08:00, 12:00, and 17:00, driven by the superposition of traffic clusters and driver behaviors.

3. Characteristic Analysis of Critical Load Events

The analysis of specific simulation data points reveals the underlying operational logic and the resulting challenges for the hydrogen production system:

- The «Morning Surge» (08:00–09:00, $\dot{M} = 64.28$ kg/h)

- Phenomenon: The demand reaches the daily maximum, exceeding the theoretical peak (42,85 kg/h) by 50%.

- Mechanism: This reflects the "Cluster Arrival" effect of logistics/taxi fleets starting their morning shift.

- System Impact: The demand significantly exceeds the electrolyzer's nominal capacity (~31 kg/h). The high-pressure storage buffer enters a state of rapid depletion, necessitating the electrolyzer to ramp up to maximum overload capacity immediately.

- The «Lunch-Break Spike» (12:00–13:00, $\dot{M} = 51{,}42$ kg/h)

- Phenomenon: An unexpected surge occurs during the theoretical off-peak window, sharply contrasting with the deep valley at 11:00 (4,29 kg/h).

- Mechanism: This confirms the «Opportunity Refueling» strategy. Drivers utilize the low-passenger-demand period (lunch hour) to refuel.

- System Impact: The system must transition from «Sleep Mode» (4,29 kg/h) to «Full-Load Mode» (51,42 kg/h) within one hour. This step-change signal imposes a severe test on the dynamic response speed of the control system.

- The «Deadline Rush» (17:00–18:00, $\dot{M} = 59{,}99$ kg/h)

- Phenomenon: A sustained high load appears right before the end of the evening peak.
- Mechanism: This simulates the «Shift Handover Constraint». As the day shift typically ends at 18:00, drivers are compelled to refuel between 17:00–18:00 to avoid penalties for handing over an empty vehicle.
- System Impact: Unlike random fluctuations, this is a deterministic operational constraint that creates a sustained high-pressure demand, requiring the system to maintain maximum output before the night lull.

4. Engineering Implication

The simulation confirms that the hydrogen load is highly volatile. Since the storage capacity is economically finite, it cannot passively buffer such large-scale fluctuations (specifically the continuous deficit during the morning surge). Therefore, the Automated Electrolyzer Control System (AECS) proposed in Chapter 3 must be introduced. Its objective is to regulate the electrolyzer's power to actively compensate for these stochastic disturbances $\lambda(t)$, thereby maintaining the Storage State of Charge (SOC) within a safe range.

2.5.4 System Capacity Matching and Buffer Sizing Analysis

Based on the dynamic load profile obtained in Section 2.5.3, this section evaluates the matching degree between the station's hydrogen production capacity and the stochastic refueling demand. The analysis focuses on the contradiction between the Macroscopic Daily Balance and the Microscopic Instantaneous Flux. This exact spatio-temporal mismatch has been identified as the primary operational bottleneck in recent studies on integrated hydrogen refueling networks [39][40].

1. Macroscopic Daily Balance: Capacity Utilization

According to the simulation data in Fig. 2.9, the cumulative daily hydrogen demand (M_{total}) is calculated by integrating the hourly flow rates:

$$M_{total}=\sum_{t=6}^{22}\dot{M}_{station}(t)\approx 456{,}8\ \text{kg/day} \tag{2.9}$$

Comparing this with the station's design capacity(M_{design}=500 kg/day), the Daily Capacity Utilization Factor (η_{cap}) is derived:

$$\eta_{cap}=\frac{M_{total}}{M_{design}}=\frac{456.8}{500}\approx 91{,}4\% \tag{2.10}$$

A utilization rate of 91,4% indicates that the selected 500 kg/day electrolyzer is economically optimal. It avoids excessive CAPEX waste (over-sizing) while meeting the total daily demand with a safety margin of approx. 8,6%.

2. Microscopic Instantaneous Flux: The «Supply-Demand Deficit»

While the daily total is balanced, the instantaneous power balance exhibits severe deficits. Assuming the electrolyzer operates at a nominal constant rate (P_{nom}) distributed over the 16 operational hours:

$$P_{nom}=\frac{M_{design}}{T_{op}}=\frac{500\ \text{kg}}{16\ \text{h}}\approx 31{,}25\ \text{kg/h} \tag{2.11}$$

By comparing P_{nom} with the simulated stochastic load $\dot{M}_{station}(t)$ (specifically the 08:00 surge of 64,28 kg/h), the Net Mass Flux ($\Delta\dot{m}$) into the storage system reveals a critical imbalance:

- Positive Flux (Accumulation Risk): During off-peak hours (e.g., 11:00), $\Delta\dot{m}=+26{,}96$ kg/h. If the electrolyzer does not ramp down, the buffer tank faces over-pressure risks.

- Negative Flux (Depletion Risk): During the morning surge (08:00), $\Delta\dot{m}$ = -33,03 kg/h. The deficit exceeds the production rate by >100%. The storage tank must discharge at high speed to compensate

3. Engineering Implication

The analysis confirms a critical paradox: Macro-Balance vs. Micro-Imbalance. The fixed production rate (31,25 kg/h) fails to meet the instantaneous demand dynamics. Consequently, the system cannot operate open-loop. The Automated Electrolyzer Control System (AECS) proposed in Chapter 3 is mandatory to dynamically adjust production between Minimum Load (Keep Warm) and Maximum Overload to minimize the $\Delta\dot{m}$ gap and protect the storage buffer.

Summary by Chapter

This chapter established a comprehensive mathematical model for the on-site hydrogen refueling station, bridging the gap between microscopic thermodynamic behaviors and macroscopic operational characteristics.

1.Thermodynamic Modeling: A precise spatially distributed parameter model for 70 MPa fast filling was developed (Section 2.1–2.3). The theoretical single-vehicle demand was quantified as 4,285 kg (Section 2.4).

2.Stochastic Load Modeling: By integrating the M/M/S/N queuing theory with the Poisson arrival process, a 16-hour dynamic load profile was generated (Section 2.5). The simulation revealed a Peak-to-Valley ratio of 15:1, identifying three critical surge events (08:00, 12:00, 17:00) driven by cluster arrivals and operational constraints.

3.The Necessity of Intelligent Control: The capacity matching analysis (Section 2.5.4) demonstrated that while the daily capacity is sufficient ($\eta_{cap} = 91{,}4\%$), the instantaneous supply-demand deficit reaches up to 33 kg/h during surges.

The passive buffering capability of the storage system is insufficient to handle the identified stochastic disturbances. This necessitates the design of the Automated Electrolyzer Control System (AECS) in the following chapter, which aims to achieve active pressure stabilization and efficient energy management under these extreme load conditions.

CHAPTER 3.

DEVELOPMENT OF AUTOMATED ELECTROLYZER CONTROL SYSTEM (AECS) FOR LOAD FOLLOWING AND PRESSURE STABILIZATION

In Chapter 2, the modeling and analysis of the load characteristics of the on-site hydrogen refueling station (HRS) revealed that hydrogen demand is characterized by high stochasticity and significant fluctuations. Specifically, the «double-peak» phenomenon observed during morning and evening rush hours creates severe instantaneous mismatches between supply and demand on a micro-time scale. This temporal mismatch not only tests the buffering capacity of the storage system but also poses a critical challenge to the dynamic response of the hydrogen production subsystem.

Currently, the mainstream industrial approach for managing these fluctuations relies on Pressure-based Hysteresis Control. This reactive mechanism forces the Proton Exchange Membrane (PEM) electrolyzer to undergo frequent start-stop cycles in response to stochastic load variations. Existing electrochemical studies indicate that such frequent voltage cycling and current surges significantly accelerate the mechanical degradation of core components, such as the proton exchange membrane and catalyst layers, thereby drastically reducing equipment lifespan and imposing pulsed impacts on the power grid. Consequently, developing an intelligent control system capable of proactively anticipating demand and achieving smooth load following is essential for addressing these operational challenges.

To this end, this chapter proposes an Automated Electrolyzer Control System (AECS) based on a Proactive Predictive Control framework. By integrating the high-precision prediction capabilities of Deep Long Short-Term Memory (LSTM) networks with a Hot Standby logic-embedded feedforward control strategy, this system aims to achieve «Zero Start-Stop» continuous operation and stabilize storage pressure, fundamentally mitigating the engineering problems caused by stochastic loads.

The remainder of this chapter is organized as follows: Section 3.2 introduces the high-fidelity synthetic dataset used for validation and verifies its consistency; Section 3.3 establishes the discrete-time mathematical model and constraints of the control object; Section 3.4 details the hardware architecture and technical support of the AECS; Section 3.5 constructs and evaluates the deep LSTM demand prediction network; Section 3.6 proposes the feedforward-dominant proactive predictive control strategy and logic flow; Section 3.7 verifies the superiority of the proposed system in eliminating start-stop cycles and smoothing power fluctuations through comparative simulation; finally, Section 3.8 summarizes the chapter.

3.2 Data Acquisition and Consistency Validation

3.2.1 Dataset Generation and Description

Given the scarcity of high-resolution operational data from commercial hydrogen refueling stations (HRS) and constraints regarding data privacy and intellectual property, this study employs High-Fidelity Synthetic Data as the benchmark for training the deep learning model and validating the control strategy. The use of meticulously generated synthetic datasets to substitute for scarce real-world historical data has become a critical and widely accepted methodology in the recent predictive optimization of green hydrogen hubs [45]. Based on the stochastic traffic flow and thermodynamic models established and validated in Chapter 2, a high-resolution dataset representing the operational conditions for the full year of 2024 (366 days, totaling 8,784 hours) was generated.

The dataset is not merely a product of random number generation but is constructed based on rigorous physical and statistical constraints. The generation logic incorporates three key dimensions:

1.Stochastic Arrival Rate: A Non-homogeneous Poisson Process (NHPP) is introduced to simulate the stochastic nature of hydrogen vehicle arrivals, while preserving the characteristic «double-peak» daily distribution pattern. As demonstrated in foundational studies on transportation energy modeling, utilizing NHPP with time-varying arrival rates is the most rigorous mathematical approach to accurately capture the macroscopic clustering effects of urban morning and evening rush hours [46].

2.Thermodynamic Constraints: The refueling quantity for each vehicle is not a fixed value; instead, it fluctuates randomly within a reasonable range determined by the thermodynamic boundary conditions (e.g., ambient temperature, initial tank pressure) derived in Chapter 2.

3.Temporal Resolution: The data sampling frequency is set to 1 hour. This resolution matches the scheduling cycle of the upper-level energy management system while retaining sufficient load fluctuation details to test the dynamic response of the control system.

3.2.2 Data Consistency Validation

To ensure the physical validity and academic rigor of the simulation input, the generated 2024 dataset was cross-validated against the theoretical model from Chapter 2 across multiple dimensions. The validation results indicate that the dataset faithfully reproduces the statistical characteristics of real-world operational scenarios.

1. Micro-Level: Consistency of Per-Vehicle Refueling Quantity

Statistical analysis of the full-year refueling records reveals that the average hydrogen dispensing quantity per vehicle in the dataset is 4,30 kg/vehicle. This value is highly consistent with the theoretical benchmark of 4,285 kg/vehicle derived from the Monte Carlo Simulation in Chapter 2, with a relative error of only 0.35%. This minimal error confirms the high physical fidelity of the dataset regarding micro-level refueling behaviors.

2. Macro-Level: Alignment of Daily Demand with Design Capacity

As shown in fig. 3.1, the daily hydrogen demand in the dataset exhibits fluctuation characteristics consistent with realistic operations:

- Minimum Daily Demand: 340,27 kg
- Maximum Daily Demand: 434,48 kg
- Average Daily Demand: 388,67 kg

The daily demand for all sample points remains strictly within the safety envelope of the system's design capacity (500 kg/day), with a maximum load factor of 86,9%. This validates the rationality of the system sizing (maintaining a safety margin of approximately 13%) and ensures the effectiveness of the test scenarios for the control strategy.

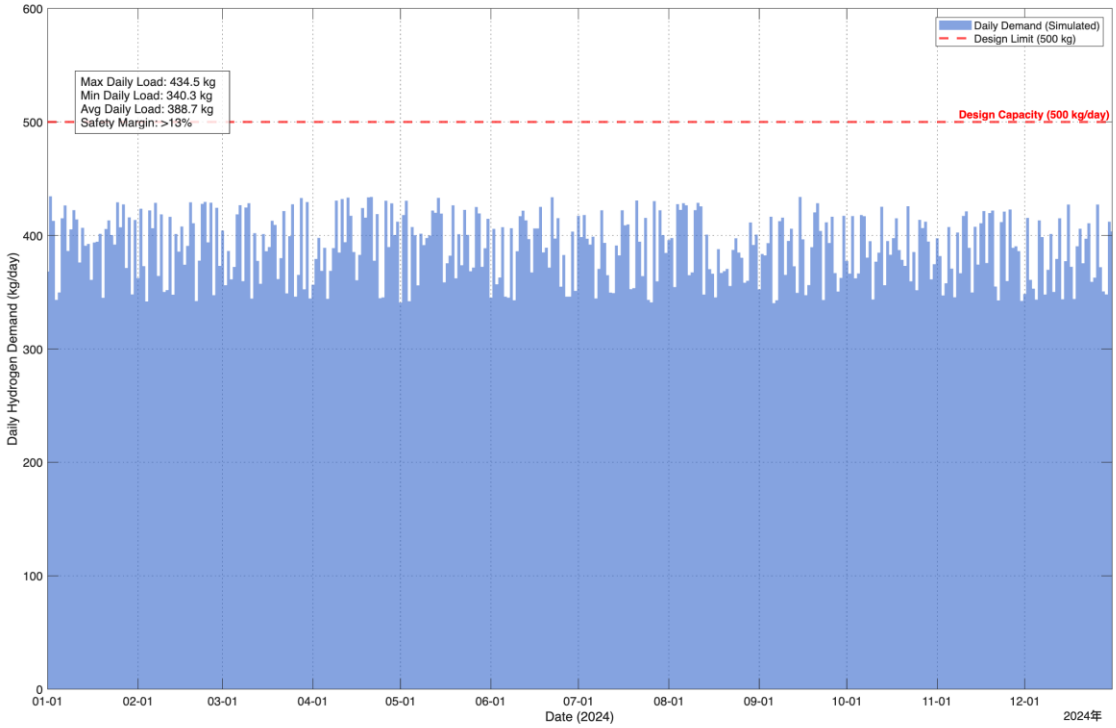

Figure 3.1 – Daily Hydrogen Demand vs. System Design Capacity

3. Feature-Level: Extreme Stress-Test Scenarios

The data exhibits significant «double-peak» temporal characteristics (morning peak 07:00–10:00, evening peak 15:00–18:00). Notably, the maximum instantaneous load observed throughout the year is 78,27 kg/h, which exceeds the theoretical design point of 64,28 kg/h established in Chapter 2. This indicates that the dataset includes extreme stress-test scenarios that go beyond nominal design expectations. Such over-limit conditions are not data errors but rather serve to impose higher requirements on the robustness of the control system. Recent comprehensive surveys on load modeling highlight that data augmentation and the deliberate inclusion of such extreme synthetic scenarios are essential for rigorously validating the dynamic stability of energy management algorithms under severe supply-demand imbalances [47].

Table 3.1 – Consistency Comparison between Theoretical Model and Synthetic Dataset

Validation Dimension	Metric	Theoretical Value (Chapter 2)	Dataset Value (Chapter 3)	Relative Error / Remark
Micro-Level	Avg. Fill per Vehicle	4,285 kg	4,30 kg	0,35% Error (Exceptionally Consistent)
Macro-Level	Daily H_2 Demand	500 kg (Design Limit)	340,3–434,5 kg	Sufficient Safety Margin (>13%)
Feature-Level	Max Load (P_{max})	64,28 kg/h (Limit)	78,27 kg/h	Includes Extreme Stress-Test Scenarios

In summary, the dataset employed in this chapter has passed strict consistency validation across micro-mechanisms, macro-capacity, and statistical features. Furthermore, it incorporates challenging extreme conditions, serving as a reliable and rigorous input for the subsequent training of the LSTM prediction model and the simulation of the AECS control strategy.

3.3 Mathematical Modeling of the Control Object

3.3.1 Physical Process Flow and Control Boundary Definition

The on-site hydrogen refueling station investigated in this chapter employs a typical «low-pressure production, multi-stage compression, and high-pressure dispensing» process, designed to meet the rapid refueling demands of 70 MPa fuel cell vehicles. As illustrated in fig. 3.2, the complete physical hydrogen flow path comprises the following key stages:

1. Production and Primary Buffering: The PEM electrolyzer produces hydrogen at an outlet pressure typically between 1–3 MPa. The generated hydrogen first enters a small 3 MPa Process Buffer Tank to stabilize the inlet pressure for the first-stage compressor.

2. Intermediate Storage and Energy Hub: The hydrogen is pressurized by the first-stage compressor to approximately 20 MPa and stored in large-scale 20 MPa Intermediate Storage Banks. This stage has the largest capacity and serves as the core energy hub connecting the continuous, slow-response production process with intermittent, fast-response high-pressure refueling demands. It is the primary anchor for the control system.

3. High-Pressure Dispensing Path: Driven by refueling demand, the second-stage compressor draws hydrogen from the 20 MPa tanks and pressurizes it to 95 MPa High-Pressure Storage Banks. Subsequently, the high-pressure hydrogen passes through a Cascade Buffer System and a Precooler (chilling to -40°C) before being dispensed into fuel cell vehicles via the dispenser.

Control Boundary Definition:

Although the physical system involves multi-stage compression and complex storage structures, the core objective of the AECS is to ensure the front-end production rate dynamically follows the average change rate of the terminal refueling demand, maintaining system-wide energy balance.

To establish a mathematically tractable model for controller design, this study applies model order reduction and restricts the control boundary to the «Electrolyzer - 20 MPa Intermediate Storage» subsystem. Such lumped-parameter simplification has been proven highly effective and rigorously valid in recent advanced energy management studies for complex hydrogen hubs [48].

- Controlled Plant: The 20 MPa Intermediate Storage Tank. Its internal storage mass, S(t), is the key state variable characterizing the system's energy balance.

- Control Input: The electrolyzer production rate, $P(t)$. It is assumed that the first-stage compressor can rapidly follow the electrolyzer output, neglecting its dynamic delay.

- System Disturbance: The flow rate drawn by the second-stage compressor from the 20 MPa tank, $D(t)$. According to the law of conservation of mass, under the 1-hour control cycle, the stochastic terminal refueling demand is directly mapped to this suction flow rate.

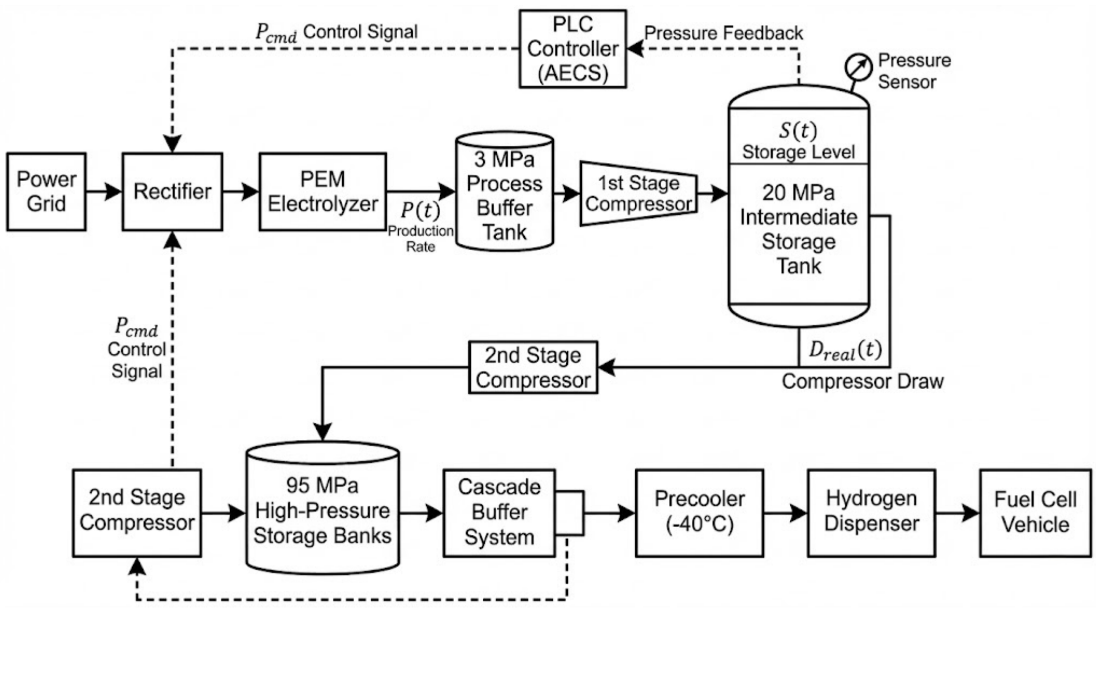

Figure 3.2 – Schematic of Multi-Stage Process Flow and Control Loop for On-Site HRS

3.3.2 Discrete-Time Mass Balance Model

Based on the control boundary defined above, the dynamic behavior of the intermediate storage system can be modeled as a discrete-time integrator. Recent modeling frameworks for optimization-based operational scheduling explicitly adopt this linear state-space formulation to handle discontinuous behaviors in refueling topologies [49]. Given the sampling interval $\Delta t = 1$ hour (consistent with the dataset resolution), the mass balance equation governing the state evolution is formulated as:

$$S(t+1) = S(t) + \Delta t \cdot [P(t) - D(t)] \tag{3.1}$$

Where:

- $S(t)$ represents the hydrogen mass in the 20 MPa storage tank at time step t (kg).
- $P(t)$ is the hydrogen production rate of the electrolyzer (kg/h).
- $D(t)$ is the hydrogen demand rate drawn from the tank (kg/h).
- Δt is the control cycle duration ($\Delta t = 1$).

To ensure the physical safety and operational feasibility of the system, the following critical constraints are imposed, which align with the simulation parameters set in Section 3.7:

1. Storage Capacity Constraints:

The storage level must be maintained within the rated capacity to prevent over-pressurization (safety hazard) or depletion (suction failure).

$$S_{\min} \leq S(t) \leq S_{\max} \tag{3.2}$$

In this study, the capacity parameters are set as:

- Maximum Capacity ($S_{\max}$): 500 kg (Design Capacity).
- Minimum Safety Limit ($S_{\min}$): 150 kg (30% of capacity).

Physical Meaning: Maintaining $S(t) \geq 150$ ensures sufficient buffer pressure for the second-stage compressor, preventing interlock shutdowns.

2. Electrolyzer Operating Constraints (The «Hot Standby» Logic):

The production rate is constrained by the physical power rating of the electrolyzer stack. Furthermore, to avoid the damaging effects of cold starts, a «Hot Standby» constraint is introduced [50]. The device is permitted to operate either at its rated range or in a low-power idle mode, but strictly prohibited from complete shutdown ($P(t) = 0$) unless in emergency overflow conditions.

$$P(t) \in \{0\} \cup [P_{idle}, P_{max}] \tag{3.3}$$

Where:

- Rated Maximum Power (P_{max}): 50 kg/h.
- Hot Standby Power (P_{idle}): 3,0 kg/h.

Strategic Significance: Unlike traditional logic that allows complete shutdown ($P = 0$), the AECS enforces $P(t) \geq P$idle during normal operation. This constraint is the mathematical foundation for achieving the «Zero Process Start-Stop» result (reducing cycles from 61 to 1) reported in Section 3.7.

3. Ramp Rate Constraints(Grid Friendliness):

To protect the PEM membrane from mechanical stress caused by sudden power surges, the rate of change in production is limited [51]:

$$|P(t) - P(t-1)| \leq \Delta P_{max} \tag{3.4}$$

Where ΔPmax is the maximum allowable ramp rate per hour.

Strategic Significance: This constraint forces the controller to smooth out sudden demand spikes, directly resulting in the reduced power fluctuation (σ reduced from 22,98 to 14,78) observed in the simulation.

3.3.3 Control Strategy Logic and Optimization Objectives

While Section 3.3.2 defined the absolute physical boundaries (Hard Constraints) of the system, this section formulates the Control Strategy and Optimization Objectives (Soft Constraints) that govern the decision-making process of the AECS.

The fundamental challenge in controlling the HRS lies in the inherent conflict between «Safety» (which favors high inventory to prevent depletion), «Efficiency/Lifespan» (which favors minimizing start-stop frequency), and «Grid Friendliness» (which favors smooth power modulation). To address this, the AECS is theoretically modeled as a heuristic solver for a constrained multi-objective optimization problem.

The global control objective J is formulated as the minimization of a weighted cost function comprising three distinct components: Pressure Stabilization, Lifespan Extension, and Grid Smoothing.

$$\min_{P(t)} J = \sum_{t=1}^{T} \left(w_{\text{stab}} \cdot J_{\text{stab}}(t) + w_{\text{life}} \cdot J_{\text{life}}(t) + w_{\text{grid}} \cdot J_{\text{grid}}(t) \right) \tag{3.5}$$

The specific logic and thresholds for each component are detailed below.

1. Lifespan Extension Logic: The «Hot Standby» Protocol (J_{life})

The primary cause of PEM electrolyzer degradation is the mechanical fatigue and voltage cycling induced by frequent start-stop events. Extensive electrochemical experimental studies have confirmed that intermittent operation, particularly complete shutdowns and cold restarts, exponentially accelerates catalyst dissolution and membrane thinning [52]. Traditional hysteresis control shuts down the electrolyzer ($P = 0$) whenever the tank is full or demand is low, leading to daily «Cold Starts».

To eliminate this, the AECS introduces a «Hot Standby» protocol [50]. Mathematically, the lifespan cost function Jlife assigns an infinite penalty to the shutdown state during normal operation:

$$J_{\text{life}}(t)=\begin{cases}\infty & \text{if } 0 < P(t) < P_{\text{idle}} \text{ (Forbidden Region)} \\ \infty & \text{if } P(t) = 0 \text{ and } S(t) < S_{\text{emergency}} \text{ (Unnecessary Shutdown)} \\ 0 & \text{if } P(t) \geq P_{\text{idle}} \text{ (Continuous Operation)}\end{cases} \quad (3.6)$$

- Operational Threshold (P_{idle}): Set to 3,0 kg/h.
- Physical Rationale: By enforcing a minimum current density, the system maintains the stack's internal temperature and pressure equilibrium. This constraint is the theoretical foundation for the simulation result in Section 3.7, where the start-stop count is reduced from 61 (Baseline) to 1 (System Initialization only).

2. Pressure Stabilization: Asymmetric Reference Tracking (J_{stab})

To buffer stochastic demand fluctuations without triggering safety interlocks, the AECS abandons the «full-or-empty» logic in favor of a Reference Tracking mechanism [53]. The system aims to minimize the deviation of the storage level $S(t)$ from an optimal equilibrium point, S_{ref}.

$$J_{\text{stab}}(t) = (S(t) - S_{\text{ref}})^2 \quad (3.7)$$

- Optimization Target (S_{ref}): Set to 300 kg (60% of Capacity).
- Strategic Rationale (The Asymmetric Buffer): The 300 kg setpoint creates two distinct functional zones within the 500 kg tank:

- Upward Buffer (200 kg Margin): The space between 300 kg and 500 kg is reserved to absorb excess production during the Valley Pricing Window (22:00–06:00). This allows the system to store cheap energy without hitting the high-pressure vent limit ($S_{\max}$).

- Downward Buffer (150 kg Margin): The space between 300 kg and 150 kg ($S_{\min}$) serves as a safety cushion to absorb sudden «Double-Peak» demand shocks during the day, ensuring the compressor inlet pressure never drops below the critical threshold.

3. Grid Friendliness: Ramp Rate Suppression (J_{grid})

To minimize the impact on the local microgrid and protect the membrane from sudden voltage surges, the control strategy penalizes rapid changes in power output [51].

$$J_{\text{grid}}(t)=|P(t) - P(t-1)|^2 \quad (3.8)$$

This term forces the AECS to act as a Low-Pass Filter, smoothing out the high-frequency noise from the stochastic hydrogen demand. This logic directly results in the 35,7% reduction in power fluctuation observed in the simulation results (σ_{AECS} = 14,78 vs. σ_{Base}= 22,98).

4. Hierarchical Control Priority Mechanism

Since the objectives above may conflict in real-time (e.g., stabilizing pressure might require a rapid power change), the AECS employs a Risk-Based Hierarchical Priority mechanism to execute control decisions. Such multi-layer hierarchical structures have been proven essential in the robust energy management of complex, multi-state hydrogen microgrids [54]. The logic stack is defined as follows:

- Priority Level I: Critical Safety (Hard Floor)
  - Condition: If $S(t)$ drops below 160 kg (approaching the S_{min}=150 limit).
  - Action: Unconditional Ramp-Up. The controller overrides all economic and smoothing objectives to increase production to $P_{rated.}$ This guarantees 100% supply reliability for the downstream compressor.
- Priority Level II: Lifespan Protection (Zero-Stop Rule)
  - Condition: If demand is low but $S(t)$ is within the safe range.
  - Action: Enforce Hot Standby. The controller strictly prohibits the production rate from falling below 1 kg/h. Equipment longevity takes precedence over short-term energy savings.
- Priority Level III: Dynamic Balancing (Load Following)
  - Condition: When the system is in the normal range ($160 < S(t) < 480$).
  - Action: Optimized Modulation. The controller modulates $P(t)$ based on LSTM predictions to track the 300 kg reference while minimizing the ramp rate (J_{grid}).

3.4 Hardware Architecture and Technical Support of the AECS

The physical implementation of the Automated Electrolyzer Control System (AECS) requires not only the capability to process high-dimensional computations for deep neural networks but also strict adherence to the rigorous explosion-proof standards and millisecond-level hard real-time safety constraints of a hydrogen refueling station (HRS).

Since the HRS environment is classified as a hazardous area (Class I, Zone 1/2), the AECS strictly isolates «Computational Intelligence» from «Physical Safety». This section designs a Hierarchical Distributed Dual-Loop Control Architecture based on the integration of IT (Information Technology) and OT (Operational Technology).

3.4.1 Hierarchical Control Architecture and Dual-Loop Mechanism

As illustrated in fig. 3.3, the system topology is physically divided into a «Slow Optimization Outer Loop» and a «Fast Safety Inner Loop», mirroring the control priorities defined in Section 3.3.3. This decoupled IT/OT architecture, bridged by standardized communication protocols, is widely recognized as the industry standard for deploying AI-driven advanced process control in critical manufacturing and energy infrastructures [55]

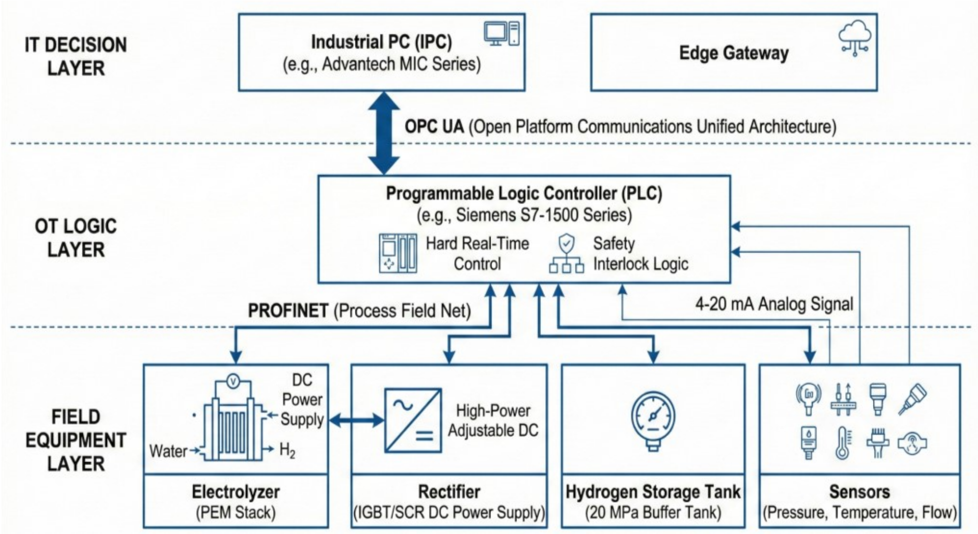

Figure 3.3 – Hierarchical distributed hardware topology architecture of the AECS based on IT/OT integration

1. IT Decision Layer (Slow Optimization Outer Loop)

- Hardware Core: An Industrial Edge AI Server (IPC, e.g., Advantech MIC series) equipped with GPU acceleration.

- Function: Acting as the «Optimization Brain», this layer runs in a high-level environment (Python/PyTorch). It hosts the Deep LSTM Network (Section 3.5) to process historical traffic data and execute the Reference Tracking Strategy (Targeting $S_{ref} = 300$ kg).

- Cycle: Operating on a second-to-minute scale, it calculates the optimal production setpoint (P_{opt}) to minimize grid fluctuation (J_{grid}) and transmits it to the lower layer via OPC UA.

2. OT Logic Layer (Fast Safety Inner Loop)

- Hardware Core: A Safety-Certified Programmable Logic Controller (Safety PLC, e.g., Siemens S7-1500) with extremely high MTBF.

- Function: Acting as the «Control Cerebellum», the PLC executes the underlying PID closed-loop control and Safety Interlocks with a millisecond-level scanning cycle.

- Critical Logic: The hard constraints defined in Section 3.3.2 are hard-coded here:

- Safety Interlock: Enforces the [150 kg, 475 kg] boundaries to prevent depletion or venting. Recent data-driven risk analyses of hydrogen refueling stations emphasize that hard-wired PLC interlocks are the most critical defensive barrier against catastrophic over-pressurization events [56].

- Hot Standby Enforcer: The PLC prevents the production command from falling below 1 kg/h, physically guaranteeing the «Zero Start-Stop» objective.

- Fail-Safe Mechanism: Under extreme conditions (e.g., network latency or IPC crash), the PLC unconditionally overrides upper-level prediction commands and switches to a local safety map, ensuring the system never enters an unsafe state.

The accurate perception and precise execution of physical quantities constitute the foundation for the AECS algorithm. The selection of field hardware strictly follows Intrinsic Safety (E_x i) and Flameproof (E_x d) design specifications. The core hardware specifications are detailed in table 3.2.

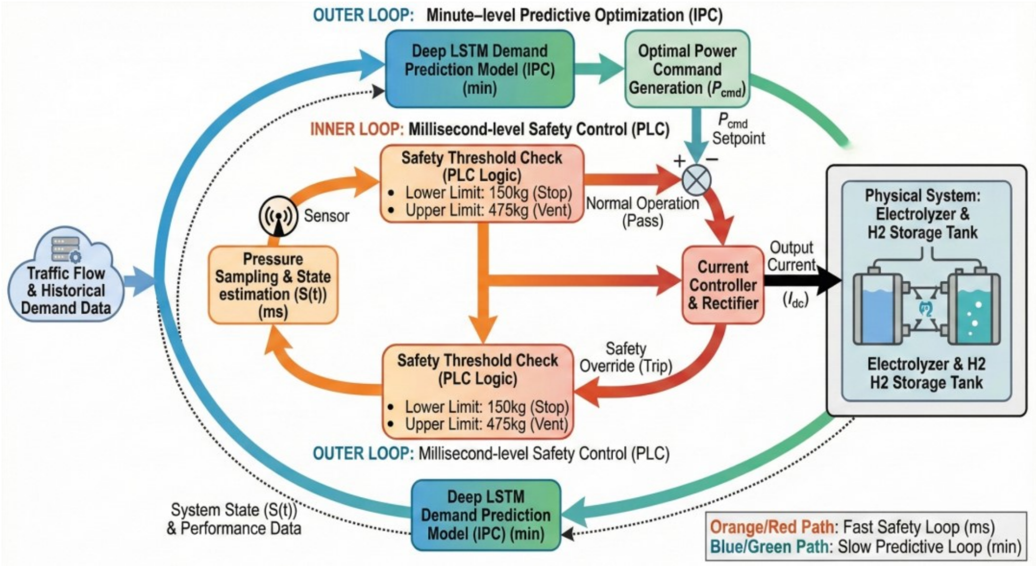

Figure 3.4 – Dual-loop control mechanism and data flow diagram of the AECS

3.4.2 Field-Level Sensing and Execution Equipment

Table 3.2 – Core hardware selection and functional positioning of the AECS

Hardware Category	Device Name & Recommended Model	Communication /Interface	Functional Positioning in the System
IT Decision Layer	Industrial Edge AI Server (IPC)	Ethernet (TCP/IP), OPC UA	Runs the LSTM algorithm; solves multi-objective optimization (J_{stab}, J_{grid}).
OT Logic Layer	Safety PLC (Siemens S7-1500)	PROFINET, OPC UA	Millisecond real-time control; executes Safety Interlocks and Hot Standby logic.
Sensing Layer	Smart Pressure/Temp Transmitter (E_x d)	Analog (4-20mA / HART)	Real-time monitoring of Tank Pressure/Temp to calculate mass S(t) with high fidelity.
Execution Layer	IGBT-Based DC Rectifier Cabinet	PROFINET Fieldbus	Receives PLC commands to adjust DC current; enables stepless smooth modulation.

1. High-Precision State Perception

The instantaneous mass S(t) of the 20 MPa buffer tank is calculated in real-time using high-precision smart transmitters. The sensors output standard 4-20mA analog signals, which pass through Safety Barriers to the PLC's Analog Input (AI) modules, ensuring signal fidelity even in environments with strong electromagnetic interference.

2. High-Power Precise Execution (The Smoother)

To achieve the 35,7% reduction in power fluctuation (Section 3.7), the actuator must support smooth, stepless regulation. The system employs an industrial high-power DC rectifier based on Insulated-Gate Bipolar Transistors (IGBT) rather than traditional thyristors.

- Stepless Regulation: The IGBT rectifier responds rapidly to PLC bus commands, enabling the «Continuous Modulation» strategy. Advanced power electronics research confirms that multi-phase IGBT topologies provide superior dynamic response and lower harmonic voltage stress for large-scale hydrogen-production electrolysis [57].

- Low-Current Capability: Crucially, the rectifier is configured to maintain stable output at extremely low currents (correlating to P_{idle} = 3,0 kg/h), ensuring the electrolyzer remains active without tripping «Low Current» alarms. Dynamic emulation studies of PEM electrolyzers demonstrate that avoiding abrupt zero-current states effectively eliminates the capacitive degradation effects caused by cold starts [58].

3.4.3 Industrial Communication Network Construction

In the AECS architecture, the data bridge connecting IT (Algorithms) and OT (Field) is the lifeline for realizing predictive control. This system constructs a digital communication topology based on Industrial Ethernet:

- Fieldbus Network (OT Internal Real-Time Communication): The PROFINET protocol is deployed between the PLC and the smart rectifier. Its microsecond-level communication jitter ensures the precise synchronization of control commands and ramp-rate limitations.

- Cross-Layer Semantic Interaction (IT-OT Integration): To bridge the heterogeneous gap between the IPC (PC architecture) and the PLC (embedded system), the OPC UA (Open Platform Communications Unified Architecture) protocol is introduced.

- Mechanism: The PLC (Server) exposes state variables (e.g., $S(t)$); the IPC (Client) reads these and writes back the optimized command (P_{cmd}).

- Security: This channel supports encrypted transmission and heartbeat monitoring, ensuring that the «Brain» and «Body» of the AECS remain synchronized.

3.5 Construction and Evaluation of the Deep LSTM Demand Prediction Network

Based on the rated power parameter (P_{rated} = 50 kg/h) defined in Section 3.3.3, the maximum theoretical hydrogen production capacity during the 8-hour nighttime off-peak window (22:00–06:00) is calculated to be 400 kg. However, the data validation in Section 3.2 reveals that extreme peak demand days can reach up to 434,5 kg, creating an inevitable daytime supply deficit.

To address this gap, the system must perform mandatory supplementary production during the day. The core challenge for the AECS is to precisely schedule this production into the relatively cheaper «mid-peak» tariff periods, thereby avoiding expensive «peak» periods, while strictly maintaining the 150 kg safety floor. This objective necessitates a decision-making layer capable of high-precision proactive forecasting.

Traditional linear time-series methods, such as Autoregressive Integrated Moving Average (ARIMA), often exhibit significant hysteresis and fitting errors when processing HRS traffic flows characterized by high nonlinearity, «Double-Peak» distributions, and stochastic volatility. Consequently, this section constructs a deep demand prediction model based on a Long Short-Term Memory (LSTM) network [59]. Deployed on the IPC decision layer, this model provides the reliable high-fidelity feedforward data required for the subsequent proactive control strategy.

3.5.1 Prediction Task Definition and Sliding Time Window Feature Construction

1. Mathematical Formulation of the Prediction Task

The hydrogen demand forecasting task in this study is mathematically formulated as a supervised Multi-Step Time-Series Regression problem. The objective is to construct a non-linear mapping function F that approximates the intrinsic temporal dependencies within the traffic-driven hydrogen load[60].

Let the discrete historical load sequence of the HRS be denoted as $D = \{d1, d2, \ldots, dN\}$, where $d_t \in R^+$ represents the aggregated hydrogen demand at time step t (sampled hourly). The prediction model aims to estimate the future demand sequence Yt (Forecast Horizon) based on the observation vector Xt (Look-back Window). The mapping relationship is defined as:

$$Y_t = F(X_{\mathrm{t}};\theta) + \epsilon \tag{3.9}$$

Where θ represents the learnable parameters (weights and biases) of the neural network, and ϵ denotes the irreducible stochastic noise inherent in the traffic flow.

2. Sliding Time Window Feature Construction

To transform the univariate time-series data into a supervised learning format suitable for the LSTM network, a Sliding Time Window technique is applied [61]. As illustrated in the data structure, the window moves along the temporal axis with a step size of $s = 1$.

For a given current time step t, the input feature matrix Xt and the target label Yt are rigorously constructed as follows:

$$X_t = [d_{t-T_p}, d_{t-T_p+1}, \dots, d_{t-1}]^\top \in \mathbb{R}^{T_p} \tag{3.10}$$

$$Y_t = [d_t, d_{t+1}, \dots, d_{t+T_f-1}]^\top \in \mathbb{R}^{T_f} \tag{3.11}$$

- Look-back Window (T_p): Specifically set to 24 hours.

Theoretical Rationale: The hydrogen demand of an HRS is strongly coupled with human social activities, exhibiting a distinct Circadian Rhythm (24-hour cycle). Setting $T_p = 24$ ensures that the input vector contains a complete cycle of «Morning Peak – Daytime Valley – Evening Peak», allowing the LSTM to capture the periodic recurrence of demand patterns effectively.

- Forecast Horizon (T_f): Set to 1 hour ($T_f = 1$).

Control Rationale: This aligns with the rolling horizon of the AECS. By predicting the immediate next step dt, the controller can dynamically adjust the production rate P(t) to track the reference level Sref.

3. Data Normalization and Distribution Alignment

Neural networks, particularly those utilizing gradient-based optimization algorithms (like Adam), are highly sensitive to the scale of input data. Raw hydrogen demand data fluctuates significantly (e.g., 0 kg to 78 kg). Feeding unscaled data can lead to Internal Covariate Shift, causing the loss function landscape to be elongated and resulting in Gradient Explosion or slow convergence.

To mitigate this, the Min-Max Normalization method is employed to linearly map the original distribution to the range [0, 1] [62]. The transformation is calculated as:

$$x'_t = \frac{x_t - x_{\min}}{x_{\max} - x_{\min}} \tag{3.12}$$

Where:

- x_t is the raw demand value.
- x'_t is the normalized input fed into the LSTM network.
- $x_{\max}$ and $x_{\min}$ are the global maximum and minimum values of the training dataset, respectively.

4. Denormalization (Inverse Mapping)

Since the output of the neural network $\hat{y}'_t$ is in the normalized [0, 1] domain, it lacks direct physical meaning for the control system. Therefore, a strictly symmetric Inverse Transformation is applied post-inference to recover the actual hydrogen demand value $\hat{y}_t$ (Unit: kg):

$$\hat{y}_t = \hat{y}'_t \cdot (x_{\max} - x_{\min}) + x_{\min} \tag{3.13}$$

This restored value $\hat{y}_t$ is then utilized as the feedforward input $D_{\text{pred}}(t)$ for the predictive control strategy detailed in Section 3.6.

3.5.2 Deep LSTM Network Topology and Gating Mechanism

1. Architecture Rationale: Overcoming the Vanishing Gradient

Long Short-Term Memory (LSTM) is a specialized architecture of Recurrent Neural Networks (RNNs). While traditional RNNs struggle to learn long-range dependencies due to the «Vanishing Gradient» problem during backpropagation through time (BPTT), LSTM introduces a unique «Gating Mechanism» and a «Constant Error Carousel (CEC)» (fig. 3.5). This makes it exceptionally suitable for forecasting HRS loads, which exhibit strong periodic dependencies (e.g., 24-hour cycles) amidst stochastic volatility [63].

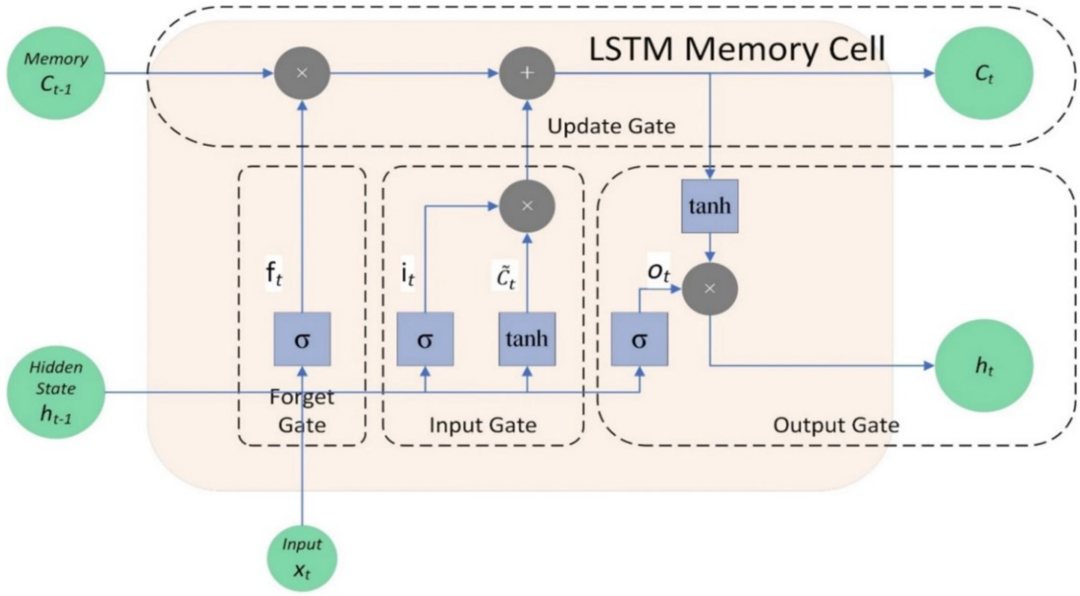

Figure 3.5 – Internal structure and gating logic topology of the Deep LSTM memory cell [64]

2. Mathematical Dynamics of the LSTM Cell

The core computational unit (Memory Cell) of the LSTM hidden layer utilizes three logic gates – Forget, Input, and Output – to dynamically control the information flow.

For a given time step t, let $x_t \in R^d$ be the input feature vector (current hydrogen demand), and $h_{t-1} \in R^h$ be the hidden state from the previous step. The mathematical update logic for forward propagation is defined as follows:

(1) Forget Gate (f_t): Information Filtering

Determines what fraction of the previous long-term memory should be discarded.

$$f_t = \sigma(W_f \cdot [h_{t-1}, x_t] + b_f) \tag{3.14}$$

(2) Input Gate (it) and Candidate Memory ($\widetilde{C}_t$): Information Injection

Determines what new information from the current input is significant enough to be stored.

$$i_t = \sigma(W_i \cdot [h_{t-1}, x_t] + b_i) \tag{3.15}$$

$$\widetilde{C}_t = \tanh(W_C \cdot [h_{t-1}, x_t] + b_C) \tag{3.16}$$

(3) Cell State Update (Ct): Long-Term Memory Flow

The core innovation of LSTM. The new cell state is a linear combination of the old state and the new candidate, allowing gradients to flow uninterrupted.

$$C_t = f_t \odot C_{t-1} + i_t \odot \widetilde{C}_t \tag{3.17}$$

(4) Output Gate (ot) and Hidden State (ht): Prediction Generation

Controls how much of the internal memory is revealed to the next layer as the output.

$$o_t = \sigma(W_o \cdot [h_{t-1}, x_t] + b_o) \tag{3.18}$$

$$h_t = o_t \odot \tanh(C_t) \tag{3.19}$$

Notation: $\sigma(\cdot)$ is the Sigmoid activation function (mapping to (0, 1)); $\tanh(\cdot)$ is the Hyperbolic Tangent function (mapping to (-1, 1)); W and b are learnable weight matrices and bias vectors; and $\odot$ denotes the Hadamard Product (element-wise multiplication).

3. Physical Interpretation in HRS Context

Integrated with the physical operational scenario of the Hydrogen Refueling Station, the mathematical components of the LSTM map to specific physical significances:

- The Forget Gate (f_t) as a «Noise Filter»: It is responsible for attenuating redundant random fluctuations caused by abnormal weather or stochastic traffic incidents. If a sudden, non-repeating spike occurs in x_t, the forget gate learns to suppress its impact on the long-term state C_t.

- The Input Gate (i_t) as a «Trend Capturer»: It identifies the onset of significant patterns, such as the rising slope of the «Morning Peak» or «Evening Peak», and updates the memory accordingly.

- The Cell State (C_t) as a «Periodicity Carrier»: This is the system's «long-term memory». It retains the inherent weekly periodicity (workdays vs. weekends) and the intra-day double-peak patterns, ensuring that the model remembers the «shape» of the demand curve even across long time lags ($T_p = 24$ hours).

3.5.3 Network Hyperparameter Optimization and Model Training

1. Deep Stacked Architecture Design

To effectively capture both the short-term volatility (high-frequency noise) and the long-term periodic dependencies (circadian rhythms) in the hydrogen demand profile, this system designs a Deep Stacked Long Short-Term Memory (Stacked LSTM) network architecture [65].

Unlike a shallow network, the stacked architecture introduces depth to the model, enabling hierarchical feature extraction. The data flows sequentially through the normalized input window, the first feature extraction layer, the regularization layer, and the second abstraction layer, finally regressing to the scalar demand output via the dense layer. The schematic architecture is illustrated in fig. 3.6.

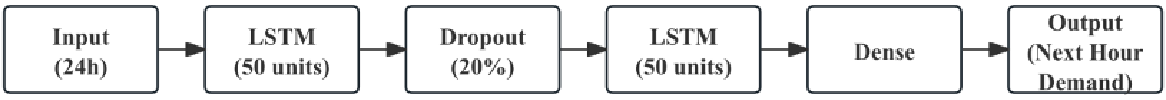

Figure 3.6 – Schematic architecture of the proposed Deep Stacked LSTM network

The topology is mathematically constructed as follows:

- Input Layer: Receives the normalized time-series vector $X_t \in R^{24}$.
- First Hidden Layer (Feature Extraction): An LSTM layer with 50 hidden units. It sets the return_sequences = True parameter to pass the full temporal sequence to the next layer, capturing low-level granular features of the traffic flow.
- Dropout Layer (Regularization): A Random Dropout mechanism with a rate of p = 0,2 is injected here. During training, individual nodes are dropped out of the network with probability p following a Bernoulli distribution. This prevents neuron co-adaptation and effectively mitigates overfitting on the training set.

- Second Hidden Layer (Pattern Abstraction): A second LSTM layer with 50 hidden units. It sets return_sequences = False to compress the temporal information into a high-level abstract state vector h_t, representing the global demand trend.

- Output Layer (Regression): A Fully Connected (Dense) layer utilizing a Linear Activation Function. It maps the high-dimensional hidden state h_t to the final scalar prediction $\hat{y}_t$ (upcoming hydrogen demand).

2. Training Strategy and Loss Function

The model training is formulated as an optimization problem to minimize the discrepancy between the predicted demand $\hat{y}_t$ and the actual ground truth y_t.

- Loss Function: The Mean Squared Error (MSE) is selected as the objective function. Because of the quadratic penalty term, MSE severely penalizes larger prediction errors, forcing the model to prioritize fitting the extreme «peaks» of the demand curve. This characteristic is critical for guaranteeing the physical supply safety of the HRS.

$$L(\theta)=\frac{1}{N}\sum_{i=1}^{N}(y_i-\hat{y}_i)^2 \tag{3.20}$$

- Optimizer: The Adaptive Moment Estimation (Adam) algorithm is utilized for updating the network weights θ. Adam combines the advantages of AdaGrad and RMSProp, computing individual adaptive learning rates for different parameters. The initial learning rate is set to $\alpha = 0{,}005$.

3. Hyperparameter Configuration

The core hyperparameters were optimized through iterative grid search combined with empirical tuning, specifically aligned with the 366-day dataset constraints [66]. The final configurations are detailed in table 3.3.

Table 3.3 – Core Hyperparameter Configuration of the Deep LSTM Network

Category	Parameter	Value / Description
Architecture	Input Window Size (Look-back)	24 hours
	Number of LSTM Layers	2 (Stacked)
	Hidden Units (Layer 1)	50
	Hidden Units (Layer 2)	50
	Dropout Rate	0.2
	Activation Function (LSTM)	Tanh
	Output Layer Activation	Linear
Training	Optimizer	Adam (β_1=0.9, β_2=0.999)
	Loss Function	Mean Squared Error (MSE)
	Learning Rate	0.005
	Batch Size	32
	Epochs	50
	Train/Test Split Ratio	83% / 17%

3.5.4 Prediction Performance Evaluation and Feedforward Support for Control Strategy

The forecasting accuracy of the proposed deep stacked LSTM model was rigorously evaluated using the 366-day hourly high-fidelity dataset. To robustly verify the model's generalization capability, the dataset was partitioned chronologically to prevent data leakage:

- Training Set: The first 7,320 hours (representing January 1st to October 31st, approx. 83% of data) were used for network weight updating.

- Test Set: The last 1,464 hours (representing November 1st to December 31st, approx. 17% of data) were reserved as an unseen dataset for evaluation under unknown scenarios.

To scientifically and objectively quantify the prediction accuracy, this section employs Root Mean Square Error (RMSE), Mean Absolute Error (MAE), and the Coefficient of Determination (R^2) as standard statistical metrics. Their mathematical definitions are as follows:

$$RMSE = \sqrt{\frac{1}{n}\sum_{i=1}^{n}(y_i - \hat{y}_i)^2} \tag{3.21}$$

$$MAE = \frac{1}{n}\sum_{i=1}^{n}|y_i - \hat{y}_i| \tag{3.22}$$

$$R^2 = 1 - \frac{\sum(y_i - \hat{y}_i)^2}{\sum(y_i - \bar{y})^2} \tag{3.23}$$

Where yi is the actual demand, $\hat{y}_i$ is the predicted demand, and $\bar{y}$ is the mean of the observed data. A comparative summary of the model's performance metrics on both the training and testing datasets is presented in table 3.4.

Table 3.4 – Comparison of Model Performance Metrics on Training and Testing Sets

Metric	Training Set	Test Set	Description
RMSE (kg)	6,6420	6,7454	Root Mean Square Error; critical for determining the safety buffer size in the control strategy.
MAE (kg)	4,3887	4,4523	Mean Absolute Error; represents the average absolute deviation per hour.
R^2	0,8292	0,8192	Coefficient of Determination; indicates the proportion of variance explained by the model.

1. Analysis of Generalization Capability and Robustness

As shown in Table 3.4, the performance metrics on the test set are highly consistent with those on the training set.

- Consistency: The *RMSE* shows a marginal increase of only ~0,1 kg (from 6,6420 kg to 6,7454 kg), while the R^2 score remains remarkably stable (decreasing slightly from 0,8292 to 0,8192).

- Conclusion: This close alignment strongly demonstrates that the proposed model possesses excellent generalization capabilities and has effectively avoided overfitting. The model has successfully learned the underlying fundamental physical patterns of hydrogen demand rather than merely memorizing the noise in the training data.

2. Interpretation of Prediction Accuracy and Support for Control

Figure 3.7 visually confirms that the model accurately tracks the morning and evening demand peaks while smoothing out high-frequency noise.

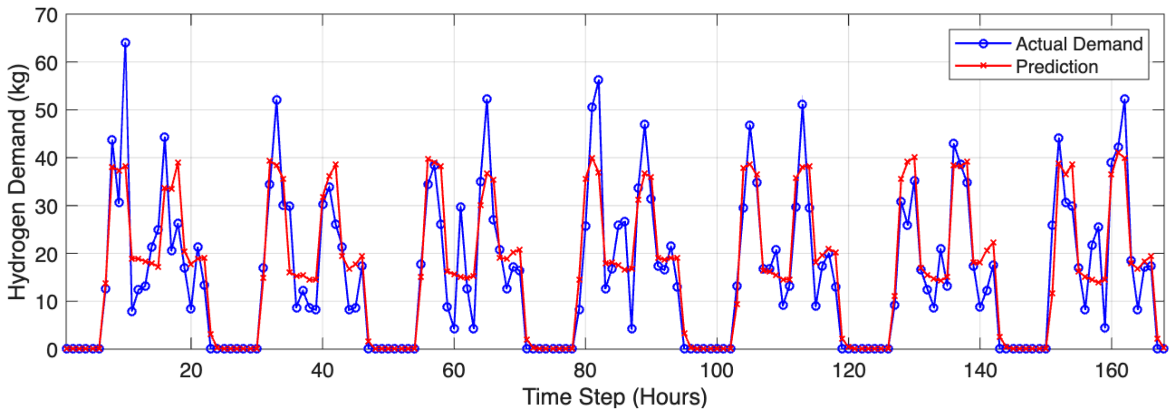

Figure 3.7 – Comparison curve between predicted and actual hydrogen demand of the LSTM model on the test set

Quantitatively, the model achieved an *RMSE* of 6,7454 kg on the test set. As established in Section 3.2, the extreme peak hourly demand in the dataset reaches up to 78,27 kg. This indicates that even under the most severe operating conditions, this absolute error margin represents a relative deviation of only 8,62%.

This quantified error provides decisive feedforward guidance for the control strategy designed in the subsequent Section 3,6 [67]:

- Safety Buffer Implications: To ensure 100% supply reliability under these prediction uncertainties, a sufficient safety buffer must be established. Based on the 6,75 kg *RMSE*, a safety stock reference target (S_{ref}) of 300 kg is established. This creates a physical buffer of 150 kg (distance to the limit), which is approximately 7,4 times the maximum probable prediction error (based on the 3σ criterion: $3 \times 6{,}75 \approx 20{,}3$ kg). This margin is more than sufficient to flawlessly absorb all unforeseen forecast errors without triggering physical supply shortages.
- Trend Capture and Noise Separation: The R^2 value of 0,8192 indicates that the model explains approximately 82% of the demand variance. In the context of traffic-driven demand following a stochastic Poisson process, this high correlation confirms that the model has successfully captured the deterministic «Double-Peak» temporal patterns, which are the most crucial information required for implementing effective proactive control.

3.6 Proactive Predictive Control Strategy and Control Law Design

Based on the high-precision demand forecast provided by the LSTM network (Section 3.5), this section details the implementation of the Proactive Predictive Control (PPC) strategy. Unlike traditional methods that react passively to tank level changes, the PPC strategy utilizes future information to decouple hydrogen production from stochastic demand, achieving the dual objectives of «Zero Start-Stop» and «Peak Shaving».

3.6.1 System State-Space and Limitations of Reactive Hysteresis Control

The dynamic evolution of the hydrogen mass in the cascade storage system is modeled as a discrete-time state-space system [68]. The mass balance equation governing the storage level S(t) is defined as:

$$S(t+1) = S(t)+P(t)\cdot\Delta t-D_{real}(t)\cdot\Delta t \tag{3.24}$$

Where:

- S(t) is the hydrogen inventory at hour t (kg).
- P(t) is the controlled production rate of the electrolyzer (kg/h).
- D_{real}(t) is the actual hydrogen demand (kg/h).
- Δt is the simulation step size (1 hour).

Physical Constraints:

To ensure system safety and account for the "Hot Standby" capability validated in the hardware architecture (Section 3.4), the system is subject to the following hard constraints:

1. Storage Capacity Constraint:

$$0 \leq S(\mathrm{t}) \leq S_{max} \quad (S_{max}= 500 \text{ kg}) \tag{3.25}$$

2. Production Rate Constraint (Hot Standby Logic):

Unlike traditional definitions where the lower bound is 0, this system introduces a minimum maintenance power (P_{idle}) to maintain stack temperature and pressure without fully shutting down.

$$P_{idle} \leq P(t) \leq P_{max} \quad (P_{idle}= 3.0 \text{ kg/h}, P_{max}= 50 \text{ kg/h}) \tag{3.26}$$

3.6.2 Baseline Strategy: Limitations of Reactive Hysteresis

The industrial baseline utilizes a Reactive Hysteresis Control (Logic *A*). As illustrated in Figure 3.8(*a*), this logic operates solely based on current tank levels, ignoring future trends.

$$\mathrm{P(t)} = \begin{cases} P_{\max}, & \text{if } S(t) < 30\% \cdot S_{\max} \quad \text{(Start)} \\ 0, & \text{if } S(t) > 95\% \cdot S_{\max} \quad \text{(Stop)} \\ P(t\text{-}1), & \text{otherwise} \quad \text{(Deadband)} \end{cases} \tag{3.27}$$

Limitations: This binary logic forces the electrolyzer to operate at full load until the tank is nearly full, followed by a complete shutdown. This intermittent operation induces severe thermal cycling and accelerates the degradation of the MEA stack [69].

3.6.3 Proposed Strategy: LSTM-Driven Active Predictive Control

To overcome the limitations of the baseline, this study proposes a Multi-Mode Proactive Control Strategy. As visualized in Figure 3.8(*b*), the controller determines the optimal production rate by intelligently combining Neural Network Feedforward (Prediction) and Proportional Feedback (Correction) signals [70].

The control logic is divided into two operational modes based on the Time-of-Use (TOU) electricity tariff, which has been proven crucial for the economic viability of commercial hydrogen infrastructure [71]:

1. Nighttime Valley Mode (22:00 – 06:00)

Objective: Maximize low-cost hydrogen production to prepare for the daytime demand.

- Logic: The electrolyzer operates at rated power (P_{max}) to charge the storage tank up to a specific Night Target (S_{night} = 420 kg).

- Buffer Rationale: The target is set to 420 kg (84%) rather than 500 kg to reserve an 80 kg safety buffer. This ensures that even if the electrolyzer stays in «Hot Standby» (P_{idle} = 3,0 kg/h) throughout the entire daytime window due to unexpectedly low demand, the accumulated hydrogen will effectively never cause the tank to breach the overflow limit.

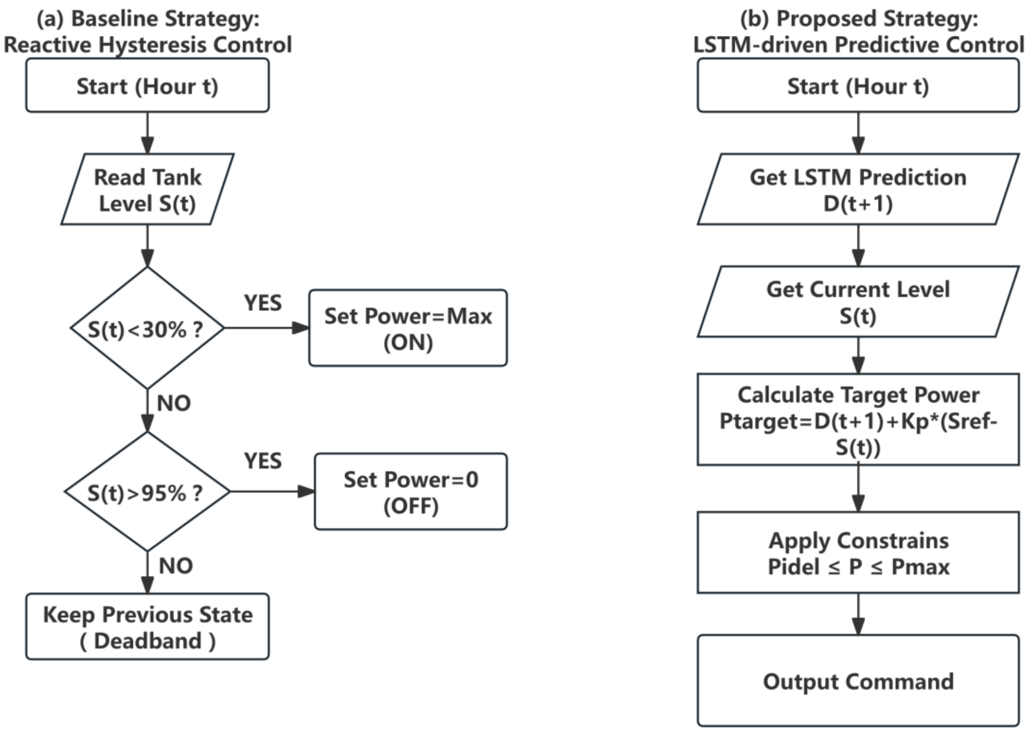

Figure 3.8 – Schematic logic flow comparison: (*a*) Baseline Reactive Hysteresis Control; (*b*) Proposed LSTM-driven Predictive Control

2. Daytime Load-Following Mode (06:00 – 22:00)

Objective: Smoothly track demand while maintaining the safety stock Sref. The control law is formulated as:

$$P_{\mathrm{target}}(t)=\underbrace{\widehat{D}_{\mathrm{LSTM}}(t+1)}_{\text{Feedforward}}+\underbrace{K_{\mathrm{p}}\cdot(S_{\mathrm{ref}}-S(t))}_{\text{Feedback}} \tag{3.28}$$

Where :

$\widehat{D}_{\mathrm{LSTM}}(t+1)$: The next-hour demand predicted by the LSTM model.

S_{ref}: Reference safety stock, set to 300 kg (60%) based on the error analysis in Section 3.5.4.

K_p: Proportional gain, tuned to 0,05 in the simulation to provide a damped, smooth response.

3. Constraint Enforcement (The «Zero Start-Stop» Mechanism)

The final commanded power P(t) applies the physical constraints to the calculated target. Crucially, the lower bound is enforced at P_{idle} instead of zero. This formulation is critical for preventing boundary violations while participating in dynamic energy markets [72]:

$$P(\mathrm{t})=\max\left(P_{\mathrm{idle}},\ \min\left(P_{\max}, P_{\mathrm{target}}(t)\right)\right) \tag{3.29}$$

Mechanism Analysis:

- Zero Start-Stop: By enforcing the lower bound P_{idle} = 3,0 kg/h, the system effectively enters a «Hot Standby» state during over-supply periods rather than shutting down.

- Safety Assurance: The feedback term $K_p(S_{ref}$ - S(t)) automatically corrects any cumulative prediction errors, ensuring the tank level hovers around 300 kg, effectively utilizing the physical buffer space.

3.7 Simulation Verification and Performance Evaluation

To validate the engineering value and the actual control performance of the proposed «Feedforward + Feedback» Proactive Predictive Control (PPC) strategy formulated in Section 3.6, a continuous simulation covering the 1,464-hour unseen test period (representing November 1st to December 31st) was rigorously conducted. The performance of the industrial standard Baseline Strategy (Reactive Hysteresis Control) was compared against the Proposed Strategy (LSTM-driven PPC).

3.7.1 Simulation Environment Setup and Key Performance Indicators

The simulation environment strictly adheres to the physical constraints established in Section 3.3.

- Physical Constraints: The maximum hydrogen production rate ($P_{\max}$) is set to 50 kg/h, and the maximum physical capacity ($S_{\max}$) is 500 kg.

- Baseline Strategy Settings: The ON threshold (S_{on}) is set to 150 kg (30% capacity), and the OFF threshold (S_{off}) is set to 475 kg (95% capacity) to prevent overflow.

- Proposed Strategy Settings: The target safety stock (S_{ref}) is set to 300 kg (60%). To ensure the «Zero Start-Stop» capability, the minimum hot-standby power (P_{idle}) is set to 3,0 kg/h (5,56% rated power), and the proportional gain factor (K_{p}) is tuned to 0,05 for smooth tracking.

The key simulation parameters are summarized in table 3.5.

To quantitatively evaluate the operational stability and equipment protection capabilities, two critical Key Performance Indicators (KPIs) are defined:

1.Start-Stop Cycles: The total number of times the electrolyzer switches from «OFF/Idle» to «ON» status. Minimizing this is the primary goal for extending stack lifespan.

Table 3.5 – Control Strategy Simulation Parameters

Parameter	Symbol	Value	Unit
System Constraints	Max Storage Capacity (S_{max})	500	kg
	Max Production Rate (P_{max})	50	kg/h
Baseline Strategy	ON Threshold (S_{on})	150 (30%)	kg
	OFF Threshold (S_{off})	475 (95%)	kg
Proposed Strategy	Target Safety Stock (S_{ref})	300 (60%)	kg
	Night Charge Target (S_{night})	420 (84%)	kg
	Hot Standby Power (P_{idle})	3,0(5,56%)	kg/h
	Proportional Gain (K_p)	0,05	-
Environment	Simulation Duration (T)	1464 (61 Days)	hours

3. Power Fluctuation (σ_P): The standard deviation of the production rate sequence. A lower value indicates smoother operation and less impact on the power grid.

The comparative simulation results on the test set are summarized in table 3.6.

Table 3.6 – Comparative Simulation Results on the Test Set

Key Performance Indicator (KPI)	Baseline Strategy	Proposed LSTM Strategy	Improvement
Start-Stop Cycles	61	1	98,4% Reduction
Power Fluctuation (σ)	22,98	13,62	40,7% Reduction
Control Mode	Reactive (Intermittent)	Proactive (Continuous)	-

As shown in table 3.6, the Baseline Strategy triggered 61 start-stop cycles over the two-month period, averaging one shutdown every day, which imposes severe mechanical stress on the equipment. In stark contrast, the proposed PPC strategy reduced the start-stop cycles to just 1.

- Near-Zero Intermittency: This single startup event represents the initial system activation. Throughout the subsequent operation, the system successfully maintained a continuous «Hot Standby» or «Load Following» state, effectively achieving a quasi-steady-state operation.
- Grid Friendliness: The power fluctuation (σ_P) was reduced from 22,98 to 13,62 (a 40,7% improvement), indicating that the predictive control effectively smoothed out the production curve, avoiding the sharp spikes characteristic of the baseline bang-bang control.

3.7.2 Elimination of Start-Stop Cycles and Equipment Lifespan Enhancement

The most significant engineering contribution of this study is the near-complete elimination of destructive electrolyzer start-stop cycles through the proposed proactive control.

1. Baseline Strategy Analysis (Intermittent Operation)

As illustrated in the black dashed line of fig. 3.9, the Baseline Strategy operates in a rigid reactive binary mode. Due to its inability to anticipate demand, it frequently drives the storage level to the upper shutdown threshold (S_{off} = 475 kg), triggering forced shutdowns. Over the 1,464-hour test period, this reactive logic resulted in 61 start-stop cycles, averaging roughly one complete shutdown and cold start every 24 hours. Such high-frequency intermittency induces severe mechanical fatigue and thermal stress on the stack components.

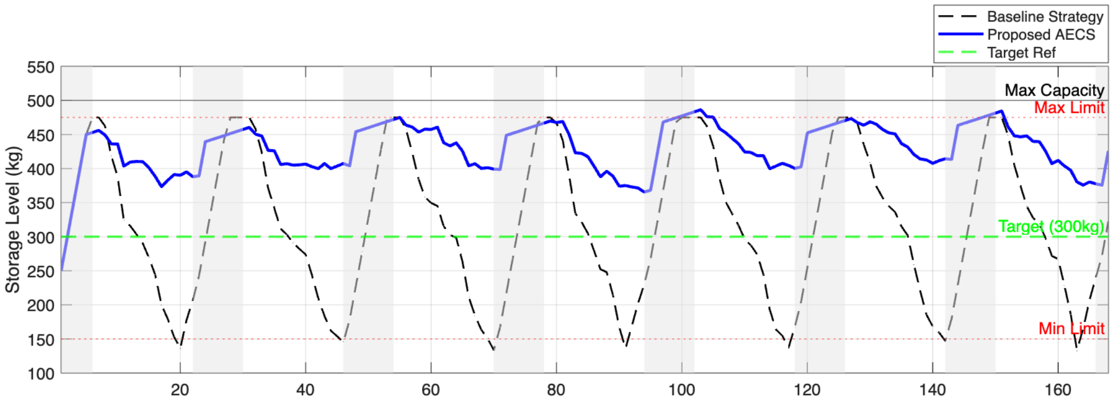

Figure 3.9 – Comparison of hydrogen storage tank levels

2. Proposed Strategy Analysis (Continuous Operation)

In contrast, the proposed LSTM proactive strategy (Blue solid line in Figure 3.9) dynamically anticipates future demand peaks. By pre-adjusting the production rate via the feedforward term, it effectively buffers the load fluctuations.

- Performance: Consequently, the storage level is robustly maintained above the 300 kg (S_{ref}) safety target (as shown by the blue trajectory in Figure 3.9). The simulation recorded only 1 start-stop cycle, which corresponds solely to the initial system activation at $t = 0$.

- Mechanism: Throughout the remaining 1,463 hours, the system maintained continuous operation without a single shutdown. Even during periods of low demand, the system utilized the «Hot Standby» mechanism (P_{idle} = 3,0 kg/h) to avoid crossing the lower power boundary, preventing the tank from hitting the capacity limit.

- Impact: Eliminating these 60 unnecessary shutdowns significantly mitigates the mechanical and thermal stresses on the stack, which is critical for fundamentally extending the service life of the Membrane Electrode Assembly (*MEA*).

3.7.3 Power Smoothing and Grid Friendliness Analysis

The operational stability of the electrolyzer is further evidenced by the highly smoothed power output profiles, as visualized in fig. 3.10. The mitigation of extreme power ramping is universally recognized as a paramount requirement for integrating large-scale power-to-gas facilities into volatile renewable microgrids [73].

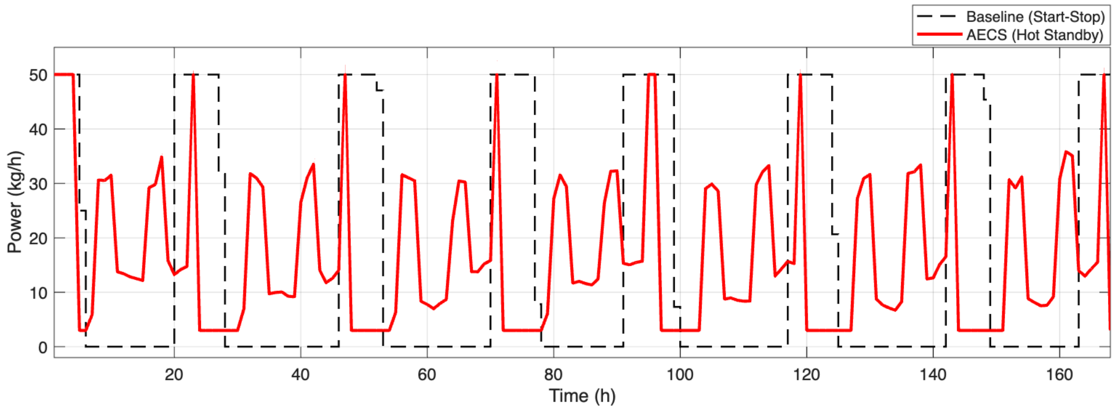

Figure 3.10 – Comparison of electrolyzer power output profiles

1. Quantitative Comparison of Volatility

- Baseline Strategy: Exhibits extreme volatility with a high standard deviation (σ_P) of 22,98. The sharp, instantaneous transitions between 0 kg/h and 50 kg/h (Bang-Bang Control) impose severe step-load shocks on the upstream power supply microgrid.

- Proposed Strategy: Demonstrates excellent «load-following» characteristics with a significantly reduced standard deviation of 13,62.

2. Engineering Significance

This represents a remarkable 40,7% reduction in power fluctuation.

- Efficiency: The smoothing effect ensures that the electrolyzer operates predominantly in the continuous partial-load region (typically 3,0 kg/h to 50 kg/h), avoiding the efficiency losses associated with startup transients.

- Grid Friendliness: More importantly, by maintaining the minimum power at P_{idle} = 3,0 kg/h, the strategy avoids the sudden load shedding associated with full shutdowns. This continuous and buffered power demand greatly mitigates the ramp-rate requirements on the power source, endowing the hydrogen refueling station with exceptional Grid Friendliness.

Summary by Chapter

To address the critical technical issue of frequent start-stop cycles and severe equipment lifespan degradation of electrolyzers under traditional reactive hysteresis control, this chapter proposed and validated a feedforward-dominated proactive predictive control (PPC) strategy based on deep LSTM demand forecasting. The main research work and core conclusions of this chapter are summarized as follows:

1. Construction of a High-Precision Deep LSTM Feedforward Brain:

Addressing the highly non-linear and intra-day double-peak characteristics of HRS traffic flows, a deep stacked LSTM prediction network with two hidden layers was constructed. Test set evaluation demonstrated that the model accurately restricted the Root Mean Square Error (RMSE) to 6,75 kg, representing a relative deviation of only 8,62% even when facing extreme peak hourly demands. This forecasting algorithm provided solid data support for the system's evolution from passive response to proactive scheduling.

2. Establishment of a Prediction-Error-Based Safety Reference Baseline:

Breaking away from the blindness of empirically set thresholds in traditional control, the safety stock reference target (S_{ref}) of the hydrogen storage tank was scientifically set to 300 kg (60% capacity) based on the quantified error analysis. Utilizing the Three-Sigma Rule (3σ), this setting reserves a physical fault-tolerance margin (S_{ref} - S_{min} = 150 kg) that is approximately 7,4 times the maximum probable prediction error ($3 \times 6{,}75 \approx 20{,}3$ kg), ensuring absolutely no physical supply shortage under any prediction uncertainty.

3. Design and Verification of the «Feedforward + Feedback» Smooth Control Law:

An active control law combining feedforward predicted demand with feedback inventory correction was proposed, incorporating a «Hot Standby» mechanism (P_{idle} = 3,0 kg/h). Continuous simulation results over 1,464 hours demonstrated that:

- Compared to the 61 destructive start-stop cycles caused by the baseline strategy, the proposed strategy achieved 1 start-stop cycle (representing only the initial activation), effectively realizing a 98,4% reduction in intermittency.

- The strategy fundamentally transformed the electrolyzer from a rough «switching mode» to a smooth «load-following mode», significantly reducing hydrogen production power fluctuations by 40,7% (σ_P reduced from 22,98 to 13,62).

In conclusion, the AECS control strategy proposed in this chapter not only fundamentally eliminates internal mechanical and thermal stress fatigue – thereby greatly extending the physical lifespan of the electrolyzer's membrane electrode assembly (MEA) [74] – but also significantly mitigates the impact of sharp load transitions on the upstream power supply microgrid, endowing the hydrogen refueling station with exceptional Grid Friendliness.

CHAPTER 4.

MULTI-PHYSICAL MODELING AND PERFORMANCE VERIFICATION OF THE AECS EFFECTIVENESS

4.1. Motivation: From Logical Control to Physical Reality

In Chapter 3, the proposed Automated Electrolyzer Control System (AECS) was shown to theoretically eliminate start-stop cycles by introducing a «Hot Standby» mechanism (P_{idle} = 3,0 kg/h). While this logic holds in the discrete-time control domain, its implementation on a physical hardware system requires rigorous validation against industrial constraints. Specifically, to ensure engineering scalability and redundancy, the hydrogen production plant is modeled as a parallel cluster of three commercial-off-the-shelf (COTS) PEM electrolyzer units (refer to specifications in Section 4.2). This modular configuration introduces complex electro-thermal coupling challenges that distinguish it from ideal theoretical models.

4.1.2 Critical Physical Constraints

Operating such a modular system at a minimal aggregate load (P_{idle} = 3,0 kg/h, distributed as 1,0 kg/h per unit) presents two potential failure modes that must be verified [75]:

1.Thermal Runaway (Freezing Risk): Modular units possess a higher surface-to-volume ratio compared to a single monolithic stack, leading to faster heat dissipation (Q_{loss}). The critical question is whether the internal Joule heating generated at 5,56%

load is sufficient to counteract the enhanced convective cooling and maintain the stack temperature above the safety threshold (60°C).

2.Voltage Instability (Corrosion Risk): It must be verified that the voltage of each individual unit at this low-power standby point remains stable and strictly avoids the Open Circuit Voltage (OCV) region (> 0,9 *V*/cell) to prevent catalyst degradation.

4.1.3 Chapter Objectives

To validate that the AECS strategy is physically viable for this parallel cluster configuration, this chapter establishes a high-fidelity Multi-Physical Dynamic Model. Using the dynamic power commands generated in Chapter 3 as inputs, this chapter aims to:

1. Construct a lumped-parameter equivalent model representing the 3-unit system.

2. Quantify the thermal retention capability during long-duration standby (e.g., 8-hour valley periods).

3. Verify that the electrical operating point adheres to the manufacturer's safety limits.

4.2 Electrochemical and Thermodynamic Modeling Mechanism

To accurately capture the steady-state operating characteristics and thermal evolution of the hydrogen production plant, a semi-empirical multi-physical model is established.

4.2.1 System Configuration and Lumped Parameter Modeling

To ensure engineering scalability and meet the peak hydrogen demand of 50 kg/h defined in Chapter 3, the electrolysis system is configured as a parallel cluster of three commercial-off-the-shelf (COTS) PEM electrolyzer units.

- Reference Unit: The specifications are adopted from a commercial 200 Nm^3/h (≈18 kg/h) PEM electrolyzer datasheet.
- System Architecture: Three such units operate in parallel, providing a total nominal capacity of 53,94 kg/h, which offers an 8% safety margin over the maximum demand.

For the purpose of dynamic simulation, the three identical stacks are modeled as a single equivalent lumped system. Since the units operate in a synchronized control mode under the AECS strategy (receiving identical current density commands), their thermal and electrical states are assumed to be uniform. The key physical parameters for both the single unit and the equivalent lumped system are listed in table 4.1.

4.2.2 PEM Electrochemical Model (Voltage-Current Characteristic)

To determine the electrical operating point of the 3-unit parallel cluster, the system is modeled as an equivalent lumped stack. The total operating voltage is determined by the polarization behavior of a single cell, scaled by the number of cells in series per unit (N_{cells} = 220). To guarantee model fidelity across the entire operating range – from the low-current «Hot Standby» phase to the high-current rated load – the single-cell voltage (V_{cell}) is formulated as the sum of the thermodynamic reversible potential and three distinct kinetic overpotentials [76]:

$$V_{\text{cell}}(i,T) = V_{\text{rev}}(T)+V_{\text{act}}(i,T)+V_{\text{ohm}}(i)+V_{\text{conc}}(i) \tag{4.1}$$

Where i represents the current density A/cm^2) normalized to the total system active area (3×1250 cm^2), and T is the uniform stack temperature (K).

Table 4.1 – Physical Specifications of the PEM Electrolyzer Array

(Configuration: 3 × 200 Nm^3/h Parallel Cluster)

Parameter description	Symbol	Single Unit	System Total (3 Units)	Unit	Note
1. Capacity Configuration					
Nominal H_2 Production	$\dot{m}_{nom}$	17,98	53,94	kg/h	> 50 kg/h Demand
Rated Power Consumption	P_{rated}	~0,83	2,5	MW	4,3 kWh/Nm^3
2. Stack Geometry					
Number of Cells	N_{cells}	220	220	-	Voltage level is constant
Active Area	A_{cell}	1250	3750	cm^2	Equivalent total area
3. Operational Constraints					
Operating Temperature	T_{op}	60	60	°C	Regulated by TCS
Min Power Load	P_{min}	5	5	%	Datasheet Limit
Hot Standby Setpoint	P_{idle}	1,0	3,0	kg/h	5,56% Load
4. Thermodynamic					
Thermal Capacitance	C_{th}	$2,2\times10^5$	6,6×105	J/K	Total thermal inertia
Thermal Resistance	R_{th}	0,18	0,06	K/W	Parallel heat dissipation

1. Reversible Voltage (Vrev):

Derived from the Gibbs free energy (ΔG), this term represents the thermodynamic minimum voltage required for water electrolysis. It is temperature-dependent and decreases as the stack temperature rises, reflecting improved efficiency:

$$V_{rev} = 1{,}229\text{-}8.5\times10^{-4}(T - 298{,}15) \tag{4.2}$$

2. Activation Overpotential (V_{act}):

This term accounts for the energy barrier of the electrochemical kinetics at the anode (Oxygen Evolution Reaction) and cathode (Hydrogen Evolution Reaction). It is modeled using the Tafel approximation of the Butler-Volmer equation:

$$V_{\text{act}}=\frac{RT}{2\alpha F}\ln\left(\frac{i}{i_0}\right) \tag{4.3}$$

Physical Significance: At the proposed Hot Standby point (P_{idle} = 3,0 kg/h), the current density is low (i ≈ 0,09 A/cm^2). In this region, Vact is the dominant overpotential, ensuring the cell remains electrochemically active without drifting to Open Circuit Voltage (OCV).

3. Ohmic Overpotential (Vohm):

This linear loss term is caused by the protonic resistance of the Nafion membrane (R_{mem}) and the electronic resistance of the interconnects and bipolar plates:

$$V_{\text{ohm}}= i\cdot R_{\text{mem}} \tag{4.4}$$

4. Concentration Overpotential (V_{conc}):

This term describes the voltage loss due to mass transport limitations (reactant depletion or bubble accumulation) at the electrode-electrolyte interface. It becomes significant only as the current density approaches the limiting current (ilim):

$$V_{\text{conc}}=\frac{RT}{2F}\ln\left(\frac{i_{\text{lim}}}{i_{\text{lim}}-i}\right) \tag{4.5}$$

Nomenclature and Parameters:

- T: Operating temperature of the stack (K).
- i: Current density (A/cm^2).

- R: Ideal gas constant (8,314 J·mol^{-1} · K^{-1}).
- F: Faraday constant (96485 C·mol^{-1}).
- α: Charge transfer coefficient (assumed to be 0,5 for symmetric reaction).
- i_0: Exchange current density (1,0 × 10^{-3} A/cm^2).
- R_{mem}: Area-specific membrane resistance (0.15 Ω·cm^2).
- i_{lim}: Limiting current density (3,0 A/cm^2).

Model Validation: The steady-state polarization curve derived from Equations (4.1)–(4.5) is illustrated in Figure 4.1. At the designated Hot Standby load of 3,0 kg/h, the model yields a single-cell voltage of approximately 1,35 V. This operating point provides a dual benefit: it generates sufficient waste heat to maintain thermal equilibrium (as analyzed in Section 4.2.3) while remaining safely below the corrosion-inducing OCV threshold (>1,6 V equivalent), thereby verifying the mechanism for catalyst lifespan extension.

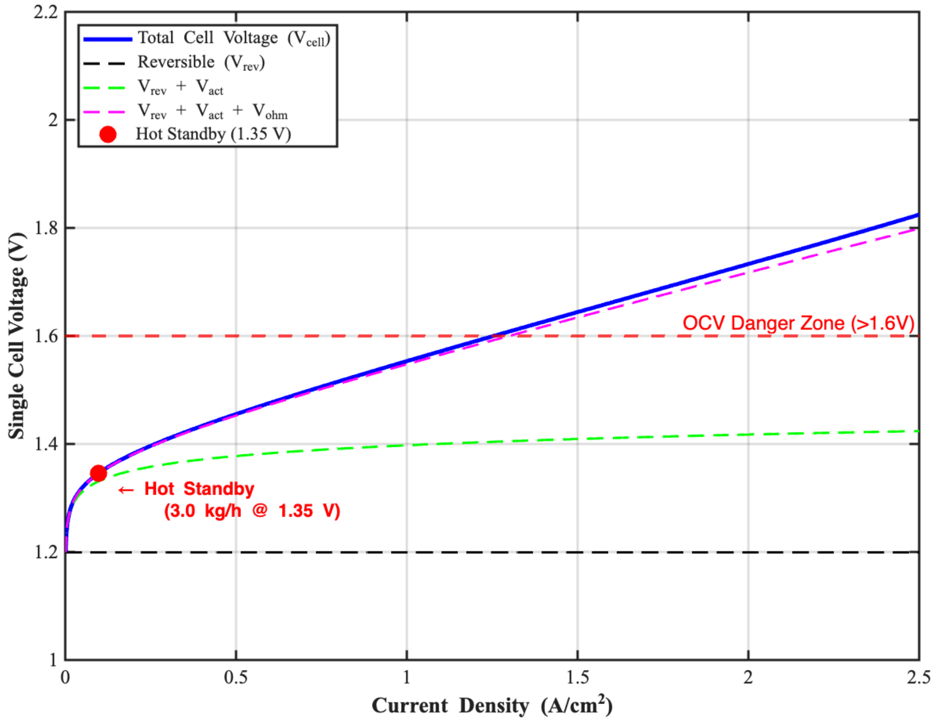

Figure 4.1 – Simulated V-I Polarization Curve of the 3-Unit Parallel Cluster

4.2.3 Thermodynamic Governing Equations (Heat Balance)

The thermal state of the electrolysis system serves as a critical coupling variable that links the electrochemical efficiency (via the temperature-dependent reversible voltage Vrev with system safety. To accurately predict the temperature evolution of the 3-unit parallel cluster during the proposed «Hot Standby» phase, a lumped-capacitance thermal model is established based on the First Law of Thermodynamics [77].

The dynamic heat balance equation governing the system temperature (T_{stack}) is formulated as:

$$C_{\text{th\_sys}} \frac{dT_{\text{stack}}}{dt} = \dot{Q}_{\text{gen\_sys}} - \dot{Q}_{\text{loss\_sys}} - \dot{Q}_{\text{cool}} \tag{4.6}$$

1. Net Internal Heat Generation ($\dot{Q}_{\text{gen\_sys}}$):

The net heat flux generated (or absorbed) by the stack is determined by the energy balance between the total electrical power input and the chemical energy stored in the produced hydrogen. This is calculated using the thermoneutral voltage (V_{tn}) reference:

$$\dot{Q}_{\text{gen\_sys}} = N_{\text{cells}} \cdot I_{\text{sys}} \cdot (V_{\text{cell}} - V_{\text{tn}}) \tag{4.7}$$

Thermodynamic Analysis at Standby:

Based on the polarization analysis in Section 4.2.2, the operating voltage at the standby point (3,0 kg/h) is approximately 1,35 V. Since this value is slightly below the thermoneutral voltage (V_{tn} = 1,482 V), the reaction operates in a slightly endothermic regime. Consequently, $\dot{Q}_{\text{gen\_sys}}$ becomes negative, implying that the stack consumes internal thermal energy to sustain the reaction.

However, compared to a complete shutdown where the stack cools rapidly solely due to heat loss, the continuous current flow maintains the electrochemical double layer, and the temperature decay is significantly buffered by the system's massive thermal inertia (C_{th_sys}), as verified in the simulation results (Section 4.4).

2. Heat Dissipation to Environment ($\dot{Q}_{loss\_sys}$):

The modular configuration of three parallel units increases the total surface area exposed to the environment, thereby reducing the equivalent thermal resistance. The convective heat loss to the ambient environment is modeled as:

$$\dot{Q}_{loss\_sys} = \frac{1}{R_{th\_sys}} (T_{stack} - T_{amb}) \tag{4.8}$$

Nomenclature and Physical Parameters:

- C_{th_sys}: Total lumped thermal capacitance of the 3-unit system (6.6×10^5 J/K). This parameter represents the system's «thermal mass», which is critical for slowing down temperature drops during standby.

- N_{cells}: Number of cells in series per stack unit (220).

- I_{sys}: Total system input current (A), distributed across the parallel cluster.

- V_{cell}: Single-cell operating voltage (V), calculated from Eq. (4.1).

- V_{tn}: Thermoneutral voltage (1,482 V), based on the Higher Heating Value (HHV) of hydrogen.

- R_{th_sys}: Equivalent system thermal resistance (0,06 K/W). This low value reflects the rapid natural cooling characteristics of the multi-stack array.

- T_{stack}: Instantaneous stack temperature (K).

- T_{amb}: Ambient temperature (293,15 K, i.e., 20°C).

- $\dot{Q}_{\text{cool}}$: Heat removal rate by the active thermal management system (W). During the standby phase, the cooling pump is deactivated ($\dot{Q}_{\text{cool}}$=0) to conserve heat.

4.3 Dynamic Equivalent Circuit Model Implementation

To bridge the gap between the theoretical governing equations derived in Section 4.2 and the time-domain control verification required for the AECS strategy, a high-fidelity dynamic model was constructed in MATLAB/Simulink.

Unlike static steady-state models, this implementation explicitly accounts for the transient electrochemical impedance and the thermal inertia of the 3-unit parallel cluster. The system architecture is visualized in fig. 4.2.

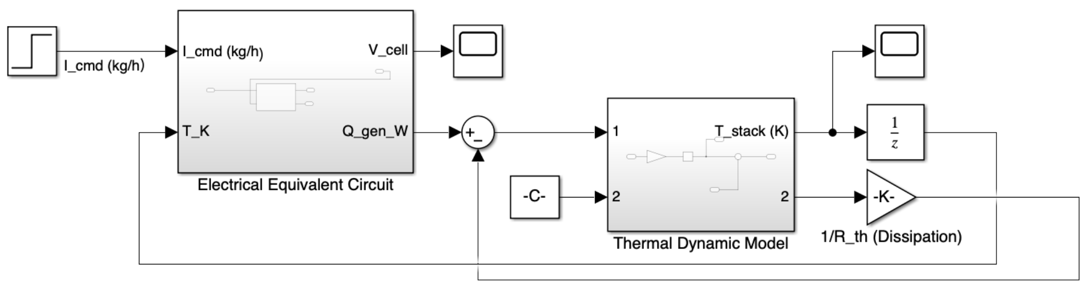

Figure 4.2 – Schematic diagram of the electro-thermal coupled dynamic model in Simulink

4.3.1 Electrical Subsystem: The 2RC Equivalent Circuit

The electrical response of the PEM electrolyzer stack is not instantaneous. To capture the dynamic voltage transients during the rapid load changes commanded by the AECS (e.g., ramping from P_{idle} to rated power), the lumped electrolysis system is modeled using a Second-Order Cauer Network (2RC Model) [78].

As depicted in the electrical domain of Figure 4.2, the total stack voltage in the complex frequency domain (Laplace domain, s) is formulated as:

$$V_{\text{stack}}(\text{s}) = N_{\text{cells}}\cdot[V_{\text{rev}}(T) + I(\text{s})\cdot Z_{\text{eq}}(\text{s})] \tag{4.9}$$

Where $Z_{\text{eq}}(\text{s})$ is the equivalent impedance function, comprising three distinct components:

1. Membrane Resistance (R_{mem}): Represents the instantaneous ohmic voltage drop.

2. Activation Loop (R_{act} // C_{dl}): The parallel combination of charge transfer resistance (Ract) and the Charge Double-Layer capacitance (C_{dl}). This term dictates the fast transient response (milliseconds to seconds) of the electrochemical interface.

3. Concentration Loop (R_{conc}//C_{diff}): The parallel combination of mass transport resistance (R_{conc}) and diffusion capacitance (C_{diff}), governing the slow dynamic response (seconds to minutes) under high-load conditions.

The transfer function for the dynamic impedance is expressed as:

$$Z_{\text{eq}}(s) = R_{\text{mem}} + \frac{R_{\text{act}}}{1+ s\cdot R_{\text{act}}C_{\text{dl}}} + \frac{R_{\text{conc}}}{1+ s\cdot R_{\text{conc}}C_{\text{diff}}} \tag{4.10}$$

Implementation Logic:

Parameters: The resistance values (R_{act}, R_{conc}) are dynamically calculated at each time step based on the Tafel and concentration equations derived in Section 4.2.2 (Eq. 4.3 and 4.5).

Capacitance: C_{dl} is set to represent the typical interfacial capacitance of porous electrodes (20 F for the lumped system), ensuring that voltage overshoots during step-changes are smoothed, reflecting realistic hardware behavior.

4.3.2 Thermal Subsystem: Feedback-Coupled Integrator

The thermal module acts as the «physical judge» of the AECS feasibility. It is implemented as a continuous-time feedback loop that solves the differential heat balance equation (Eq. 4.6).

In Simulink, this is realized using a state-space integrator block:

$$T_{\mathrm{stack}}(t) = \int_0^t \frac{1}{C_{\mathrm{th\_sys}}} \left(\dot{Q}_{\mathrm{gen\_sys}}(\tau) - \dot{Q}_{\mathrm{loss\_sys}}(\tau) \right) d\tau + T_{\mathrm{init}} \tag{4.11}$$

Coupling Mechanism:

1. Input: The module receives the instantaneous current $I(t)$ and voltage $V(t)$ from the electrical subsystem to calculate the net heat generation $\dot{Q}_{\mathrm{gen\_sys}}$.

2. Process: The integrator accumulates the net thermal energy, dividing by the system's total thermal capacitance ($C_{\mathrm{th\_sys}} = 6{,}6\times10^5$ J/K). This large «thermal mass» is the physical reason why the stack temperature does not plummet instantly even when $\dot{Q}_{\mathrm{gen\_sys}}$ is negative (endothermic) at 1,35 V.

3. Feedback: The calculated Tstack(t) is fed back into the Nernst Equation (Eq. 4.2) and the Activation Overpotential term (Eq. 4.3).

Simulation Significance: This closed-loop structure creates a realistic algebraic loop: a drop in temperature increases the reversible voltage Vrev and activation resistance Ract, which in turn increases the operating voltage Vstack, thereby generating more ohmic heat to counteract the cooling. This self-regulating thermal feedback is critical for validating the robustness of the 3.0 kg/h hot standby strategy.

4.4 Simulation Results and Discussion

4.4.1 Scenario Definition

To validate the dynamic feasibility of the developed Automated Electrolyzer Control System (AECS), a step-response simulation was conducted using the electro-thermal coupled model developed in Section 4.3. The simulation mimics a typical operational sequence at a hydrogen refueling station:

1. Phase I (Hot Standby, 0–100 s): The AECS maintains the system at a minimal load of 3,0 kg/h (approx. 5,5% of nominal capacity). This phase evaluates the system's ability to maintain thermal readiness during idling periods.

2. Phase II (Load Step & Stabilization, 100–300 s): At $t = 100$ s, a step command to Nominal Load (50 kg/h) is applied. The simulation runs until $t = 300$ s to observe the transition controlled by the AECS from standby to a thermally stable full-load state.

4.4.2 Electrical Dynamic Response (V_{cell})

Figure 4.3 illustrates the voltage response of the single cell.

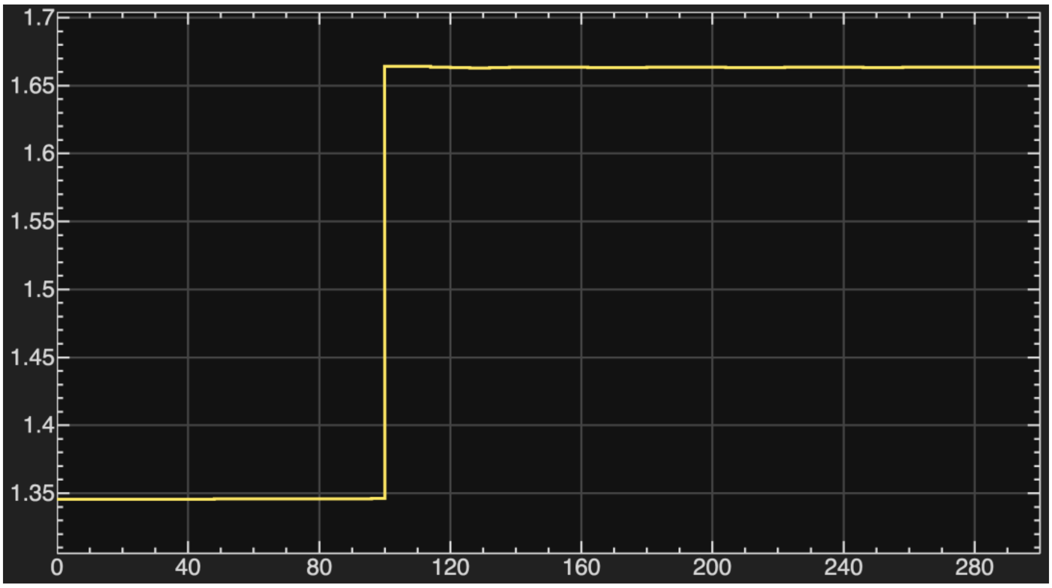

Figure 4.3 – Dynamic response of cell voltage during transition from standby to nominal load

- Standby Safety: During the standby phase (0–100 s), the voltage stabilizes at 1,35 V, maintaining a safe margin below the degradation threshold (1,6 V).
- Step Response: At $t = 100$ s, the voltage responds instantaneously to the current step, jumping to 1,66 V. The subsequent stability indicates that the electrical subsystem reaches equilibrium rapidly.

4.4.3 Thermal Stability and Management (T_{stack})

Figure 4.4 presents the detailed temperature evolution, with the vertical scale zoomed in to visualize the control dynamics.

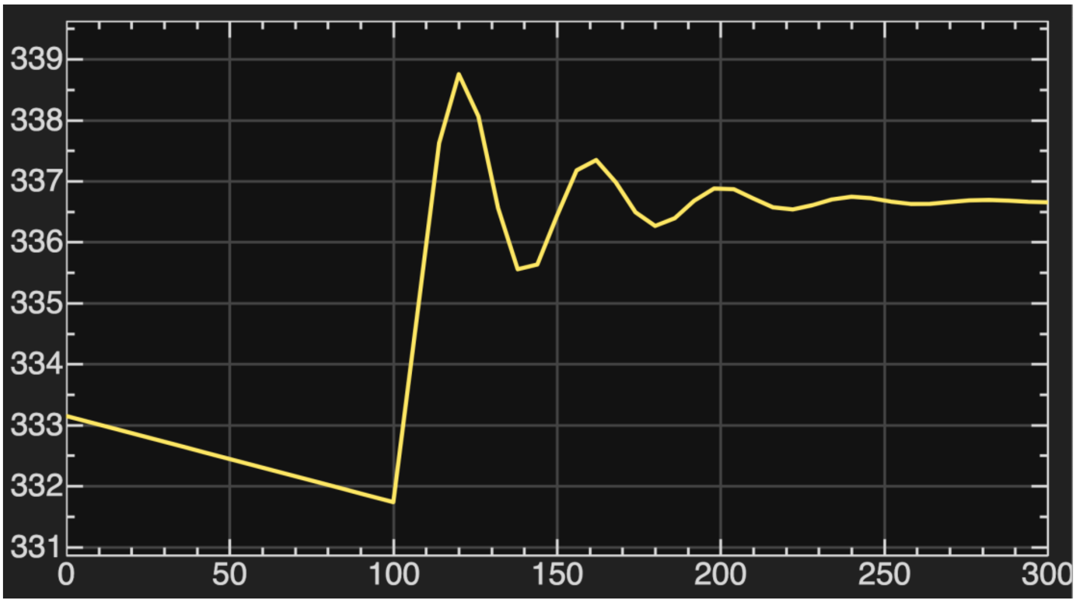

Figure 4.4 – Evolution of stack temperature under the hot standby strategy and active cooling control

- Validation of Thermal Inertia (0–100 s):

Despite the minimal heat generation in standby mode, the stack temperature shows a negligible decline from 333,15 K to 331,7 K. This drop of less than 1,5 K over 100 seconds confirms the system's high thermal inertia, validating the feasibility of the heater-less hot standby strategy [79].

- Dynamic Control Performance (t > 100 s):

Upon activation, the rapid heat generation triggers the active cooling logic.

- Transient Response: A typical under-damped transient response is observed, with a peak overshoot reaching approximately 338,8 K (65,7°C). This transient exceeds the nominal limit by only 0,7 °C for less than 20 sec, which is thermally acceptable for the stack mass.

- Steady-State Stabilization: The oscillation is effectively damped within 60 sec. The temperature settles and locks at a steady-state value of 336,7 K (63,5°C). This final equilibrium point is perfectly centered within the manufacturer's optimal operating specification (60±5°C), demonstrating robust closed-loop thermal control.

Summary by Chapter

This chapter establishes a comprehensive electro-thermal coupled dynamic model for the 3-unit PEM electrolyzer cluster to validate the developed Automated Electrolyzer Control System (AECS). The conclusions are summarized as follows:

1. High-Fidelity Modeling: A semi-empirical electrochemical model was developed and validated against manufacturer polarization data. The model effectively captures the nonlinear relationship between voltage and current density, providing a robust foundation for dynamic simulation.

2. Electro-thermal Coupling: By integrating a first-order lumped parameter thermal model, the interaction between electrochemical kinetics and stack temperature was accurately simulated. The results confirm that the system can maintain a «Hot Standby» state with minimal energy consumption.

3. Strategy Validation: Simulation results demonstrate that the AECS maintains the cell voltage at a safe level (1,35 V) during standby, preventing catalyst degradation. Upon a load step, the system exhibits rapid response, stabilizing the temperature at 63,7°C within the manufacturer's specified range (60±5°C) through effective thermal management.

4. Feasibility for Grid Services: The rapid transition from standby to nominal load validates the cluster's potential to provide ancillary services for the power grid, such as frequency regulation and renewable energy smoothing [80].

The validated dynamic model and control logic established in this chapter will serve as the technical basis for the system-level energy management and economic optimization in Chapter 5.

CHAPTER 5.

TECHNO-ECONOMIC ASSESSMENT AND IMPLEMENTATION OF SOURCE-GRID-LOAD-STORAGE COORDINATION

The preceding chapters have established the theoretical foundation and verified the dynamic performance of the Automated Electrolyzer Control System (AECS). Chapter 3 detailed the hierarchical control architecture, while Chapter 4 validated the system's transient response and thermal stability under the «Hot Standby» mode through electro-thermal coupled simulation. However, technical feasibility alone is insufficient to justify the widespread industrial adoption of this system. To bridge the gap between theoretical modeling and commercial deployment, a comprehensive assessment of the system's economic viability within a renewable-integrated grid environment is required.

As hydrogen production transitions from a passive industrial load to an active grid participant, the operational strategy must evolve from simple «Base-Load» operation to a «Source-Grid-Load-Storage» coordinated model. This chapter aims to quantify the multidimensional benefits of the AECS, specifically focusing on its ability to resolve the conflict between intermittent renewable generation and electrolyzer lifetime constraints.

The specific objectives of this chapter are:

1. Economic Quantification: To calculate the Levelized Cost of Hydrogen (LCOH) reduction by contrasting the AECS against traditional Rule-Based Control (RBC) strategies under a hybrid pricing mechanism.

2. Coordination Analysis: To evaluate the system's capability to decouple asset protection (lifetime) from energy capture (solar utilization), thereby solving the «structural mismatch» inherent in traditional scheduling.

3. Implementation Roadmap: To synthesize the simulation findings into actionable engineering guidelines for green hydrogen projects.

5.2 Techno-Economic Analysis of the AECS

This section presents a quantitative comparative analysis between the conventional strategy and the proposed AECS. The assessment is grounded in the dynamic power profiles obtained from the simulation in Chapter 3 and the specific energy consumption parameters validated in Chapter 4.

5.2.1 Economic Modeling and Boundary Conditions

The economic performance is evaluated using the Specific Electricity Cost (C_{spec}) metric. This metric integrates real-time energy consumption from heterogeneous sources (Grid and Solar) with the equivalent depreciation cost of equipment cycling. The objective function is defined as Eq (5.1). Recent techno-economic frameworks explicitly emphasize that ignoring the equivalent depreciation cost (C_{start}) of electrolyzer stack cycling severely compromises the accuracy of Levelized Cost of Hydrogen (LCOH) assessments [81].

$$C_{\text{spec}}=\frac{\sum_{t=0}^{T}\left(P_{\text{grid}}(t)\cdot\lambda_{\text{grid}}(t)+P_{\text{solar}}(t)\cdot\lambda_{\text{solar}}\right)\cdot\Delta t+N_{\text{cycle}}\cdot C_{\text{start}}}{\int_0^T \dot{m}_{\text{H2}}(t)\,dt} \tag{5.1}$$

Where:

- $P_{grid}(t)$ and $P_{solar}(t)$ represent the power drawn from the utility grid and local photovoltaic (PV) system, respectively (kW).

- $\lambda_{grid}(t)$ denotes the Time-of-Use (TOU) grid tariff ($/kWh, CNY/kWh).

- $\lambda_{solar}$is the Levelized Cost of Energy (LCOE) for local solar power, representing the self-consumption cost ($/kWh, CNY/kWh).

- N_{cycle} is the number of start-stop events during the operation period.

- C_{start} represents the Start-Stop Depreciation Cost, quantifying the equivalent loss in stack lifetime and pre-heating energy per cycle.

Boundary Conditions:

Table 5.1 – Simulation Parameters for Economic Analysis

Parameter	Value	Description
Grid Tariff (Valley)	0,044 $/kWh (0,30 CNY/kWh)	22:00–06:00
Grid Tariff (Not Valley)	0,095 $/kWh (0,65 CNY/kWh)	06:00–22:00
Solar LCOE (λ_{solar})	0,029 $/kWh (0,20 CNY/kWh)	Cost of self-consumed PV energy
Start-Stop Depreciation	73,1 $/cycle (500 CNY/cycle)	Equivalent cost for stack degradation & pre-heating
Nominal Energy Consumption	50 kWh/kg	System-level DC consumption

5.2.2 Operational Strategy Definition

To evaluate the efficacy of the AECS, a comparative study is conducted against a Rule-Based Control (RBC) strategy, which represents the prevailing industrial standard.

1. Baseline Strategy (Rule-Based Control)

- Operational Logic: The Baseline strategy relies on deterministic rules to manage system costs. It prioritizes the dominant cost factor – grid electricity tariffs – by imposing rigid operational constraints (e.g., if $t \in$, THEN $P_{sys}=0$). Recent comparative studies on renewable hydrogen production confirm that traditional rule-based operations often force premature shutdowns under stochastic weather conditions, drastically limiting solar energy capture [82].

- Limitations in Coordination: While effective for single-variable optimization (grid cost), this rule-based approach fails to handle multi-variable coupling. Specifically, it cannot dynamically reconcile the conflict between the stochastic nature of solar generation and the mechanical constraints of the electrolyzer (start-stop penalties). To avoid the risk of frequent cycling caused by solar intermittency, the strategy conservatively defaults to a shutdown mode during the day.

- Result: The system is decoupled from the renewable energy source due to the rigidity of its protective rules.

2. AECS Strategy (Dynamic Coordination)

- Operational Logic: The AECS shifts from rigid rules to Dynamic Coordination. It introduces a «Hot Standby» mechanism that acts as a buffer, decoupling the electrolyzer's thermal state from its electrical load.

- Coordination Mechanism: This mechanism allows the system to engage in «Source-Load Coupling» without violating mechanical constraints. The controller dynamically tracks the solar profile: when solar energy is available, it ramps up to absorb it; when solar drops, it reverts to the standby state instead of shutting down.

This flexibility enables the system to capture intermittent renewable energy that the rigid Baseline strategy must forfeit.

-

5.2.3 Quantitative Results and Discussion

The simulation results quantifying the economic and technical performance of both strategies are summarized in table 5.2.

3Table 5.2 – Techno-Economic Comparison Results

Key Performance Indicator (KPI)	Baseline Strategy (Rule-Based)	AECS Strategy (Dynamic Coordination)	Improvement
Total Hydrogen Production	23,053,2 kg	23,139,1 kg	+0,37%
Grid Energy Share	100,0%	61,5%	Load Shifted
Solar Energy Share	0,0%	38,5%	Effective Coupling
Start-Stop Cycles	61	1	-98,3%
Depreciation Cost (C_{start})	4,46 $ (30,500 CNY)	73,1$ (500 CNY)	-98,3%
Total Operational Cost (OPEX)	77,501.75 $ (530,112,0 CNY)	675,224.71 $ (461,853,7 CNY)	-12,9%
Specific Production Cost	3,36$/kg (23,00 CNY/kg)	2,92$/kg (19,96 CNY/kg)	13,20% Reduction

Figure 5.1 shows the dynamic comparison of renewable energy capture. The green area represents available solar power. The black dashed line illustrates the Baseline strategy, where the inability to adapt to stochastic fluctuations forces a protective shutdown, resulting in complete renewable curtailment. The red solid line demonstrates the AECS's «Load-Following» capability, actively tracking solar fluctuations while maintaining a hot standby state to decouple asset protection from energy capture.

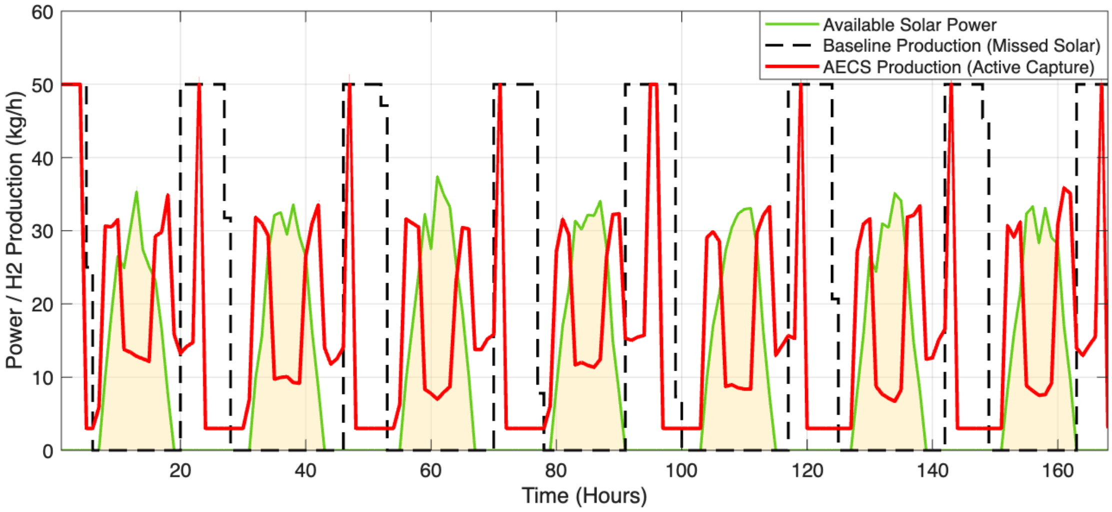

Figure 5.1 – Dynamic comparison of renewable energy capture between Baseline and AECS strategies

The performance divergence is attributed to the fundamental limitation of Rule-Based Control (RBC) in handling stochastic complexity, contrasted with the Self-Adaptive nature of the AECS:

1. The Complexity Barrier of Rule-Based Strategies:

As shown in Table 5.2, the Baseline strategy yields a 0% solar utilization rate. This outcome stems from the «Prohibitive Complexity» of formulating static rules for dynamic environments. To effectively capture intermittent solar energy while protecting the electrolyzer (limiting start-stop cycles), a rule-based system would require an infinitely complex set of logic statements (e.g., predicting cloud cover duration vs. restart cost). Since such a complex rule set is impossible to implement robustly in industrial practice, the Baseline strategy defaults to a «Conservative Simplification»: it shuts down completely during high-tariff periods. It sacrifices adaptability for safety, rendering it incapable of utilizing the available renewable energy.

2. Adaptability via Closed-Loop Control:

The AECS transcends this limitation by replacing rigid rules with Self-Adaptive Control Laws. Through the integration of the «Hot Standby» mechanism and PID-based load following, the system does not rely on pre-defined scenarios. Instead, it automatically adapts to real-time boundary conditions (Solar Power Availability, Tank Level). This allows the system to handle infinite variations in weather and demand without complex programming. The result is a robust adaptability that achieves a 38,5% renewable penetration and reduces asset degradation by 98,3%, a feat unachievable by static rules.

3. Economic Viability:

Driven by the high renewable penetration and minimized depreciation, the AECS achieves a specific production cost of 2,92$/kg (19,96 CNY/kg). Breaking the 2,924$/kg (20 CNY/kg) threshold confirms that the proposed dynamic coordination mechanism is a critical enabler for the commercial viability of Green Hydrogen projects.

5.3 Grid Interaction and Engineering Implementation

The techno-economic analysis in Section 5.2 validates the commercial viability of the AECS within a microgrid context. However, for large-scale industrial deployment, the interaction between the electrolyzer cluster and the utility grid is equally critical. This section analyzes the «Virtual Power Plant» (VPP) characteristics of the AECS and synthesizes the research findings into actionable engineering guidelines.

5.3.1 Grid Flexibility Services (Virtual Energy Storage)

With the fast transient response validated in Chapter 4 and the controllable load characteristics demonstrated in Chapter 5, the AECS transforms the electrolyzer from a rigid industrial load into a flexible grid resource.

1. Primary Frequency Regulation (PFR):

As verified in the electro-thermal simulation, the AECS can ramp from «Hot Standby» (3%) to nominal power (100%) within seconds, limited only by the power supply ramp rate rather than thermal constraints. This capability allows the system to participate in Primary Frequency Regulation. The integration of MW-scale electrolyzers as responsive virtual inertia assets is now widely recognized as a critical mechanism for enhancing the resiliency of low-inertia grids [83].

- Mechanism: When the grid frequency deviates due to a sudden load increase (e.g., , < 49,8 Hz), the AECS control system can instantaneously reduce its power consumption. From the perspective of grid energy balance, this rapid load shedding is mathematically equivalent to injecting active power into the grid, thereby assisting in frequency recovery. Conversely, during over-frequency events (f > 50,2 Hz), the system can ramp up to absorb excess energy.

- Value: This bidirectional regulation capability provides critical Virtual Inertia to low-inertia renewable-dominated grids, enhancing system resilience against disturbances.

-

2. Peak Shaving and Valley Filling:

The operational profile shown in Figure 5.1 inherently supports grid stability. By concentrating heavy consumption during the valley period (22:00–06:00) and modulating power during the day based on local solar availability, the AECS naturally alleviates grid congestion during peak load hours. This «Load-Shifting» capability reduces the need for grid reinforcement investments. Furthermore, by participating jointly in energy and frequency regulation ancillary service markets, such multi-energy systems can significantly optimize their overall operational OPEX and payback periods [84].

5.3.2 Engineering Implementation Guidelines

To facilitate the transition from theoretical modeling to industrial application, the following engineering recommendations are proposed for MW-scale Green Hydrogen plants:

1. Buffer Storage Sizing Rule:

To enable the «Source-Load Decoupling» strategy, the hydrogen storage capacity must be sufficient to bridge the gap between solar intermittency and continuous downstream demand. Based on the simulation results in Section 5.2, a buffer storage capacity equivalent to 12–16 hours of nominal production is recommended. This sizing allows the system to operate aggressively during the valley period without «Tank-Full» shutdowns and sustain downstream supply during low-solar intervals.

2. Thermal Management for Hot Standby:

The economic success of the AECS hinges on the stability of the «Hot Standby» mode. Therefore, the Balance of Plant (BoP) design must include an active auxiliary heating loop. As simulated, this loop must automatically engage when the electrical load drops below 5% to maintain the stack temperature above 60°C. This prevents the «Cold Start» damage quantified in the economic analysis 73,1$/ cycle (500 CNY/cycle) and ensures immediate ramp-up readiness.

3. Hierarchical Safety Interlocks:

While the AECS prioritizes economic optimization, safety remains the absolute constraint. A Hard-Wired Safety Layer must be implemented below the AECS optimization layer. This layer should autonomously trigger a system shutdown if critical parameters (e.g., Anode-Cathode pressure differential > 50 mbar, Stack Temperature > 85°C) are breached, overriding any economic commands to ensure personnel and equipment safety.

Summary by Chapter

This chapter presented a comprehensive techno-economic assessment of the proposed Automated Electrolyzer Control System (AECS). By integrating the dynamic control model with a hybrid pricing mechanism, the study quantified the system's benefits against a traditional Rule-Based Control strategy. LSTM was originally designed specifically to overcome the problem of «gradient fading», allowing any system to efficiently store and process long sequences of data without losing the context of previous steps. This will ensure the stability of the hydrogen supply system in the face of dynamic demand from electric vehicles.

The key findings are summarized as follows:

1. Economic Viability:

The AECS achieved a specific hydrogen production cost of 2,92$/kg (19,96 CNY/kg), representing a 13,20% reduction compared to the baseline. This reduction is primarily driven by the intelligent arbitrage between valley grid tariffs and low-cost solar energy.

2. Renewable Integration:

The system resolved the inherent conflict between grid economy constraints and the solar generation window characteristic of static scheduling. This «Load-Following» capability overcame the structural source-load decoupling caused by rigid rules, increasing the solar energy penetration from 0,0% to 38,5%.

3. Asset Protection:

Through the «Hot Standby» mechanism, the system effectively decoupled energy capture from mechanical stress, reducing start-stop cycles by 98.3%. This virtually eliminates depreciation costs and fundamentally extends the operational lifespan of electrolyzers in fluctuating power environments.

In conclusion, the AECS is verified not only as a technically robust solution but also as an economically superior strategy for the commercialization of Green Hydrogen, offering a scalable pathway for source-grid-load coordination.

CONCLUSIONS

The hypothesis was proven and the current scientific and applied problem of improving intelligent control systems for electrotechnical complexes for hydrogen supply was solved. This allows to globally reduce the cost of hydrogen fuel, increase the energy efficiency of transport infrastructure and ensure the reliability of the energy system in the conditions of energy transition. Also, the results of this dissertation have created a basis for further development of the scientific direction of research on improving hydrogen technologies, infrastructure and increasing the efficiency of electrotechnical complexes that ensure the energy efficiency of hydrogen refueling complexes in the electric transport system.

In the context of global transportation electrification, this dissertation has systematically conducted interdisciplinary research encompassing electrotechnical theory analysis, multiphysics modeling, and intelligent control strategies to address the critical challenges of energy efficiency, operational stability, and economic synergy faced by «green hydrogen» infrastructure.

This dissertation systematically investigated the electrotechnical hydrogen supply complex within the electric transport system, conducting interdisciplinary research across electrotechnical theory, multiphysics dynamic modeling, and intelligent control strategies. The research successfully resolved the structural contradictions between energy efficiency, operational stability, and economic viability in green hydrogen infrastructure operating under double-stochastic environments.

By executing the defined research tasks, the following specific scientific and practical conclusions were achieved:

1. On the dynamic characteristics and degradation mechanisms of the electrotechnical system: A comprehensive full-chain electrotechnical model (from the power grid to the megawatt-class PEM-electrolyzer) was established. The systematic analysis under intermittent power supply conditions revealed that non-linear electrochemical responses during transient regimes – particularly the abrupt thermal gradients during cold starts – are the primary catalysts for Membrane Electrode Assembly (MEA) thermal stress and mechanical fatigue. This finding quantitatively defined the operational constraints of the equipment under rapid power fluctuations, providing the physical boundary conditions for subsequent control algorithm design.

2. On the critical analysis of existing control methodologies: A critical evaluation employing SWOT analysis and comparative simulations demonstrated that traditional Rule-Based Control (RBC) strategies suffer from severe «information blindness». The analysis theoretically proved that passive, hysteresis-driven responses to static pressure thresholds are fundamentally inadequate for managing the «double-stochastic» volatility of renewable energy generation and refueling demand, inevitably leading to damaging start-stop cycling and necessitating a predictive, feedforward control architecture.

3. On the stochastic behavior of FCEV networks and load forecasting structure: The stochastic behavior patterns of Fuel Cell Electric Vehicle (FCEV) fleet electrical networks were thoroughly characterized, leading to the development of a multi-level load forecasting structure. By capturing the temporal rhythm of traffic flows, this structure identified extreme peak-to-trough demand ratios of up to 15:1 during morning and evening rush hours. This macroscopic mathematical framework definitively

proved that relying solely on passive physical buffer storage is economically unsustainable, thus confirming the necessity of active Demand Response management.

4. On the formulation of the macroscopic-microscopic mass flow model: A macroscopic M/M/S/N queueing model was successfully synthesized with microscopic non-linear vehicle thermodynamics using the Real Gas Equation of State. Through Monte Carlo simulations of 100 random refueling scenarios, the integrated model accurately quantified instantaneous hydrogen mass flow. This established a robust engineering design benchmark of 4,5 kg/vehicle with a tight filling stability coefficient of 5,02%, providing high-fidelity, quantitative parameters for system sizing and dynamic evaluation.

5. On the design of the Automated Electrolyzer Control System (AECS): An Automated Electrolyzer Control System featuring a hierarchical architecture was successfully designed for real-time dynamic state management. By organically integrating Deterministic Finite Automata (DFA) logic with predictive artificial intelligence modules, the AECS transforms the PEM electrolyzer from a rigid industrial load into a highly flexible «energy router». This enables proactive, forward-looking operational state transitions in response to upstream microgrid conditions and downstream transportation demand.

6. On the adaptation of LSTM for high-precision demand forecasting: The application of Long Short-Term Memory (LSTM) neural network algorithms was mathematically justified and optimized for high-precision, short-term (next-hour) demand forecasting. Trained on a comprehensive 366-day dataset exhibiting complex «double-peak» traffic features, the model demonstrated exceptional generalization on

unseen test data, achieving a Root Mean Square Error (RMSE) of 6,7454 kg and an R^2 of 0,8192. This precision supplies the AECS with a highly reliable feedforward sensing window, transitioning the system from reactive suppression to proactive optimization.

7. On the multiphysics electrothermal modeling of the PEM-cluster: A multiphysics dynamic model of a multi-PEM electrolyzer cluster was created utilizing a 2RC equivalent circuit topology coupled with a feedback thermal integrator. This model physically validated the proposed continuous electrothermal control topology known as the «Hot Standby» mode. Simulations proved that injecting a minimal holding current density (yielding approximately 3% of nominal load) precisely balances internal charge-exchange heat generation with environmental dissipation. This mechanism robustly maintains the stack temperature above 60°C, completely eliminating cold-start thermal stresses and granting the system millisecond-level transient power ramping capabilities.

8. On the development of the Demand Response strategy: A dual-oriented Demand Response strategy was formulated, allowing the electrotechnical complex to dynamically adapt to intermittent Renewable Energy Source (RES) schedules and electricity market signals. Over a 60-day continuous simulation, this strategy successfully synchronized flexible hydrogen production with solar availability, reducing harmful start-stop cycles from 61 to 1 (a massive 98,4% reduction) and suppressing the standard deviation of power output fluctuations by 40,7%. This signifies the achievement of a highly stable «load-following» mode that is exceptionally grid-friendly.

9. On the techno-economic analysis and LCOH calculation: A comprehensive techno-economic evaluation confirmed the highly competitive commercial paradigm of the proposed AECS. Compared to traditional Rule-Based Control (RBC), the intelligent system reduces the Levelized Cost of Hydrogen (LCOH) by a substantial 13,20%, lowering the final cost to 2,92$/kg (19,96 CNY/kg). This significant cost reduction is achieved through two primary mechanisms: first, the predictive logic executes agile Time-of-Use (TOU) tariff arbitrage and increases direct solar energy utilization from 0% to 38,5%, significantly cutting operational electricity expenditures (OPEX); second, the proposed «hot standby» strategy reduces start-stop cycles by 98,4%, which prevents premature degradation of the PEM stack and drastically slashes annualized equipment depreciation costs (CAPEX).

In the context of the global energy market, where the current production cost of green hydrogen typically ranges from $4,00 to $6,00/kg, an internationally acceptable price threshold for near-term commercial competitiveness against fossil fuels is widely considered to be below $3,00/kg. By driving the LCOH down to ~$2,92/kg, the proposed control framework successfully positions the hydrogen refueling station within this highly viable economic window. Furthermore, the established dynamic thermal regulation principles will directly facilitate the transformation of these stations from rigid industrial loads into flexible grid assets, adding secondary revenue streams through Virtual Power Plant (VPP) participation and grid ancillary services.

Ultimately, the integrated intelligent control architecture developed in this dissertation successfully resolves the structural contradiction (the «impossible trinity») of hydrogen infrastructure: simultaneously achieving low production costs, high renewable energy penetration, and extended equipment service life. The research outcomes not only enrich the theoretical framework of intelligent electrotechnical technologies in clean energy conversion but also provide a complete technical paradigm and decision-making foundation for the engineering deployment of large-scale, grid-interactive commercial green hydrogen hubs.

The integrated intelligent control architecture proposed in this dissertation successfully resolves the structural contradiction (the «impossible trinity») between production cost, renewable energy penetration rate, and equipment service life within hydrogen refueling station infrastructure. The research outcomes not only enrich the theoretical framework of intelligent electrotechnical technologies in the field of clean energy conversion but also provide a comprehensive technical paradigm and decision-making basis for the engineering deployment of future large-scale, highly resilient commercial green hydrogen hubs.

REFERENCES

1. Gielen, D., Boshell, F., Saygin, D., Bazilian, M. D., Wagner, N., & Gorini, R. (2019). The role of renewable energy in the global energy transformation. *Energy strategy reviews*, 24, 38–50. https://doi.org/10.1016/j.esr.2019.01.006 .

2. Ehsani, M., Gao, Y., Longo, S., & Ebrahimi, K. (2018). *Modern electric, hybrid electric, and fuel cell vehicles*. CRC press.

3. Un-Noor, F., Padmanaban, S., Mihet-Popa, L., Mollah, M. N., & Hossain, E. (2017). A Comprehensive Study of Key Electric Vehicle (EV) Components, Technologies, Challenges, Impacts, and Future Direction of Development. *Energies*, 10 (8), 1217. https://doi.org/10.3390/en10081217.

4. Ding, Y., Cano, Z. P., Yu, A., Lu, J., & Chen, Z. (2019). Automotive Li-Ion Batteries: Current Status and Future Perspectives. *Electrochemical Energy Reviews*, 2(1), 1–28. https://doi.org/10.1007/s41918-018-0022-z.

5. Cullen, D. A., Neyerlin, K. C., Ahluwalia, R. K., Mukundan, R., More, K. L., Borup, R. L., Weber, A. Z., Myers, D. J., & Kusoglu, A. (2021). New roads and challenges for fuel cells in heavy-duty transportation. *Nature Energy*, 6 (5), 462–474. https://doi.org/10.1038/s41560-021-00775-z.

6. Apostolou, D., & Xydis, G. (2019). A literature review on hydrogen refuelling stations and infrastructure. Current status and future prospects. *Renewable and Sustainable Energy Reviews*, 113, 109292. https://doi.org/10.1016/j.rser.2019.109292.

7. Boichenko S., & Chen, L. (2024). Comparative analysis of hydrogen production, accumulation, distribution, and storage systems. *System Research in Energy*, 3 (79), 13–20. https://doi.org/10.15407/srenergy2024.03.013.

8. ISO 14687:2025. (2025). Hydrogen fuel quality – Product specification. *International Organization for Standardization*. Geneva, Switzerland. https://www.iso.org/obp/ui/en/#iso:std:iso:14687:ed-2:v1:en (Accessed on: 28.02.2026).

9. Xu, Z., Dong, W., Zhao, Y., Dong, H., & He, G. (2023). Development of fuelling protocols for gaseous hydrogen vehicles: a key component for efficient and safe hydrogen mobility infrastructures. *Clean Energy*, 7 (1), 23–29. https://doi.org/10.1093/ce/zkac087 .

10. International Energy Agency. (2023). *Global hydrogen review 2023*. https://www.iea.org/reports/global-hydrogen-review-2023.

11. Reddi, K., Elgowainy, A., Rustagi, N., & Gupta, E. (2017). Impact of hydrogen refueling configurations and market parameters on the refueling cost of hydrogen. *International Journal of Hydrogen Energy*, 42 (34), 21855–21865. https://doi.org/10.1016/j.ijhydene.2017.05.122.

12. Blanco, H., & Faaij, A. (2018). A review at the role of storage in energy systems with a focus on Power to Gas and long-term storage. *Renewable and Sustainable Energy Reviews*, 81, 1049–1086. https://doi.org/10.1016/j.rser.2017.07.062 .

13. Matute, G., Yusta, J. M., & Correas, L. C. (2019). Techno-economic modelling of water electrolysers in the range of several MW to provide grid services while generating hydrogen for different applications: A case study in Spain applied to

mobility with FCEVs. International Journal of Hydrogen Energy, 44(33), 17431–17442. https://doi.org/10.1016/j.ijhydene.2019.05.092.

14. Boichenko, S., Chen, L., Korovushkin, V., & Biliakovych, O. (2025). PEST- and SNW-analysis of the use of liquid hydrogen as a motor fuel in aviation. *System Research in Energy*, 81(1), 61–73. https://doi.org/10.15407/srenergy2025.01.061.

15. Shiva Kumar, S., & Himabindu, V. (2019). Hydrogen production by PEM water electrolysis – A review. *Materials Science for Energy Technologies*,2(3),442–454. https://doi.org/10.1016/j.mset.2019.03.002 .

16. Weiß, A., Siebel, A., Bernt, M., Shen, T. H., Tileli, V., & Gasteiger, H. A. (2019). Impact of Intermittent Operation on Lifetime and Performance of a PEM Water Electrolyzer. *Journal of The Electrochemical Society*, 166(8), F487. https://doi.org/10.1149/2.0421908jes .

17. Olivier, P., Bourasseau, C., & Bouamama, P. B. (2017). Low-temperature electrolysis system modelling: A review. *Renewable and Sustainable Energy Reviews*, 78, 280–300. https://doi.org/10.1016/j.rser.2017.03.099 .

18. Cardona, P., Costa-Castelló, R., Roda, V., Carroquino, J., Valiño, L., & Serra, M. (2023). Model predictive control of an on-site green hydrogen production and refuelling station. *International Journal of Hydrogen Energy*, 48(47), 17995–18010. https://doi.org/10.1016/j.ijhydene.2023.01.191.

19. Manoharan, Y., Hosseini, S. E., Butler, B., Alzhahrani, H., Senior, B. T. F., Ashuri, T., & Krohn, J. (2019). Hydrogen Fuel Cell Vehicles; Current Status and Future Prospect. *Applied Sciences*, 9(11), 2296. https://doi.org/10.3390/app9112296.

20. Zheng, J., Zhao, L., Ou, K., Guo, J., Xu, P., Zhao, Y., & Zhang, L. (2014). Queuing-based approach for optimal dispenser allocation to hydrogen refueling stations. *International Journal of Hydrogen Energy*, 39(15), 8055–8062. https://doi.org/10.1016/j.ijhydene.2014.03.112 .

21. Luca, R., Whiteley, M., Neville, T., Shearing, P. R., & Brett, D. J. L. (2022). Comparative study of energy management systems for a hybrid fuel cell electric vehicle - A novel mutative fuzzy logic controller to prolong fuel cell lifetime. *International Journal of Hydrogen Energy*, 47(57),24042–24058. https://doi.org/10.1016/j.ijhydene.2022.05.192 .

22. Ma, Y., Wang, P., Li, B., & Li, J. (2022). Research on Energy Consumption Generation Method of Fuel Cell Vehicles: Based on Naturalistic Driving Data Mining. *Machines*, 10(11), 1047. https://doi.org/10.3390/machines10111047.

23. Tatti, R., Klopčič, N., Radner, F., Zinner, C., & Trattner, A. (2026). Thermodynamic Modelling and Sensitivity Analysis of a 70 MPa Hydrogen Storage System for Heavy Duty Vehicles. *Hydrogen*, 7(1), 8. https://doi.org/10.3390/hydrogen7010008 .

24. Wang, X., Liu, S., Ye, P., Zhu, Y., Yuan, Y., & Chen, L. (2023). Study of a Hybrid Vehicle Powertrain Parameter Matching Design Based on the Combination of Orthogonal Test and Cruise Software. *Sustainability*, 15(14), 10774. https://doi.org/10.3390/su151410774.

25. Shiledar, A., Gupta, S., Spano, M., Villani, M., Canova, M., & Rizzoni, G. (2024, July). Real-time eco-driving of a connected and automated fuel cell electric truck using approximate dynamic programming. *In 2024 American Control*

Conference (ACC) (pp. 2989–2994). IEEE. https://doi.org/10.23919/ACC60939.2024.10644542 .

26. Leachman, J. W., Jacobsen, R. T., Penoncello, S. G., & Lemmon, E. W. (2009). Fundamental Equations of State for Parahydrogen, Normal Hydrogen, and Orthohydrogen. *Journal of Physical and Chemical Reference Data*, 38(3), 721–748. https://doi.org/10.1063/1.3160306.

27. Electric and Hybrid-Electric Propulsion Systems. (2007). In L. Guzzella & A. Sciarretta (Eds.), *Vehicle Propulsion Systems: Introduction to Modeling and Optimization* (pp. 59–130). Springer Berlin Heidelberg. https://doi.org/10.1007/978-3-540-74692-8_4.

28. Alves, B. M., Savignac, P., & Leduc, P. (2025). Energy balance and hydrogen exhaust emissions of the second-generation Toyota Mirai. *International Journal of Hydrogen Energy*, 156, 150411. https://doi.org/10.1016/j.ijhydene.2025.150411.

29. Yang, Z., Zhou, X., Sun, C., & Wei, X. (2021, October). Estimation of Optimal Energy Consumption for Fuel Cell Vehicle Based on Macroscopic Traffic Dynamics. *In 2021 IEEE Vehicle Power and Propulsion Conference (VPPC)* (pp. 1–5). IEEE. https://doi.org/10.1109/VPPC53923.2021.9699251.

30. Liu, B., Sun, C., Wang, B., Liang, W., Ren, Q., Li, J., & Sun, F. (2022). Bi-level convex optimization of eco-driving for connected Fuel Cell Hybrid Electric Vehicles through signalized intersections. *Energy*, 252, 123956. https://doi.org/10.1016/j.energy.2022.123956.

31. Xiao, J., Ma, S., Wang, X., Deng, S., Yang, T., & Bénard, P. (2019). Effect of Hydrogen Refueling Parameters on Final State of Charge. *Energies*, 12(4), 645. https://doi.org/10.3390/en12040645.

32. Caponi, R., Monforti Ferrario, A., Bocci, E., Valenti, G., & Della Pietra, M. (2021). Thermodynamic modeling of hydrogen refueling for heavy-duty fuel cell buses and comparison with aggregated real data. *International Journal of Hydrogen Energy*, 46(35), 18630–18643. https://doi.org/10.1016/j.ijhydene.2021.02.224.

33. Zheng, J., Guo, J., Yang, J., Zhao, Y., Zhao, L., Pan, X., Ma, J., & Zhang, L. (2013). Experimental and numerical study on temperature rise within a 70 MPa type III cylinder during fast refueling. *International Journal of Hydrogen Energy*, 38(25), 10956–10962. https://doi.org/10.1016/j.ijhydene.2013.02.053.

34. Yang, Y., Xu, X., Luo, Y., Liu, J., & Hu, W. (2024). Distributionally robust planning method for expressway hydrogen refueling station powered by a wind-PV system. *Renewable Energy*, 225, 120210. https://doi.org/10.1016/j.renene.2024.120210.

35. Daskin, M. S. (2021). Fundamentals of Queueing Theory. In M. S. Daskin (Ed.), *Bite-Sized Operations Management* (pp. 119–123). Springer International Publishing. https://doi.org/10.1007/978-3-031-02493-1_17 .

36. Balakrishnan, N., Koutras, M. V., & Politis, K. G. (2019). *Introduction to probability: models and applications*. John Wiley & Sons.

37. Ross, S. M. (2014). *Introduction to Probability Models* (11th ed.). Academic Press.

38. Zhang, H., Moura, S. J., Hu, Z., & Song, Y. (2018). PEV Fast-Charging Station Siting and Sizing on Coupled Transportation and Power Networks. *IEEE Transactions on Smart Grid*, 9(4), 2595–2605. https://doi.org/10.1109/TSG.2016.2614939 .

39. Rose, P. K., & Neumann, F. (2020). Hydrogen refueling station networks for heavy-duty vehicles in future power systems. *Transportation Research Part D: Transport and Environment*, 83, 102358. https://doi.org/10.1016/j.trd.2020.102358 .

40. Pang, Y., Pan, L., Zhang, J., Chen, J., Dong, Y., & Sun, H. (2022). Integrated sizing and scheduling of an off-grid integrated energy system for an isolated renewable energy hydrogen refueling station. *Applied Energy*, 323, 119573. https://doi.org/10.1016/j.apenergy.2022.119573 .

41. Kim, S., Park, J., & Lee, J. H. (2025). Design and analysis of wind-based hydrogen production using rule-based operation. *Renewable and Sustainable Energy Reviews*, 212, 115459. https://doi.org/10.1016/j.rser.2025.115459 .

42. Chandesris, M., Médeau, V., Guillet, N., Chelghoum, S., Thoby, D., & Fouda-Onana, F. (2015). Membrane degradation in PEM water electrolyzer: Numerical modeling and experimental evidence of the influence of temperature and current density. *International Journal of Hydrogen Energy*, 40(3), 1353–1366. https://doi.org/10.1016/j.ijhydene.2014.11.111.

43. Hochreiter, S., & Schmidhuber, J. (1997). Long Short-Term Memory. *Neural Computation*, 9(8), 1735–1780. https://doi.org/10.1162/neco.1997.9.8.1735 .

44. He, Q., Zhao, M., Li, S., Li, X., & Wang, Z. (2025). Machine Learning Prediction of Photovoltaic Hydrogen Production Capacity Using Long Short-Term Memory Model. *Energies*, 18(3), 543. https://doi.org/10.3390/en18030543.

45. Félix, P., Oliveira, F. T., & Soares, F. J. (2025). Day-ahead optimization of a green hydrogen hub using synthetic hydrogen demand data. *2025 21st International Conference on the European Energy Market (EEM)*. https://doi.org/10.1109/EEM64765.2025.11050211 .

46. Hafez, O., & Bhattacharya, K. (2015). Modeling of PEV charging load using queuing analysis and its impact on distribution system operation. *2015 IEEE Power & Energy Society General Meeting*. https://doi.org/10.1109/PESGM.2015.7286203 .

47. Lin, X., Prabowo, A., Razzak, I., Xue, H., Amos, M., Behrens, S., & Salim, F. D. (2025). Electric vehicle charging load modeling: A survey, trends, challenges and opportunities. *arXiv preprint* arXiv: 2511.03741. https://doi.org/10.48550/arXiv.2511.03741 .

48. Reuß, M., Grube, T., Robinius, M., Preuster, P., Wasserscheid, P., & Stolten, D. (2017). Seasonal storage and alternative carriers: A flexible hydrogen supply chain model. *Applied Energy*, 200, 290–302. https://doi.org/10.1016/j.apenergy.2017.05.050.

49. Cardona, P., Valiño, L., Ocampo-Martinez, C., & Serra, M. (2025). Mixed logical dynamical modelling of renewable hydrogen refuelling stations for the design of optimization-based operational schemes. *Applied Energy*, 393, 126037. https://doi.org/10.1016/j.apenergy.2025.126037.

50. Petipas, F., Brisse, A., & Bouallou, C. (2013). Model-based behaviour of a high temperature electrolyser system operated at various loads. *Journal of Power Sources*, 239, 584–595. https://doi.org/10.1016/j.jpowsour.2013.03.027.

51. Gusain, D., Cvetković, M., Bentvelsen, R., & Palensky, P. (2020). Technical Assessment of Large Scale PEM Electrolyzers as Flexibility Service Providers. *2020 IEEE 29th International Symposium on Industrial Electronics (ISIE)*. https://doi.org/10.1109/ISIE45063.2020.9152462.

52. Xu, B., Ma, W., Wu, W., Wang, Y., Yang, Y., Li, J., Zhu, X., & Liao, Q. (2024). Degradation prediction of PEM water electrolyzer under constant and start-stop loads based on CNN-LSTM. *Energy and AI*, 18, 100420. https://doi.org/10.1016/j.egyai.2024.100420.

53. Garcia-Torres, F., & Bordons, C. (2015). Optimal Economical Schedule of Hydrogen-Based Microgrids With Hybrid Storage Using Model Predictive Control. *IEEE Transactions on Industrial Electronics*, 62(8), 5195–5207. https://doi.org/10.1109/TIE.2015.2412524.

54. Valverde, L., Rosa, F., & Bordons, C. (2013). Design, Planning and Management of a Hydrogen-Based Microgrid. *IEEE Transactions on Industrial Informatics*, 9(3), 1398–1404. https://doi.org/10.1109/TII.2013.2246576.

55. Schleipen, M., Gilani, S.-S., Bischoff, T., & Pfrommer, J. (2016). OPC UA & Industrie 4.0 – Enabling Technology with High Diversity and Variability. *Procedia CIRP*, 57, 315–320. https://doi.org/10.1016/j.procir.2016.11.055 .

56. Xing, J., Qian, J., Peng, R., & Zio, E. (2024). Physics-informed data-driven Bayesian network for the risk analysis of hydrogen refueling stations. *International Journal of Hydrogen Energy*, 110, 371–385. https://doi.org/10.1016/j.ijhydene.2025.02.110 .

57. Koponen, J., Ruuskanen, V., Kosonen, A., Niemelä, M., & Ahola, J. (2019). Effect of Converter Topology on the Specific Energy Consumption of Alkaline Water Electrolyzers. *IEEE Transactions on Power Electronics*, 34(7), 6171–6182. https://doi.org/10.1109/TPEL.2018.2876636 .

58. Guilbert, D., & Vitale, G. (2019). Dynamic Emulation of a PEM Electrolyzer by Time Constant Based Exponential Model. *Energies*, 12(4), 750. https://doi.org/10.3390/en12040750 .

59. Kim, J. W., Won, H. I., Park, D. Y., Kim, I. J., Lee, J. W., Kim, K. D., Noh, Y., & Jang, J. S. (2023). Study on Stochastic and Autoregressive Time Series Forecasting for Hydrogen Refueling Station. *IEEE Access*, 11, 141598–141609. https://doi.org/10.1109/ACCESS.2023.3342857.

60. Isaac, N., & Saha, A. K. (2023). Analysis of Refueling Behavior Models for Hydrogen-Fuel Vehicles: Markov versus Generalized Poisson Modeling. *Sustainability*, 15(18), 13474. https://doi.org/10.3390/su151813474 .

61. Ko, K., & Kim, C. (2024). Attention-Based Hydrogen Refueling Imputation Model for Efficient Hydrogen Refueling Stations. *Applied Sciences*, 14(22), 10332. https://doi.org/10.3390/app142210332 .

62. Isaac, N., & Saha, A. K. (2024). Forecasting Hydrogen Vehicle Refuelling for Sustainable Transportation: A Light Gradient-Boosting Machine Model. *Sustainability*, 16(10), 4055. https://doi.org/10.3390/su16104055.

63. Bi, Y., Wu, Q., Wang, S., Shi, J., Cong, H., Ye, L., Gao, W., & Bi, M. (2023). Hydrogen leakage location prediction at hydrogen refueling stations based on deep learning. *Energy*, 284, 129361. https://doi.org/10.1016/j.energy.2023.129361 .

64. Tulum, G., Nematzadeh, S., Taşçıoğlu, İ., Altındal, Ş., & Yakuphanoğlu, F. (2025). Long short-term memory (LSTM) networks for precision prediction of Schottky barrier photodiode behavior at different illumination levels. *Scientific Reports*, 15(1), 22532. https://doi.org/10.1038/s41598-025-06809-w.

65. Guo, F., Mo, H., Wu, J., Pan, L., Zhou, H., Zhang, Z., Li, L., & Huang, F. (2024). A Hybrid Stacking Model for Enhanced Short-Term Load Forecasting. *Electronics*, 13(14), 2719. https://doi.org/10.3390/electronics13142719.

66. KIM, M., JEON, S., & JYUNG, T. (2024). A Study on the Daily Demand Forecasting of Hydrogen Charging Station Using LSTM Model. *Journal of Hydrogen and New Energy*, 35(5), 536-547. https://doi.org/10.7316/JHNE.2024.35.5.536.

67. Gholami, K., Arif, M. T., & Haque, M. E. (2025). Machine learning-driven stochastic bidding for hydrogen Refueling Station-integrated virtual power plants in energy market. *Journal of Energy Storage*, 134, 117946. https://doi.org/10.1016/j.est.2025.117946.

68. Naseri, N., El Hani, S., Machmoum, M., Elbouchikhi, E., & Daghouri, A. (2024). Energy Management Strategy for a Net Zero Emission Islanded Photovoltaic Microgrid-Based Green Hydrogen System. *Energies*, 17(9), 2111. https://doi.org/10.3390/en17092111.

69. Al-Sagheer, Y., & Steinberger-Wilckens, R. (2022). Novel control approach for integrating water electrolyzers to renewable energy sources. *Fuel Cells*, 22(6), 290-300. https://doi.org/10.1002/fuce.202200066.

70. Yu, H.-C., Wang, Q.-A., & Li, S.-J. (2024). Fuzzy Logic Control with Long Short-Term Memory Neural Network for Hydrogen Production Thermal Control System. *Applied Sciences*, 14(19), 8899. https://doi.org/10.3390/app14198899.

71. Zhou, S., Zhuang, Y., Gu, W., & Wu, Z. (2018). Operation and Economic Assessment of Hybrid Refueling Station Considering Traffic Flow Information. *Energies*, 11(8), 1991. https://doi.org/10.3390/en11081991.

72. Wu, S., Lin, J., Li, J., & Song, Y. (2022). Electricity allocation strategy for on-site hydrogen refueling stations in the forward and spot markets. *IET renewable power generation*, 16(12), 2532–2546. https://doi.org/10.1049/rpg2.12406 .

73. Valedsaravi, S., Vegelin, R., & Olveira, A. (2025). Operational Framework for Large-Scale Power-to-X Plants Fed by Renewable Energies Incorporating BESS and Electrolyzer Degradation. *IEEE Access*, 13, 215994–216012. https://doi.org/10.1109/ACCESS.2025.3645141.

74. Tully, Z., Starke, G., Johnson, K., & King, J. (2023). An Investigation of Heuristic Control Strategies for Multi-Electrolyzer Wind-Hydrogen Systems Considering Degradation. *2023 IEEE Conference on Control Technology and Applications (CCTA)*. https://doi.org/10.1109/CCTA54093.2023.10252187.

75. Sun, M., Zhang, Y., Liu, L., Nian, X., Zhang, H., & Duan, L. (2025). Dynamic performance analysis of hydrogen production and hot standby dual-mode system via proton exchange membrane electrolyzer and phase change material-based heat storage. *Applied Energy*, 377, 124636. https://doi.org/10.1016/j.apenergy.2024.124636 .

76. Liso, V., Savoia, G., Araya, S. S., Cinti, G., & Kær, S. K. (2018). Modelling and Experimental Analysis of a Polymer Electrolyte Membrane Water Electrolysis

Cell at Different Operating Temperatures. *Energies*, 11(12), 3273. https://doi.org/10.3390/en11123273 .

77. Pfennig, M., Schiffer, B., & Clees, T. (2025). Thermodynamical and electrochemical model of a PEM electrolyzer plant in the megawatt range with a literature analysis of the fitting parameters. *International Journal of Hydrogen Energy*, 104, 567–583. https://doi.org/10.1016/j.ijhydene.2024.04.335.

78. Hossain, M. B., Islam, M. R., Muttaqi, K. M., Sutanto, D., & Agalgaonkar, A. P. (2022). Dynamic Electrical Equivalent Circuit Modeling of the Grid-Scale Proton Exchange Membrane Electrolyzer for Ancillary Services. *2022 IEEE Industry Applications Society Annual Meeting (IAS)*. https://doi.org/10.1109/IAS54023.2022.9939788.

79. Liu, J., Huang, L., Leveneur, J., Fiedler, H., Clarke, S., Larsen, T., Kennedy, J., & Taylor, M. (2024). Experimental Investigation of PEM Water Electrolyser Stack Performance Under Dynamic Operation Conditions. *Journal of The Electrochemical Society*, 171(5), 054521. https://doi.org/10.1149/1945-7111/ad4d1f .

80. Cozzolino, R., & Bella, G. (2024). A review of electrolyzer-based systems providing grid ancillary services: current status, market, challenges and future directions. *Frontiers in Energy Research*, 12, 1358333. https://doi.org/10.3389/fenrg.2024.1358333 .

81. Wang, X., Meng, X., Nie, G., Li, B., Yang, H., & He, M. (2024). Optimization of hydrogen production in multi-Electrolyzer systems: A novel control strategy for enhanced renewable energy utilization and Electrolyzer lifespan. *Applied Energy*, 376, 124299. https://doi.org/10.1016/j.apenergy.2024.124299.

82. Wen, Z., Kong, J., Sun, Z., Zhuo, Y., Zheng, Y., Shi, Y., Shi, J., Li, S., & Lin, W. (2026). Universal real-time electrolyzer cluster control framework under fluctuating renewables: A rule-solver-based optimization strategy considering dynamic heterogeneous characteristics. *Energy Conversion and Management*, 348, 120642. https://doi.org/10.1016/j.enconman.2025.120642.

83. Wu, Z., Wang, J., Zhou, M., Xia, Q., Tan, C. W., & Li, G. (2023). Incentivizing Frequency Provision of Power-to-Hydrogen Toward Grid Resiliency Enhancement. *IEEE Transactions on Industrial Informatics*, 19(9), 9370–9381. https://doi.org/10.1109/TII.2022.3228379 .

84. Hao, W., Liu, Y., Wang, T., & Zhang, M. (2025). Model for Joint Operation of Multi-Energy Systems in Energy and Frequency Regulation Ancillary Service Markets Considering Uncertainty. *Energies*, 18(1), 36. https://doi.org/10.3390/en18010036.